Haptic-Enabled Teleoperation of Hydraulic Manipulators: Theory and Application

by

Kurosh Zarei-nia

A Thesis submitted to the Faculty of Graduate Studies of

The University of Manitoba

in partial fulfilment of the requirements of the degree of

Doctor of Philosophy

Department of Mechanical and Manufacturing Engineering

The University of Manitoba

Winnipeg, Manitoba, Canada

Abstract

Hydraulic manipulators commonly interact with environments that are highly unstructured, and thus rely on the intelligence of human operators to provide proper commands. Typically, operators use visual information, directly or through cameras, to perform a task. Providing haptic or touch sensation about the task environment to the operator, enhances her/his ability to perform telemanipulation. The focus of this thesis is on haptic teleoperation of hydraulic manipulators. The application is directed at live transmission line maintenance tasks.

In this thesis, both unilateral and bilateral haptic teleoperation of hydraulic manipulators are investigated. On the unilateral telemanipulation front, position error is shown to be an important issue in performing repetitive tasks. The most important sources of inaccuracy in position are sensors, robot controller performance, and the operator. To reduce the human operator's errors, the concept of virtual fixtures is adopted in this research. It is shown that virtual fixtures can help operators perform routine tasks related to live line maintenance.

Stability and telepresence are the main issues in reference to bilateral control. Three stable bilateral control schemes are designed for haptic teleoperation of hydraulic actuators considering nonlinear dynamics of hydraulic actuation, haptic device, and the operator. For each control scheme, stability of the entire control system is proven theoretically by constructing a proper Lyapunov function. Due to the discontinuity originating from a sign function in the control laws, the proposed control systems are non-smooth. Thus, the existence, continuation, and uniqueness of Filippov's solution to

the system are first proven for each control system. Next, the extensions of Lyapunov's stability theory to non-smooth systems and LaSalle's invariant set theorems are employed to prove the asymptotic stability of the control systems. In terms of telepresence, two types of haptic sensation are provided to the operator: (*i*) haptic based on the reflected interaction force, and (*ii*) haptic based on the position error. Performances of all proposed controllers are validated by experimental results on a hydraulic actuator controlled by a haptic device. It is shown that besides stability, the hydraulic actuator performs well in terms of position tracking while the haptic device provides telepresence for the operator.

Acknowledgment

I would like to forward my most sincere appreciation to my advisor, Dr. Nariman Sepehri, whose encouragements and supports have made this thesis possible. I feel tremendously fortunate to have such a fabulous opportunity to work with an advisor who has both solid theoretical knowledge and experimental expertise which strengthened this project in both aspects.

No word describes my heartfelt thanks to my wife Hamideh Bayrampour whose support has always been encouraging during my studies.

I also wish to sincerely thank Dr. Christine Wu who played a major role in enriching this project by her valuable guidelines and advice on the theoretical aspect of Lyapunov stability analysis, Filippov's solution, and LaSalle's invariant set theorems.

On this project, I had the opportunity of working with Mr. Ehsan Jalayeri, the Fluid Power and Telerobotics Research Laboratory's support engineer. I would like to thank him for his technical support in preparing experimental test rigs.

I also wish to thank my friends and my peers in the fluid power lab, especially Dr. Amin Yazdanpanah who made a friendly atmosphere in the lab during my course of study.

I wish to thank my mother, Ms. Touran Pourebrahim, and my father, Mr. Abdolhosein Zarei-nia, for a lifetime support and encouragement.

I also wish to acknowledge the support of NSERC, Manitoba Hydro, Mitacs, and the University of Manitoba for their financial support.

To:

My dearest wife and my son

Table of Contents

List of Figures

List of Tables

Nomenclature

$x_m, \dot{x}_m, \ddot{x}_m$	Displacement, velocity, and acceleration of the haptic device (Master)	[m], [m/s], [m/s^2]
F_m	Force generated by the master manipulator based on a control law	[N]
F_h	Force generated by the operator	[N]
$x_s, \dot{x}_s, \ddot{x}_s$	Displacement, velocity, and acceleration of the hydraulic actuator (Slave)	[m], [m/s], [m/s^2]
u	Control signal applied to the valve	[V]
F_l	Load force (interaction force)	[N]
m_m	Combined inertia of the master manipulator and the operator's arm	[kg]
m_s	Combined inertia of the piston, actuator rod and load of hydraulic actuator	[kg]
k_d	Combined viscous coefficient of the master manipulator and the operator's arm	[Ns/m]
k_h	Combined stiffness of the operator's arm and the haptic device	[N/m]
$x_{sp}, \dot{x}_{sp}$	Displacement and velocity of the valve spool	[m], [m/s]
P_s	Supply pressure	[Pa]
P_r	Tank pressure	[Pa]
P_1, P_2	Left (or right) actuator chamber pressure	[Pa]
A	Piston annulus area	[m^2]
d	Equivalent viscous damping coefficient, which describes the combined effect of the viscous friction between the piston and the cylinder walls and the damping of the load	[Ns/m]
Q_1, Q_2	Flows into and out of the actuator chambers	[m^3/s]
Q_L	Load flow	[m^3/s]
k_s	Stiffness of the environment	[N/m]
K_v	Servovalve flow gain	[m$^{3/2}$ / kg$^{1/2}$]
w	Width of the rectangular port cut into the valve bushing through which the fluid flows	[m]
β_h	Fluid bulk modulus	[Pa]
$\bar{V}_1, \bar{V}_2$	Volume of fluid contained in the connecting line between the servovalve and the left (or right) chamber of the actuator	[m^3]
L	Actuator stroke	[m]
P_L	Differential or load pressure	[Pa]
F_{fr}	Dry friction	[N]
F_C	Coulomb friction	[N]
F_S	Stiction force	[N]
$\dot{x}_{sv}$	Velocity threshold where downward bend in friction appears after the breakaway	[m/s]

c_d	Orifice coefficient of discharge	
ρ	Hydraulic fluid density	[kg/m^3]
w	Orifice area gradient	[m^2/m]
k_{sp}	Valve gain	[m/V]
τ	Valve time constant	[s]
C	Hydraulic compliance	[m^5/N]
V_t	Total compressed fluid volume	[m^3]
$\theta_1, \theta_2, \theta_3, \theta_4, \theta_5$	Joint angles of the manipulator	[rad]
k_p	Controller gain	[V/Pa$^{3/2}$]
α	Controller parameter	
K_{ps}	Position scaling factor	
K_{fs}	Force scaling factor	
K_{p1}	Controller gain	[V/mPa$^{1/2}$]
K_{p2}	Controller gain	[V/Pa$^{3/2}$]
K_{p3}	Controller gain	[N/m]
K_{p4}	Controller gain	[m^2]

Chapter 1

1 INTRODUCTION

1.1 Statement of the problem

Human-operated, heavy-duty hydraulic machines with manipulator-like implements are widely used in industry. Examples include backhoes, excavators, forklifts, and underwater manipulators [1-3]. Hydraulic manipulators offer several advantages such as good stiffness, high power-to-mass ratio, good performance at low speed, high payload capability, and fast response. Moreover, hydraulic actuators are durable and can hold in place without active control [4]. Furthermore, hydraulic actuators are capable of applying high constant torques for a long period of time, which in case of electrically-actuated manipulators causes overheating of motors.

Researchers have adopted various approaches in the teleoperation of manipulators, in order to improve safety and productivity. At one end of the spectrum, researchers aim to develop fully autonomous manipulators. In these efforts, the humans are removed from direct operation of the machine and only play the role of remote supervisors. However, many applications require interaction with various environments, most of which are highly unstructured. Since a fully autonomous machine may fail in unforeseen circumstances, they rely on the intelligence of human operators to provide proper commands [5]. This combines the accuracy, high power to mass ratio, and good performance of a robot manipulator with the intelligence and decision making capabilities of the operator.

However, the operator may not be present in the task environment for a number of reasons such as the environment is too dangerous or hazardous for humans. Therefore, separating human operators from task environment is necessary in some cases or simply for convenience [6].

Providing fast and proper commands by the operators, in the operation of these machines, requires some sensory feedback from the task environment. The most common types of feedback are direct or indirect visual/audio feedbacks. Touch, or *haptic*, sensation about the task environment to the operator is another way of enhancing the ability to perform telemanipulation [6, 7]. Haptic interaction can provide an additional link that can greatly increase task quality, productivity and safety in operation of these machines compared to traditional manual levers [7]. Fundamentally, haptic interaction is different from all other sensory modalities in that it is bidirectional. Operators exchange energy between their

hands and the haptic device when they push on it and it pushes back on them [8]. It has been shown that, in some applications of teleoperation systems, haptic feedback alone can even be more valuable than visual feedback [9].

Haptic teleoperation of electrically-actuated manipulators has been widely explored by many researchers during the last three decades and various control strategies have been proposed, in which, the stability and performance issues were addressed. Although haptic control of hydraulic systems offers many practical applications, as compared to the class of electrically-actuated robots, research on application of teleoperation control schemes applied to the class of hydraulic manipulators is sparse [10]. Lack of enough research in the field of haptic teleoperation of hydraulic manipulators is the motivation to propose haptic control strategies specially designed for the hydraulic manipulators.

Haptic bilateral teleoperation of hydraulic manipulators is, generally, more challenging than that of their electromechanical counterparts. Electric actuators generally behave as force/torque sources, while in hydraulic actuators, the control voltage acts to move the spool valve that controls the flow of hydraulic fluid into and out of the actuator. This flow in turn causes a pressure differential buildup that is proportional to the actuator force. Even if some of the systems dynamics are ignore, the control voltage fundamentally controls the derivative of the actuator force and not the force itself [11]. Hydraulic actuators also exhibit significant nonlinear characteristics [11]. These challenges make the stability analysis difficult. The focus of this thesis is on the Lyapunov stability control design, because using advanced nonlinear techniques such as

Lyapunov to design controllers that incorporates nonlinearities and guarantees the stability of the system is preferred for highly nonlinear hydraulic systems [6, 12-14].

Teleoperation systems have two major categories: unilateral and bilateral. If only information of the master (position, velocity, or force commands) is transmitted to the slave at the remote site, then the teleoperation system is called *unilateral*. If the slave manipulator reflects some information back to the master, the teleoperation system is called *bilateral* [15]. In this thesis, different categories of haptic teleoperation systems are thoroughly investigated for hydraulic manipulators. In unilateral control mode, the concept of virtual fixtures is adopted, for the first time, to control a hydraulic manipulator by a haptic device for performing live transmission line maintenance. In bilateral control front, some stability proven bilateral control schemes are developed considering the nonlinear dynamics of hydraulic actuation, haptic device, and the operator. Both force-mode and displacement-mode control strategies are explored. The stability of the proposed control systems are proven theoretically and the performances are validated by experimental results.

1.2 Objectives of this research

The objectives of this research are:

(i) To implement a technique to control a hydraulic manipulator unilaterally by a haptic device.

(ii) To design and implement a stable bilateral control scheme for haptic teleoperation of hydraulic manipulators.

In order to achieve the above objectives, two research questions are addressed:

(i) How to design and implement a technique based on the concept of virtual fixtures to control a hydraulic manipulator unilaterally by a haptic device.

(ii) How to design stable control schemes specially for the hapto-hydraulic system, to control a hydraulic actuator bilaterally with the capability of generating force by the haptic device to be applied to the operator's hand.

To address these research questions, an interface is developed to enable a commercially available hydraulic robot to work with an available haptic device. The application will focus on employing this experimental setup and the associated technologies to partially substitute for, and work cooperatively with, crew to perform interruption-free maintenance and inspection of live transmission lines.

1.3 Methodology and approaches

With respect to unilateral control of hydraulic manipulators, concept of virtual fixtures is adopted in this research to haptically control a hydraulic manipulator in performing repetitive tasks. Virtual fixtures have been found useful in many teleoperation applications [1, 16-23]. However, research on using virtual fixtures to control a hydraulic manipulator is sparse [1]. In this research, impedance-type forbidden region virtual fixtures are used for teleoperation of a hydraulic robot.

For bilateral control, different control strategies can be used at the master or slave side for controlling the slave manipulator while generating and applying force by the haptic device to the operator's hand. Two main issues in bilateral control systems are stability and performance [24]. Firstly, the overall closed-loop system should be stable irrespective of the input commands (provided by the operator) or the task environment [15]. Secondly, a feel of performing task at the remote site must be available to the operator. In general, there is a tradeoff between high performance and sufficient stability margins [25]. Many research studies have addressed this tradeoff for electrically-actuated manipulators with controllable torques and various control strategies have been proposed to maintain the stability while improving performance (see [15] and the references cited therein). As compared to the class of electrically-actuated robots, research on application of bilateral control applied to the class of hydraulic manipulators is sparse. There is some research (see [26] and the references cited therein) on applying the existing control schemes, originally designed for electrically-actuated robots, to hydraulic robots; however, none of them investigated the stability of the nonlinear system. More specifically, there is no bilateral control scheme designed for haptic control of hydraulic manipulators that includes nonlinear dynamics of hydraulic functions and the human operator's dynamics. Regarding controller design and stability analysis, comparing different control schemes showed that those using nonlinear methods achieve a higher accuracy compared to the controllers directly based on linear models [27]. Thus, choosing a nonlinear method will result in better performance. Nonlinear stability analysis techniques are usually based on the energy of a system. Two main approaches are Lyapunov stability approach and the passivity approach. The passivity approach,

however, is quite conservative in many cases degrading the transparency and performance of the system [26]. Thus, the Lyapunov stability analysis is the best tool to be used for highly nonlinear systems including electro-hydraulic manipulators [6, 12-14].

The lack of enough research in the field of stable haptic manipulation of hydraulic actuators is an adequate motivation to design and develop some stable control schemes for haptic teleoperation of hydraulic manipulators. The stability of the proposed control systems are proven in this thesis by using Lyapunov stability analysis and is validated by experimental studies. Due to complexity of dynamic equations, the stability analysis and experimental validation is provided for a single-degree-of-freedom hydraulic actuator.

1.4 Application area of interest

The application intended for this research is towards live overhead transmission line maintenance tasks. This is motivated from the fact that working on an overhead power distribution system can be a hazardous and difficult job, particularly in places having harsh climatic conditions. Live transmission line maintenance is essential for most power utilities, and the need to maintain system availability is the main factor [28]. Teleoperation has been proven useful for maintenance of power distribution networks all over the world including Japan, the United States, Canada, and Europe [29]. Using a telemanipulation system for live transmission line maintenance has shown to have the following major advantages [30]: it keeps the operator away from the hazardous areas where the task is to be performed, it allows a more compact design suitable for hard to reach and restricted working spaces, it increases the safety of linemen, and it combines

the accuracy, power, and good performance of the robot with the intelligence of the human operator.

In spite of the advantages, the adoption of robotics technology to live power line maintenance is still new and introduces challenges that need to be addressed. Enhancing robot controls to replicate desired manipulation of the human arm with respect to manipulability and base mobility using haptic-enabled robot-environment interaction and human-robot collaboration are issues requiring proper investigation. Designing a stable teleoperation system to control a hydraulic robot via a haptic device with the capability of generating and applying force to the operator's hand is one of the issues, which has not yet been explored. The adoption of robotics technology applied to utility maintenance demands proper experiments. Therefore a suitable large-scale human plus manipulator-in-the-loop simulator is constructed. Besides providing an objective assessment of techniques, the test-bed will be an excellent training simulator for operators to become familiar with the new system and acquire experience. The goal is to perform a number of live transmission line maintenance tasks using human plus manipulator-in-the-loop simulator with haptic. A number of live-line maintenance tasks were identified and then replicated using the developed experimental test rig. The system was tested successfully by some experienced linemen as well as some novice operators.

1.5 Thesis outline

In Chapter 2, a detailed literature review along with some definitions is provided. First, a definition of a teleoperation system and the advantages of using a haptic interface in telemanipulation are described. Next, the concept of virtual fixtures used in unilateral

mode is explained. Haptic teleoperation of hydraulic manipulators in unilateral and bilateral control modes is described next. At the end of Chapter 2, robotics technologies designed and applied to the application intended in the research are reviewed.

Chapter 3 describes the experimental setups used in this research. First, the experimental setup for the unilateral mode with detailed information about system elements is provided. Next, the experimental setup for bilateral control of a single-degree-of-freedom hydraulic actuator controlled by a haptic device is described along with the derivation of the dynamic model of the entire system including hydraulic actuator interacting with an environment, human operator, and the haptic device.

In Chapter 4, unilateral teleoperation of hydraulic manipulators using the concept of virtual fixtures is investigated. The practicality of the proposed concepts is shown for the application intended in this research by performing a number of live transmission line maintenance tasks using the experimental setup. First, the live transmission line maintenance tasks are explained in details and the virtual fixtures used for each one is provided, followed by the experimental results on the test-rig demonstrating the effectiveness of the proposed system. At the end of this chapter, a qualitative study is conducted based on the experience of the expert linemen who utilized the system.

In Chapter 5, bilateral control of hydraulic actuators is investigated. Three stable bilateral control schemes are designed and experimentally validated on a hydraulic actuator. The control laws are derived based on Lyapunov's feedback control design technique. Individual theoretical stability of all control schemes are proven considering nonlinear hydraulic functions, servovalve dynamics, haptic device dynamics, human operator

dynamics, and dynamics of the task environment. Effectiveness of the proposed controllers is verified by simulation and experimental studies.

Contributions made in this thesis and suggestions for future work are provided in Chapter 6.

Chapter 2

2 RELEVANT BACKGROUND AND DEFINITIONS

2.1 Basic concepts and definitions

The term “teleoperation” means “doing work at a distance”, although “work” may mean almost anything including manipulation by a robotic arm [2], [15]. The term “distance” is also vague: it can refer to a physical distance, where the operator and the robot are separated from each other by a large or small distance, but it can also refer to a change in scale, where for example in robotic surgery a surgeon may use micro-manipulator technology to conduct surgery on a microscopic level, or in telemanipulation of hydraulic machines such as excavators and backhoes, a small movement of the operator causes large displacement of the manipulator [2]. A teleoperation system is used when it is preferred to separate human operators from the task environment. This can have a

number of reasons including safety of the human operator which is the most important one [6].

In general, a teleoperation system is composed of [15]: (*i*) a local site, where a human operator handles a hand controller called master device, (*ii*) a remote site, where a manipulator (slave) follows the motion of the master, (*iii*) a communication channel which connects both sites and (*iv*), visual/audio feedback system either by direct vision or cameras. Standard teleoperation system architecture is shown in Figure 2.1.

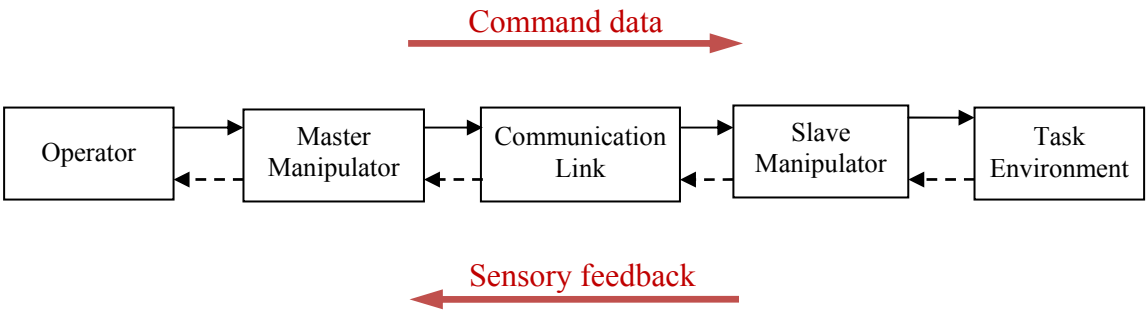

Figure 2.1 Standard teleoperation system.

Note that arrows can either be from left to right (solid arrows) or in both ways (both solid and dashed arrows). In the teleoperation system, if only information of the master is transmitted to the slave, i.e., only solid arrows are used, the teleoperation system is called unilateral (Figure 2.2). If the slave information is reflected back, to be used by the master controller, the teleoperation system is called bilateral (Figure 2.3) [15].

Figure 2.2 Unilateral teleoperation system.

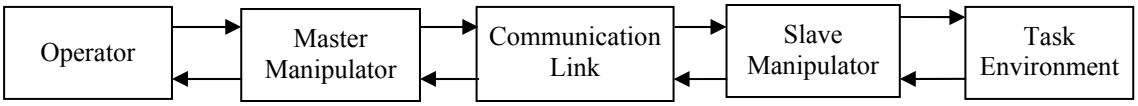

Figure 2.3 Bilateral teleoperation system.

A telemanipulator (or teleoperator) system is a device that is controlled remotely by a human operator using a hand controller. If the hand controller has the capability of generating and applying force to the operator, it is called a "haptic" device. The availability of both haptic and motion information exchange between operator and remote manipulator sites allows a sense of "telepresence" to the operator. Telepresence is the "feel" of the remote site available to the operator via the teleoperation system [24].

A "haptic" interface allows the user to feel or touch virtual objects with their hands [8]. The haptic device has the capability of generating and applying force to the human operator's hand. Touch, or *haptic* interaction is one of the most fundamental and effective ways in which a human operator perceives and influences changes in the surrounding environment. Touch interaction differs, fundamentally, from all our other sensory modalities in that it is a two directional interaction. The operators exchange energy between their hands and the haptic device when they push on it and it push back on them

[8]. It has been shown that, in some circumstances and applications, force feedback alone can be more valuable than visual feedback alone [9].

Haptic interfaces have been used in wide variety of applications such as hazardous material handling in nuclear services [31], medical robotics, tele-ultrasound, tele-surgery [32-37], underwater robotics [38], mobile robots [39-42], and micro-manipulation and assembly [43]. The application of haptics intended in this research is haptic telemanipulation of hydraulic robots. The entire hapto-hydraulic system can either work in unilateral or bilateral mode.

2.2 Unilateral teleoperation

In unilateral mode, only information of the master device is sent to the slave side to be used in slave controller. In this research, the concept of virtual fixtures is adopted for unilateral haptic control of a hydraulic manipulator. A virtual fixture is one of the most popular techniques to create the desired tracking in teleoperation systems which can be defined as active task-dependent software agents whose purpose is to assist the operator during training or performing a telemanipulation task. A virtual fixture refers to a class of guidance modes that help a manipulator to perform a predefined task by limiting the position and/or force [44]. Virtual fixtures limit the movements of the operator into constrained regions or along desired or predefined paths in the manipulator workspace [44]. The use of virtual fixtures can dramatically raise the level of safety and precision that a human operator can achieve [17]. Virtual fixtures can also be used as a source of guidance and navigation [18]. They can add virtual constraints that redirect undesirable

user movements to the useful direction [19]. The potential benefits of virtual fixtures include safer and faster operation [23].

The concept of virtual fixtures was first introduced by Rosenberg in 1993 as “abstract sensory information overlaid on top of reflected sensory feedback from a remote environment” [45]. To better understand the concept of the virtual fixtures, a simple example of a real physical fixture such as a ruler is usually used [45]. A very simple task such as drawing a straight line on a piece of paper without using any tool is a task that most humans are unable to do very fast with good accuracy. Using a very simple device like a ruler can increase the task accuracy while not influencing the task completion time or even make it less. Moreover, the ruler helps the user by guiding the pen along a straight line, which in turn, increases the task quality by reducing mental load of the operator. Without using a ruler, drawing a straight line is a manual task, which requires the user to constantly use visual feedback to correct him/herself and it also requires hand-eye coordination. In addition, when using a ruler to draw a line the task is easier and faster. Moreover, the final result is a more straight line. By “easier”, it means one does not need to use his brain to process the visual feedback information which in turn frees up that modality to be used for other purposes. By “faster” it means the task completion time is reduced. And by “more straight” it means task quality can be improved. Moreover, if the ruler is used to guide a cutting tool to cut a work-piece, it works as a barrier to protect against dangerous or destructive failures to increase safety. This safety is extremely important in medical applications such as tele-surgery as well as many other applications. In live transmission line maintenance tasks which is intended for this research, it can be

used to define a barrier for hydraulic manipulator to prevent it from hitting insulators or other elements of transmission lines which can be dangerous or destructive.

Basically, a ruler is a "perceptual overlay" which is designed to enhance performance in tasks which require a tool to be guided along a straight line. In a very similar fashion, it seems that software-generated "perceptual overlays" could be designed and developed in virtual environments to be used in guiding haptic devices in telemanipulation tasks to enhance the performance at the slave site. The success of the virtual fixtures is not only because they are used for guidance to the user, but also it provides a better telepresence and localization in the remote workspace [45]. While virtual fixtures allow precision and performance to exceed natural human abilities, they also reduce the mental processing load require to perform a telemanipulation task. There are many advantages in using virtual fixtures in telemanipulation:

(i) interact with the user and not with the task environment,

(ii) do not have any mass or mechanical constraints,

(iii) require no machining time or maintenance,

(iv) can be easily prototyped,

(v) can be easily customized and modified according to the task,

(vi) the stiffness and other characteristics of the fixture can be changed easily, and

(vii) can be designed in many types such as damped surfaces, frictional contacts, attractive or repulsive fields, or compliant surfaces.

Although the concept of virtual fixtures is mostly used for providing haptic sensations, this concept is not limited to haptics only. Visual, auditory, and even tactile sensations

can be used alone or in cross-modal combinations in virtual fixtures. Virtual fixtures can be categorized as [46]:

(i) Forbidden-Region Virtual Fixtures (FRVFs), and

(ii) Guidance Virtual Fixtures (GVFs).

In each category, two types of virtual fixtures can be defined:

(i) Impedance-type Virtual Fixtures, and

(ii) Admittance-type Virtual Fixtures.

A Forbidden-Region Virtual Fixture (FRVF) helps the user to keep the manipulator out of a defined forbidden region of the workspace. An FRVF has no effect on the manipulator when it is out of the forbidden region. FRVFs prevent the user from entering specified regions. The FRVFs can be used, for example, in a teleoperated setting where the operator has to move a manipulator in a defined working envelope to accomplish an objective. If there are some regions at the remote site which should be prohibited for the manipulator end-effector to fall into them, the forbidden regions can be defined at various regions. This prevents the operator from issuing commands that can result in the manipulation system ending up in such regions. Note that such improper commands can easily be sent by an operator because of many reasons such as poor visual or audio feedback or simply the time needed for decision making by the operator. Figure 2.4 illustrates the FRVFs and some probable linkage configurations for the tele-robotic manipulator in order to have no penetration into forbidden regions.

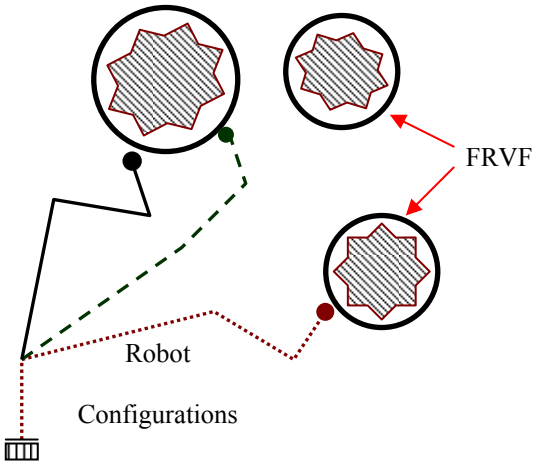

Figure 2.4 Example of a forbidden region virtual fixture (shown as circular solid lines) and robot linking configuration.

With reference to Figure 2.4, star shaped obstacles should be avoided by the en-effector of the robotic arm. Thus, forbidden region virtual fixtures are defined accordingly (shown as circular solid lines).

In an impedance[1]-type FRVF, the force generated is proportional to the manipulator's penetration into the forbidden region [47]. The force can be generated by a virtual spring which pulls the operator's hand back on track and out of the forbidden region.

In an admittance-type FRVF, the manipulator is not commanded to move into the forbidden region, i.e. if the operator pushes the master device into the forbidden region, the slave manipulator will not follow the master and stops at the border of the forbidden

[1] The term "impedance control" was first introduced by Neville Hogan in his three-part paper [100-102] as a unified approach to all manipulation. Inspired by electrical systems, Hogan argued that physical systems come into two types: admittances which accept effort (force, voltage) inputs and yield flow (motion, current) outputs; and impedances which accept flow (motion, current) inputs and yield effort (force, voltage) outputs.

region. This method is more suitable for applications in which penetration of the slave manipulator into the forbidden region can be extremely destructive, such as tele-surgery.

A Guidance Virtual Fixture (GVF) helps to keep the manipulator on a desired surface or path. The GVFs help the user steer the manipulator to a specific point or along a desired trajectory. As an example of a GVF, when the previous manipulator end-effector must follow a certain trajectory, the operator is then able to control the robot motion along the preferred direction while motion along the non-preferred direction is constrained (Figure 2.5).

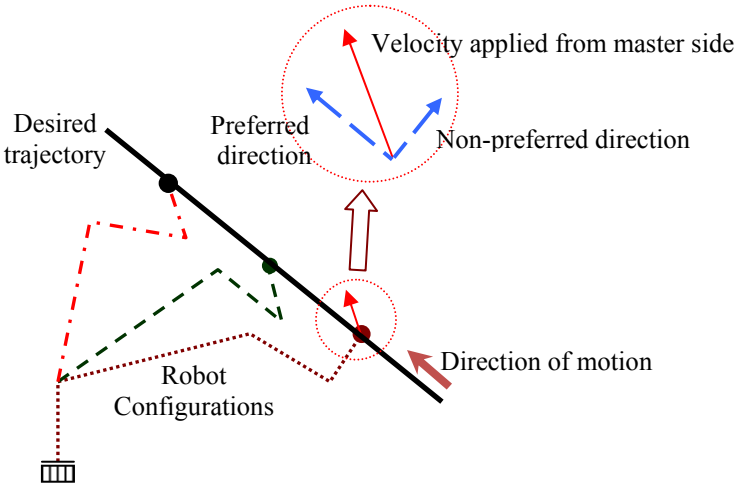

Figure 2.5 Example of a guidance virtual fixture (shown as solid straight line) and defined concept of motion directions.

An impedance-type GVF is actively influencing the movement of the robotic manipulator which can lead to undesirable or unexpected displacements of the manipulator.

In an admittance-type GVF, the velocity of the manipulator is usually controlled proportional to the force applied by the operator [20].

Each type of virtual fixture can be used in two modes:

(i) Cooperative manipulation mode, and

(ii) Telemanipulation mode.

In cooperative manipulation, the human operator directly manipulates an environment using a robotic arm or manipulator. In telemanipulation, the human operator manipulates a master manipulator, and a slave manipulator at the remote site manipulates an environment while following the position, velocity, force, or other commands of the master.

As far as previous relevant research studies are concerned, Rosenberg [45] implemented virtual fixtures for a peg-in-hole task in a teleoperated environment. Experimental results showed that guidance improved the operator performance by up to 70% [45]. Kang et al. [16] used virtual fixtures to provide passive constraint to the motion of the human operator during telemanipulation with the application in hazardous material handling. They found that virtual fixtures could improve accuracy and time for performing the tasks. Marayong et al. [21] used virtual fixtures to provide different levels of guidance to the operator for a path following task. They found that complete guidance offers the best improvement in both execution time and error reduction in tasks that involve general path-following. Eduardo et al. [22] used virtual fixtures in the teleoperation control of a remote manipulator with applications in defense and security. Abbott and Okamura [23]

considered the problem of unstable vibrations of the slave and/or master against forbidden-region virtual fixtures. Kontz et al. [1] used virtual fixtures to control a lifter for a pick and place task. They found that using virtual fixtures can significantly reduce the number of collisions between the remote manipulator and the target environment (task quality). It was also shown that using virtual fixtures can improve overall completion time (productivity). All these research studies showed that the concept of virtual fixtures has the potential of being used in telemanipulation of hydraulic robots to increase task quality, safety, and productivity in performing live transmission line maintenance tasks.

2.3 Bilateral teleoperation

Teleoperation system extends the human ability for operating and manipulating objects and performing tasks remotely by providing the operator with similar conditions, or at least partially similar conditions, as those at the remote location [24]. Two main goals of the teleoperation systems from control point of view are stability and telepresence [24]. The overall closed-loop system should be stable irrespective of the behavior of the human operator or the task environment [15]. Although providing haptic force at the master side enables the human operator to rely on his tactile senses along with the other sensory information like visual and audio, it may make the overall teleoperation system unstable [48]. This issue in haptic teleoperation systems has been one of the main challenges for researchers [15]. Telepresence is the “feel” of the remote task environment available for human operator at local site. Having transparency in the teleoperation system is a part of telepresence. However, telepresence has a more broad definition. Telepresence requires

that the users' senses be provided with such stimuli as to give the feeling of being in that other location. It can be provided by a combination of different sensory feedbacks from the task environment to the human operator. This includes, but is not limited, to audio/visual feedback, haptic and force feedback, or even temperature feedbacks. In a teleoperation system whatever improves the “feel” of being present at the remote site or task environment contributes to the telepresence. In terms of transparency in a bilateral teleoperation system, it is achieved if the position tracking of the remote robot at the slave side and force tracking of the haptic device at the master side are both faithful [24]. There is always a trade-off between stability and performance of the teleoperation system [25], [49]. Since the ideal realization of the transparent bilateral system is not possible, another bilateral teleoperation design philosophy is also proposed in literature. Rather than aiming to have a bilateral system that is fully transparent form user side, systems can be constructed in a way that impedance perceived by the human operator is shaped in order to give a feeling of a virtual tool in operator’s hand. By this method a human operator can execute a task easily and is designed suitably for a specific task [50, 51]. The best and the most up to date historical survey about bilateral teleoperation systems was provided by Hokayem and Spong [15]. It includes different control strategies proposed by researchers for bilateral teleoperation. There are also two excellent surveys by Sheridan [52, 53] which focus on interaction between human and machine, supervisory control, and software-based teleoperation systems.

2.4 Haptics and hydraulics

As far as the haptic control of hydraulic actuators is concerned, research in this area is limited to a few studies. Kontz et al. [7] showed that by shaping the impedance, a better ‘‘feel’’ of telepresence can be achieved for operators. This was evaluated in a human-in-the-loop test-bed [54]. In another application, Kontz et al. [1] used virtual fixtures to generate force signals in a forklift truck. Instead of making the system transparent, they allowed it to react to virtual forces acting on the end-effector. Kontz and Book [6] also used a hybrid position/rate haptic control for a hydraulically-actuated lifter, and showed the advantages of employing rate-mode control for moving the forklift around, and position-mode control for controlling the implement. Haptic control of excavators has also been explored by Parker et al. [5] and Lawrence et al. [55] who developed a magnetically levitated joystick with stiffness feedback to control a hydraulic excavator. Joystick stiffness was mapped to the end-effector force and joystick position was mapped to the end-effector velocity. Zarei-nia et al. [26] experimentally compared the performance of a number of teleoperation control schemes, previously used for electromechanical systems, on a hydraulic actuator. However, none of the above research studies investigated the stability of the entire control system considering combined operator-haptic-actuator-environment dynamics and nonlinear hydraulic functions. Obviously, research in the area of bilateral control of hydraulic actuators is still new, and there remain many challenges to make haptic control ready for hydraulics in practice [10]. Regarding the stability of the system, using advanced nonlinear techniques, such as Lyapunov stability to design controllers that incorporates nonlinearities and guarantees the stability of the system, is preferred for highly nonlinear hydraulic systems [6, 12-14].

With respect to the Lyapunov stability analysis, it has been extensively used in controller design for hydraulic actuators. To name a few, Sekhavat et al. [56, 57] proposed a controller to regulate the impacts of a hydraulic actuator that comes in contact with a nonmoving environment based on Lyapunov stability analysis. Niksefat et al. [58] designed a Lyapunov controller that allows a hydraulic actuator to follow a free space trajectory and then make and maintain contact with the environment for exerting a desired force. Halanay et al. [59] used Lyapunov stability analysis method for a hydraulic actuator to study the influence of the mounting structure of an airplane under hydraulic-powered control. Sekhavat et al. [60] used Lyapunov-based controller design techniques to compensate for discontinuous friction for the position regulation of a hydraulic actuator. The proposed control scheme was capable of asymptotic position regulation with no steady-state error despite friction effects. Since the performance achievable by classical linear controllers is usually limited, due to highly nonlinear behavior of the hydraulic dynamics, Sirouspour and Salcudean [12, 61] adopted the back-stepping design strategy to develop a Lyapunov-based nonlinear controller for a hydraulic servo-system. They incorporated load, hydraulic and valve dynamics in the design process. Cunha [62] proposed a cascade controller for the trajectory tracking control of a hydraulic actuator by using a suitable Lyapunov function. Becker et al. [63] presented a model-based robust controller for electro-hydraulic robots. Manipulator dynamics and actuator dynamics including the dynamics of the valves were taken into account and the stability was proven based on the Lyapunov method. The advantage of the proposed control scheme is that it is modular which simplifies the tuning of the controller parameters. None of these studies included haptic force feedback in their design. Specifically, to the best of author's

knowledge, no bilateral control scheme has been proposed in the literature based on Lyapunov's stability theory, which includes nonlinear characteristics of hydraulic actuation.

A description of the Lyapunov stability analysis method along with some other theorems and definitions used in this thesis are provided in Appendix at the end of this dissertation.

2.5 Application

The application intended for this research is live transmission line maintenance tasks. Within the context of robotics technology applied to live transmission line maintenance, Toussaint et al. [28], in a recent review paper presented extensively numerous initiatives which have been undertaken to develop robots for transmission line maintenance including different robotic technologies (e.g. LineROVer, LineScout) which has been developed at Hydro-Quebec's research institute (IREQ). Montambault and Pouliot [64] presented a literature review of innovative devices applied to power line maintenance. They [65] also designed an inspection robot system for live-line suspension insulator strings to prevent an insulator failure. Tsukahara et al. [66] formulated a conceptual design for a power distribution line maintenance robot system using a computer graphic simulator and an experimental robot system with the ability to perform tasks using task-level instructions. Aracil et al. [67] developed a teleoperated system for live-line maintenance which executes tasks directly on hot lines via a master arm. Takaoka et al. [68] developed a robotic system for executing routine jobs automatically. Lu et al. [69] developed a live working robot with local automatic and master-slave operation possibilities.

From a literature survey it was observed that the adoption of robotics technology to hydro transmission line maintenance is still new and introduces challenges that are to be further explored. Existing techniques such as virtual fixtures which has been proven to be useful in other applications for electrically-actuated manipulators has not yet been applied to hydraulic manipulators for live transmission line maintenance tasks.

2.6 Summary

To summarize, unilateral and bilateral haptic teleoperation of hydraulic manipulators are thoroughly investigated in this thesis. In the unilateral control mode, the concept of virtual fixtures is adopted to control a hydraulic manipulator by a haptic device for performing live transmission line maintenance. On the bilateral control front, some stable bilateral control schemes are designed, for the first time, considering nonlinear dynamics of hydraulic actuation, haptic device, and the human operator. Both force-mode and displacement-mode control strategies are explored thoroughly. Stability of all proposed control schemes are proven theoretically. Performances of all controllers are validated by experimental results.

Chapter 3

3 EXPERIMENTAL SETUPS AND MODELING

During the course of this research, two experimental setups were used. The first was used for implementation of the concept of virtual fixtures in unilateral mode for the application intended for this research. The second setup was used to validate the proposed control schemes designed for bilateral haptic control of a hydraulic actuator. The experimental setups are described first, followed by the modeling of the general equations describing hydraulic functions, haptic device and human dynamics, and the task environment.

3.1 Test rig for unilateral control experiments

The test rig used for unilateral control studies (see Figure 3.1) is comprised of an industrial six degrees-of-freedom hydraulic manipulator (slave), a PHANTOM haptic device that allows control of the manipulator by the operator while creating a feel of

force (master), a frame replicating a segment of transmission line, a hot stick attached to the hydraulic manipulator, and live transmission line maintenance tools.

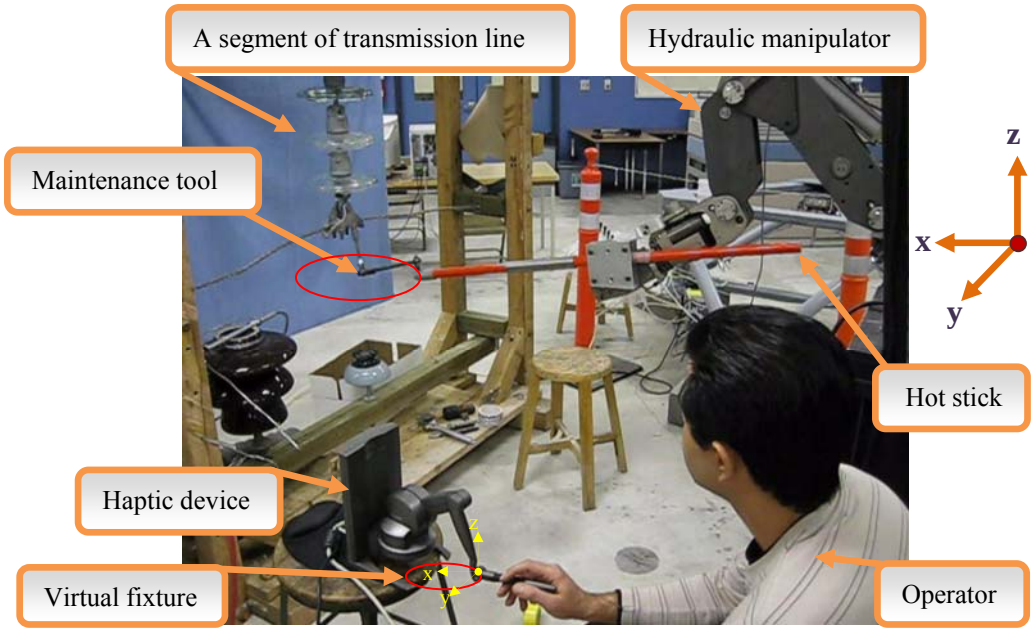

Figure 3.1 Experimental test rig for unilateral teleoperation.

The master and slave devices are connected to a PC using parallel port and data acquisition boards, respectively. The data acquisition boards are used to send control signals to the servovalves and read the manipulator's joint angle sensors. This setup can also be used for other applications such as underwater exploration. This setup is used in unilateral mode and the concept of virtual fixtures is used to control the hydraulic manipulator which will be explained in Chapter 4. Since there is no direct force feedback from slave side back to the master side, the stability of the system may not be a critical issue. However, position accuracy is an issue since there is no position feedback from the slave side to the master side. Therefore, the control method that is used for unilateral

mode should aim at minimizing the position errors. These position errors may have different sources such as human operator performance, errors caused by position or angle sensors, or errors arisen from robotic arm's controller response. The operator errors are minimized here by using the concept of virtual fixtures, sensor errors are minimized by proper sensor calibration, and the robotic arm's joint angles controllers errors are minimized by choosing an accurate controller for each joint [70].

Figure 3.2 shows the close-up picture of the system elements which includes the haptic device, hydraulic manipulator, hot stick attached to the end-effector of the hydraulic manipulator, power line insulators, and some live transmission line maintenance tools.

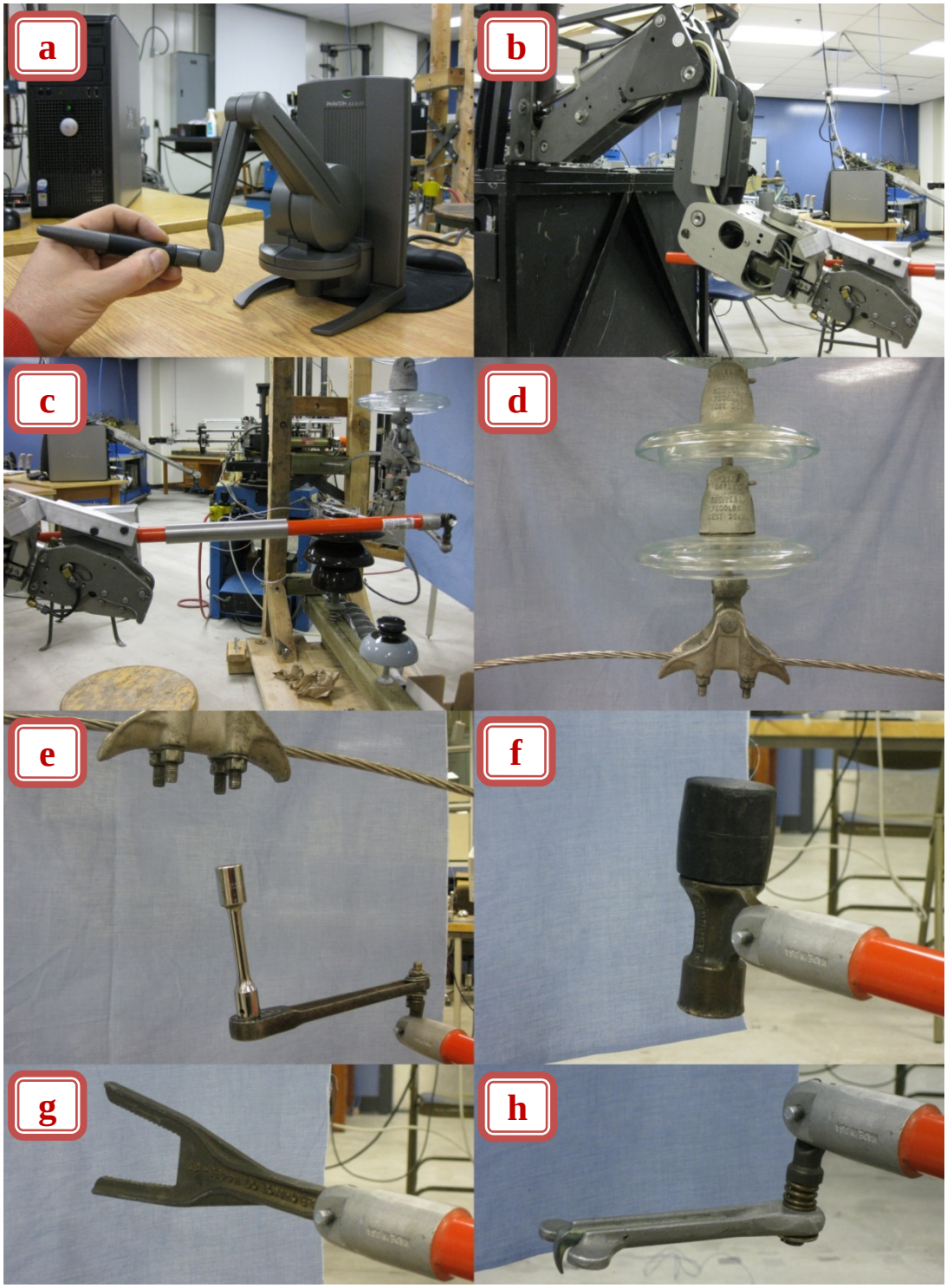

Figure 3.2 System elements used in unilateral experimental test rig: (a) haptic device; (b) hydraulic manipulator; (c) hot stick attached to manipulator's end-effector; (d) power line insulators (task environment); (e)(f)(g)(h) live-line maintenance tools.

For the hydraulic manipulator (slave), only four degrees-of-freedom are used for experiments. A schematic of the hydraulic manipulator and coordinate frames are provided in Figure 3.3.

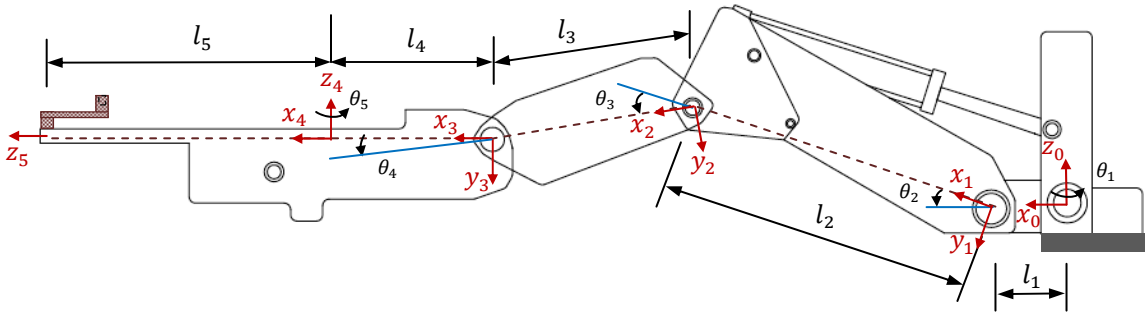

Figure 3.3 Schematic and coordinate frames of the hydraulic manipulator.

The rotational capability of the end-effector about the z_5 axis (roll) is deactivated. Also, rotation about the z_4 axis (yaw) is fixed by assigning zero as the desired value for the joint angle θ_5. For always having a horizontal hot-stick, the joint angle θ_4 (pitch) is computed according to the values of θ_2 and θ_3. Thus, only the first three joint angles, θ_1, θ_2, and θ_3, are used for positioning of the end-effector of the manipulator based on the control scheme to be designed in Chapter 4. The orientation of the end-effector is always fixed.

Coordinate frames of the haptic device (master) are shown in Figure 3.4. Only the position of the end-effector (or the first three thetas) is used in this thesis and the orientation or the last three degrees-of-freedom are not used.

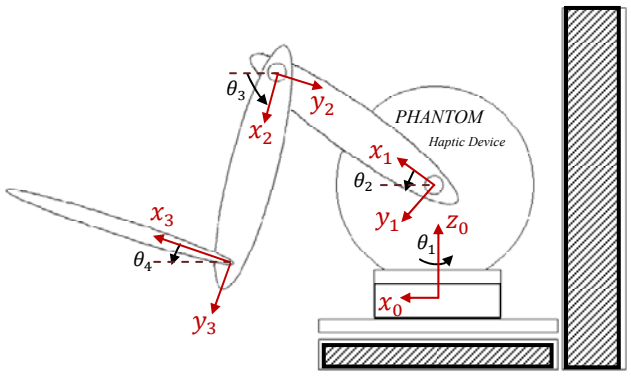

Figure 3.4 Schematic and coordinate frames of the haptic device.

3.1 Test rig for bilateral control experiments

In the bilateral control mode, although the force feedback to the master side enables the human operators to rely on their tactile senses along with the other sensory information like visual, the force feedback makes the overall teleoperation system more susceptible to instability. This issue, which has been a challenge for researchers dealing with electrically-actuated robots, is more challenging in hydraulic manipulators. Due to the complexity of the equations of a hydraulic manipulator in the bilateral control mode, a single degree-of-freedom hydraulic actuator is considered. The overall haptic-hydraulic bilateral teleoperation test-rig is shown in Figure 3.5.

The slave manipulator is a hydraulic actuator interacting with the environment emulated by a spring. The interaction force between the hydraulic actuator and the environment is measured by a force sensor mounted at the end-effector of the hydraulic actuator. The

master controller block represents a PC which controls the haptic device. The slave controller block is a PC equipped with a data acquisition board; these two PC's are connected by a Local Area Network (LAN). The communication protocol used is User Datagram Protocol (UDP). The minimum time delay has been found to be $\approx 0.2\text{ms}$ and the maximum is less than 5ms. The average round trip time for the connection is approximately 1ms ($T \approx 0.5\text{ms}$) with standard deviation of $\approx 0.03\text{ms}$. The packet loss rate is less than 5%.

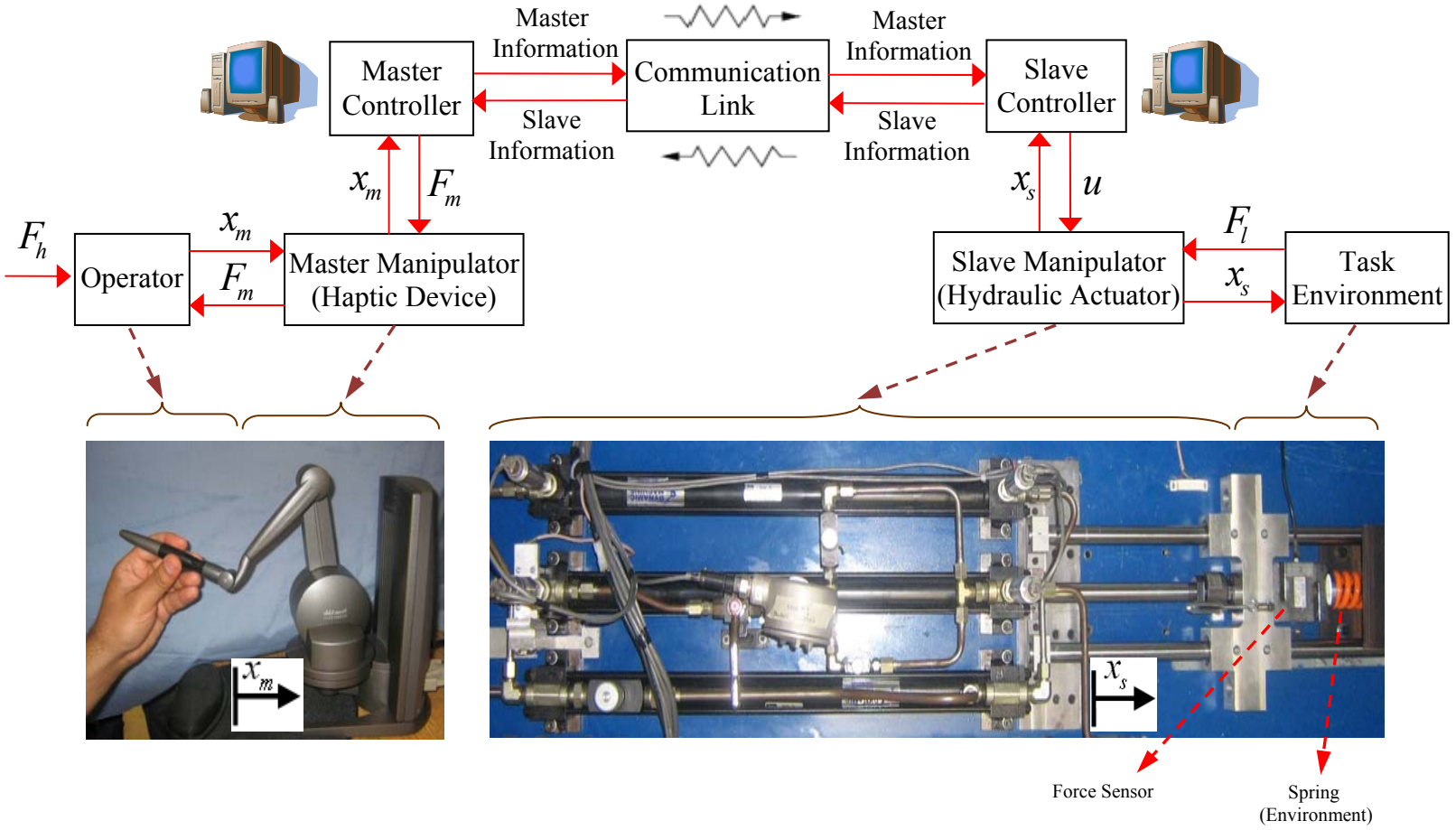

Figure 3.5 Experimental test rig for bilateral teleoperation.

3.2 Derivation of model

In this section, the dynamic model of the bilateral telemanipulation system including human operator, haptic device, hydraulic actuator, and task environment is presented. The PHANTOM desktop haptic device and operator's hand is shown in Figure 3.6.

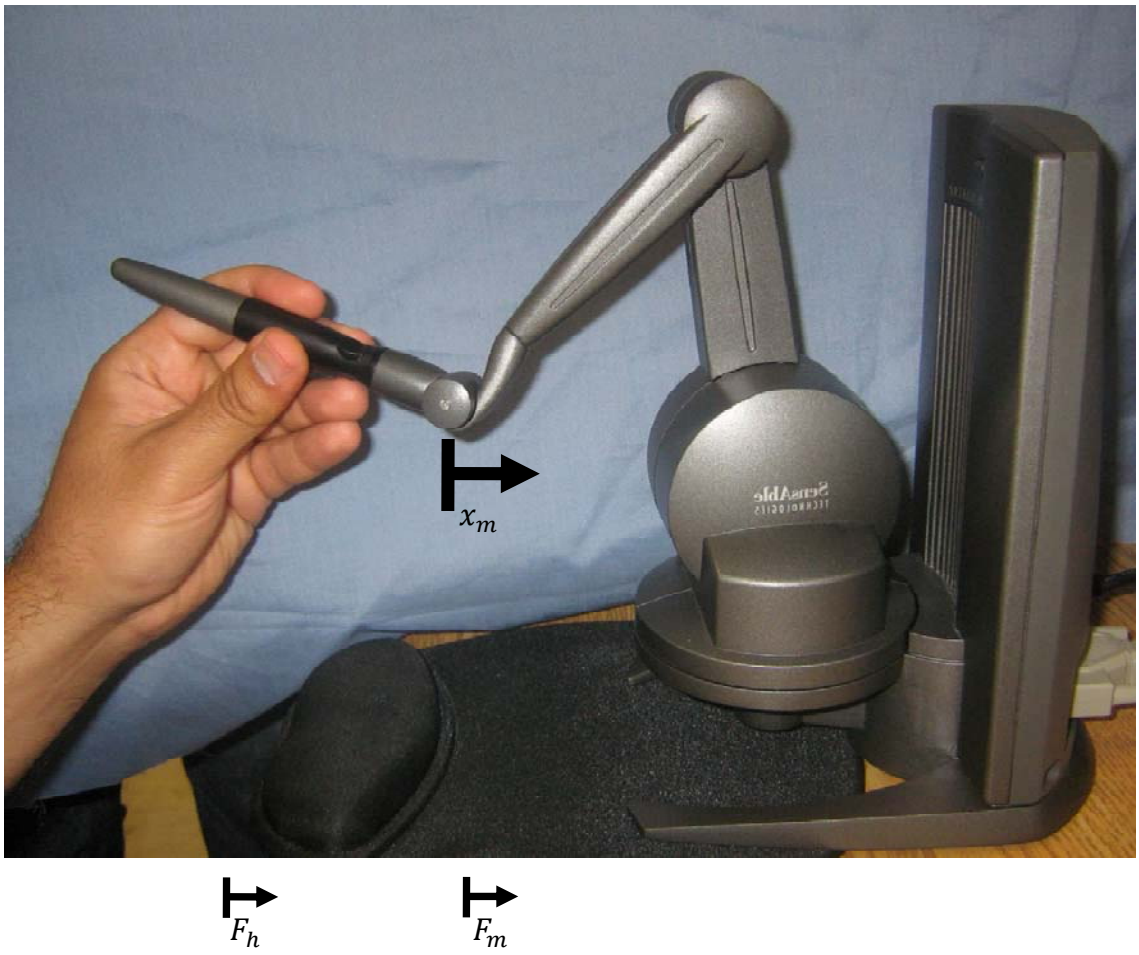

Figure 3.6 Haptic device and human operator's hand.

The combined dynamics of the master manipulator and the human arm, in one dimension, are described in (3.1) which is also used by other researchers [24, 71-76]:

$$m_m\ddot{x}_m + k_d\dot{x}_m + k_h x_m = F_h + F_m \tag{3.1}$$

where, m_m is the combined inertia of the master manipulator and human arm, k_d is the combined viscous coefficient of the master manipulator and the human arm, and k_h is the combined stiffness of the human arm and the haptic device. F_h is the force generated by the human operator's hand, x_m is the displacement of the haptic device, and F_m is the master force generated by the master manipulator actuators based on a control law. The schematic of a servovalve-controlled hydraulic actuator is shown in Figure 3.7.

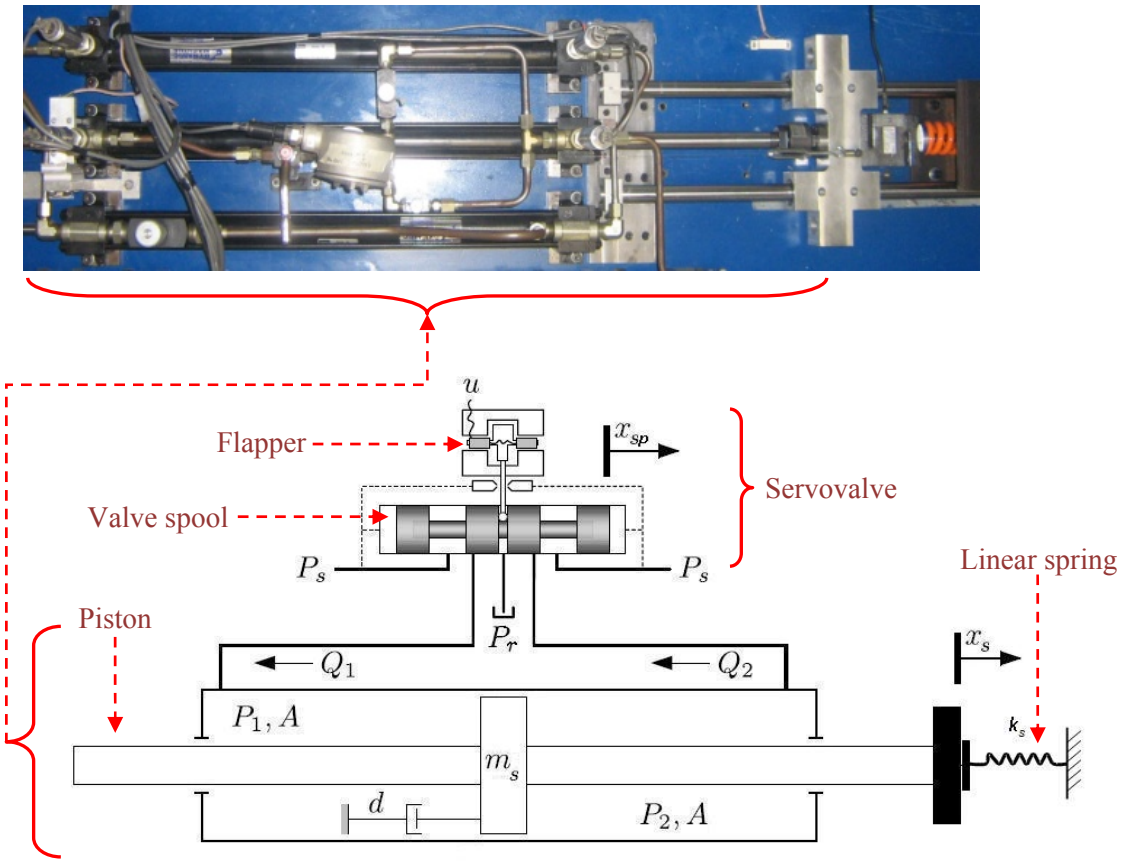

Figure 3.7 Schematic of hydraulic actuator interacting with a stiffness dominant environment.

The control input, u, is computed according to the control algorithm and causes a valve spool displacement, x_{sp}, which in turn controls flows, Q_1 and Q_2, into and out of the actuator [77, 78].

The actuator is considered to be activated by an ideal critical centre servovalve, with matched and symmetrical orifices. For control flows Q_1 and Q_2 through the valve, the nonlinear governing equations can be written in the following compact form [4]:

$$Q_1 = K_v\, w\, x_{sp} \sqrt{\frac{P_s - P_r}{2} + sgn(x_{sp})\left(\frac{P_s + P_r}{2} - P_1\right)} \tag{3.2}$$

$$Q_2 = K_v\, w\, x_{sp} \sqrt{\frac{P_s - P_r}{2} + sgn(x_{sp})\left(P_2 - \frac{P_s + P_r}{2}\right)} \tag{3.3}$$

where K_v is the valve flow gain, and w is the width of the rectangular port cut into the valve bushing through which the fluid flows. The supply and tank pressures are denoted by P_s and P_r, respectively. Variables P_1 and P_2 refer to the hydraulic pressures in each of the actuator chambers. The function $sgn(*)$ is the sign function and defined as follows:

$$sgn(*) = \begin{cases} +1 & *> 0 \\ 0 & *= 0 \\ -1 & *< 0 \end{cases} \tag{3.4}$$

The continuity equations that describe the pressure changes in each actuator chamber as a function of flows into and out of the actuator, Q_1 and Q_2, can be written as follows [4]:

$$\dot{P}_1 = \frac{\beta_h}{A\, x_s + \bar{V}_1}\,(Q_1 - A\, \dot{x}_s) \tag{3.5}$$

$$\dot{P}_2 = \frac{\beta_h}{A\,(L - x_s) + \bar{V}_2}\,(-Q_2 + A\,\dot{x}_s) \tag{3.6}$$

where A is the annulus area of the piston. The volumes of fluid contained in the connecting lines between the servovalve and the actuator are given by $\bar{V}_1$, and $\bar{V}_2$. The actuator stroke is denoted by L. The fluid bulk modulus is given by β_h , and $\dot{x}_s$ is the velocity of the actuator. The equation of motion for the hydraulic actuator is [78]:

$$AP_L = m_s\ddot{x}_s + d\dot{x}_s + F_l + F_{fr} \tag{3.7}$$

where m_s is the inertia of the moving part of the actuator. $\dot{x}_s$ and $\ddot{x}_s$ are the velocity and the acceleration of the end-effector, respectively. Parameter d is the equivalent viscous damping coefficient which describes the combined effect of the viscous friction between the piston and the cylinder walls and the damping of the load. $P_L = P_1 - P_2$ is the differential or load pressure.

The hydraulic actuator manipulates a stiffness dominant environment. Thus, the contact force, F_l, can be expressed as:

$$F_l = k_s x_s \tag{3.8}$$

where k_s is the stiffness of the environment and x_s is the displacement of the end-effector. Note that, when the hydraulic actuator moves in free motion, the stiffness of the environment is zero, i.e. $k_s = 0$, therefore $F_l = 0$, and when the hydraulic actuator is manipulating the environment, $k_s \neq 0$. A more general form for the environment, i.e.

mass-spring-damper, can also be considered, but the effect of the mass and damper of the load is already considered in m_s and d, respectively.

F_{fr} represents dry friction. Various models have been proposed to describe friction [13, 56]. They include Tustin's discontinuous model and LuGre continuous model [56]. Both are widely used in many applications including hydraulic position and force control systems [56]. The Tustin's discontinuous model, for example, is formulated as follows [56]:

$$F_{fr} = \left[F_C + (F_S - F_C)e^{-(\dot{x}_s/\dot{x}_{sv})^2}\right] sgn(\dot{x}_s) \tag{3.9}$$

where F_C is the Coulomb friction and F_S is the stiction force, needed to be overcome, in order to start the motion. At rest, the friction is opposite to the net external force and can acquire any value in the range of $[-F_S, F_S]$. This opposing static friction increases with the increase in the net external force until it reaches the breakaway force, F_S, where the piston starts to slide and the friction follows (3.9). Term $\dot{x}_{sv}$ is a threshold where the downward bend in friction appears after the breakaway (stiction) force is surmounted (Stribeck effect). F_C, F_S, and $\dot{x}_{sv}$ are normally estimated by the construction of the static friction-velocity map measured during constant velocity motions [13].

The relations between the load flow, $Q_L = (Q_1 + Q_2)/2$, the spool displacement, x_{sp}, and the load pressure, P_L, are given as [57]:

$$Q_L = \frac{c_d}{\sqrt{\rho}} w x_{sp} \sqrt{P_s - sgn(x_{sp}) P_L} = A\dot{x}_s + C\dot{P}_L \tag{3.10}$$

In (3.10), c_d is the orifice coefficient of discharge; ρ is the hydraulic fluid density. C is the hydraulic compliance which is approximated by $C \approx V_t/4\beta_h$, where V_t is the total compressed fluid volume and β_h as the effective bulk modulus of the system [79]. Note that in (3.10), C is the hydraulic compliance of the system when the actuator is centered [57].

The dynamics between the valve input voltage, u, and the spool displacement, x_{sp}, are described as a first-order model which is adequate for many industrial applications [78, 80, 81]:

$$\dot{x}_{sp} = \frac{-1}{\tau} x_{sp} + \frac{k_{sp}}{\tau} u \tag{3.11}$$

k_{sp} and τ are the valve gain and time constant, respectively.

The model described above is now employed to construct the state space model. Defining the state vector $\vec{x}$ as:

$$\vec{x} = [x_1 \quad x_2 \quad x_3 \quad x_4 \quad x_5 \quad x_6]^T = [x_s \quad \dot{x}_s \quad P_L \quad x_{sp} \quad x_m \quad \dot{x}_m]^T \tag{3.12}$$

results in the following state space model:

$$\begin{cases} \dot{x}_1 = x_2 \\ \dot{x}_2 = \dfrac{A}{m_s} x_3 - \dfrac{d}{m_s} x_2 - \dfrac{k_s}{m_s} x_1 - F_{fr} \\ \dot{x}_3 = \dfrac{1}{C}\left(-A x_2 + \dfrac{c_d}{\sqrt{\rho}} w x_4 \sqrt{P_s - sgn(x_4) x_3} \right) \\ \dot{x}_4 = \dfrac{-1}{\tau} x_4 + \dfrac{k_{sp}}{\tau} u \\ \dot{x}_5 = x_6 \\ \dot{x}_6 = \dfrac{1}{m_m}(F_h + F_m - k_d x_6 - k_h x_5) \end{cases} \tag{3.13}$$

In (3.13), u and F_m are computed by the control laws to be designed. F_h is the input force originating from the operator. Different control techniques can be used to derive the control laws for F_m and u some of which are described in the next sections.

System parameters used in simulations are given in Table 3.1. Values of the hydraulic function parameters were obtained directly from manufacturer's data or by experimental measurement/verification to resemble the test rig on which all the experiments were performed [82]. With respect to the parameters used at the master side, values for operator's parameters were obtained from references [71, 83, 84], and the values of parameters for the haptic device were obtained from the manufacturer. The accuracy of the simulation results has previously been verified [82].

Table 3.1 System parameters used in simulations.

Parameter	Symbol	Value
Supply pressure	P_s	$17.2\ MPa\ (2500\ psi)$
Combined mass of piston and rod	m_s	$12.3\ kg$
Viscous damping coefficient	d	$250\ Ns/m$
Piston area	A	$6.33 \times 10^{-4}\ m^2$
Hydraulic compliance	C	$2 \times 10^{-13}\ m^5/N$
Orifice coefficient of discharge	c_d	0.6
Hydraulic fluid density	ρ	$847.15\ kg/m^3$
Orifice area gradient	w	$0.02075\ m^2/m$
Valve gain	k_{sp}	$2.79 \times 10^{-5} m/V$
Valve time constant	τ	$0.03\ s$
Stiffness of environment	k_s	$125\ kN/m$
Inertia of master (haptic)	m_m	$0.545\ kg$
Viscous coefficient at the master side	k_d	$2.0\ Ns/m$
Stiffness of human arm	k_h	$10\ N/m$

The experimental setups and modeling described in this chapter will be used in Chapter 4 and Chapter 5 to design control schemes for unilateral and bilateral control of hydraulic manipulators while providing haptic force feedback for the operator.

Chapter 4

4 UNILATERAL CONTROL OF HYDRAULIC MANIPULATORS[2]

4.1 Implementation of the concept

In unilateral telemanipulation, only information from the master is sent to the slave side to be used in the slave controller. No information is sent back to the master system during manipulation. Thus, position accuracy is one of the most important issues that should be addressed. One source of inaccuracy in position is the human operator. It was shown that using the concept of virtual fixtures can effectively minimize the human operator's deviation from prescribed desired trajectory, in performing tasks which require general path tracing [85]. The concept of virtual fixtures is used in this research to minimize these errors. For example, consider the replacement of a faulty or broken insulator which is a common task in live-line maintenance. This task comprises of sub-tasks which are

[2] Results of this section has been presented and published in the proceedings of the: (i) 6th FPNI-PhD Symposium, June 15-19, 2010, Lafayette, IN, USA, Vol. 2, pp. 633-642; and (ii) IEEE 1st International Conference on Applied Robotics for the Power Industry (CARPI 2010), 2010, Montreal, Quebec, Canada, pp. 6.

identified by investigating the manual line maintenance tasks. For each task a forbidden region virtual fixture was designed based on the way that linemen perform the task manually. In this context, a program was developed, which allows different paths to be generated and appropriate forces to be applied to the operator's hand by the haptic device, to maintain a prescribed path. The operator defines a path based on the manual task as the prescribed path for the end-effector of the hydraulic manipulator. This path is then mapped geometrically onto the position of the haptic device to generate a virtual fixture. The real-time current position of the haptic device is then transferred to the position of the end-effector of the hydraulic manipulator. This desired position of the hydraulic manipulator is used to calculate the joint angles set-points, using inverse kinematics. The error between the current joint angles, measured by encoders, and the joint angle set-points (desired) is then used by the controller to obtain the control signal. During the operation, linemen are free to move the manipulator when it is in the desired path, but, when haptic device penetrates into the forbidden region, or the operator deviates from the desired path, an appropriate force is generated by the haptic device. The software is capable of changing the force pattern and the tolerance to deviation from the path. The way that the haptic force is generated will be shown on Figure 4.2.

Another source of position inaccuracy is the hydraulic manipulator's controller. In order to possess the manipulator exhibiting a low position error in tracking the master, the position controller is required to meet a number of stringent criteria. These criteria includes: having excellent tracking and regulating abilities, responding quickly to the changes in the set point in spite of stiction and hydraulic flow dead-band, reversing the directions quickly without overshoot, and retaining the above properties for both large

and small changes in set point. The implementation was made possible by a novel nonlinear PI (NPI) controller for each joint of the manipulator [70]. The NPI controller was shown to improve position tracking accuracy, relative to a conventional PI controller with fixed gains, without sacrificing regulation accuracy or robustness.

Figure 4.1 presents the master-slave telemanipulation control scheme which is employed with the inclusion of the corresponding modules.

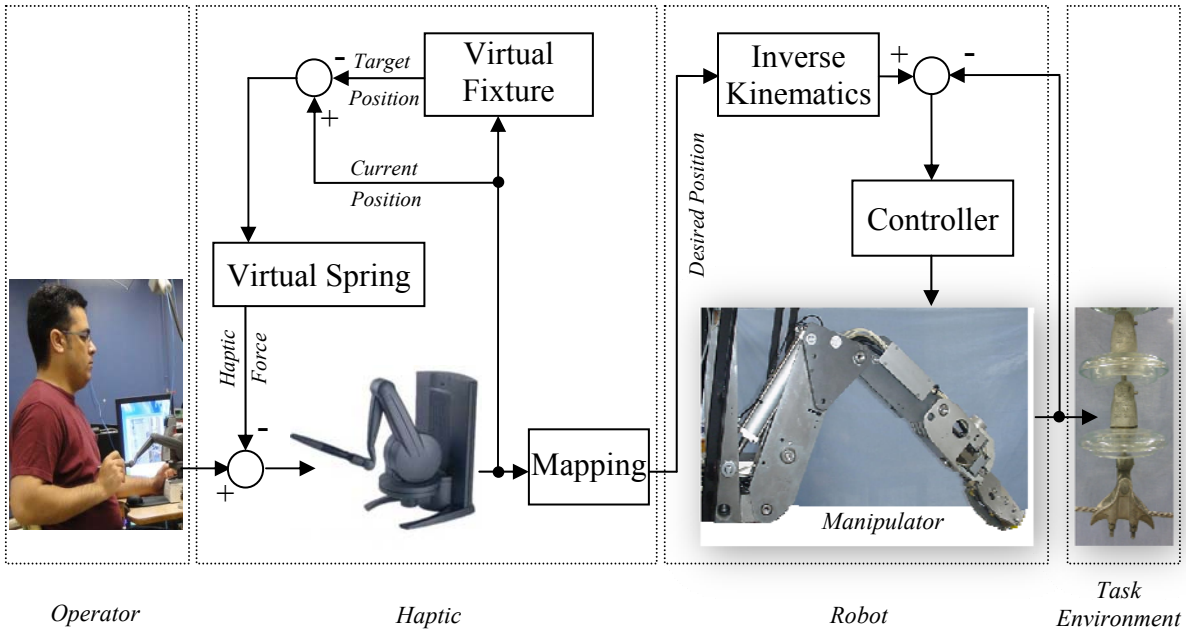

Figure 4.1 Block diagram of unilateral teleoperation control system.

With respect to Figure 4.1, the operator moves the haptic device. The current position of the haptic device (point **A** on Figure 4.2) is used by the virtual fixture software to determine the target point on the prescribed path (point **B** on Figure 4.2). The difference

between this target position and the current position of the haptic device, δx, is multiplied by the stiffness of the virtual spring, k_s, to calculate the haptic force , i.e., $f = k_s \delta x$. This haptic force is then generated and applied to the operator's hand. This type of force was shown to increase task quality and the accuracy of tasks requiring general path tracing [85]. For the slave manipulator, the current position of the haptic device is mapped geometrically onto the workspace of the hydraulic manipulator to be used as the desired position of the end-effector. This desired position is then used to calculate the desired joint angles of the robotic arm using inverse kinematics. The NPI controller provides control signals based on the difference between the desired joint angles and the actual joint angles, for each joint.

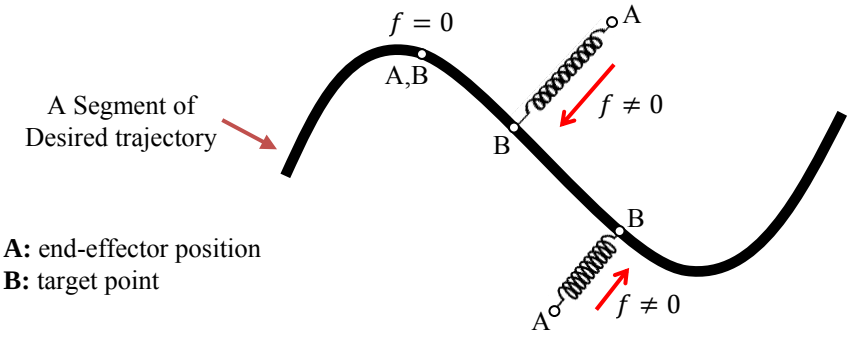

Figure 4.2 Virtual spring concept.

4.2 Application to live line maintenance

There were different tasks emulated using the experimental setup, some of which are shown in Figure 4.3 along with the virtual fixtures used for each. These tasks are

currently performed manually by operators working in locations high above the ground and near high voltage power transmission lines.

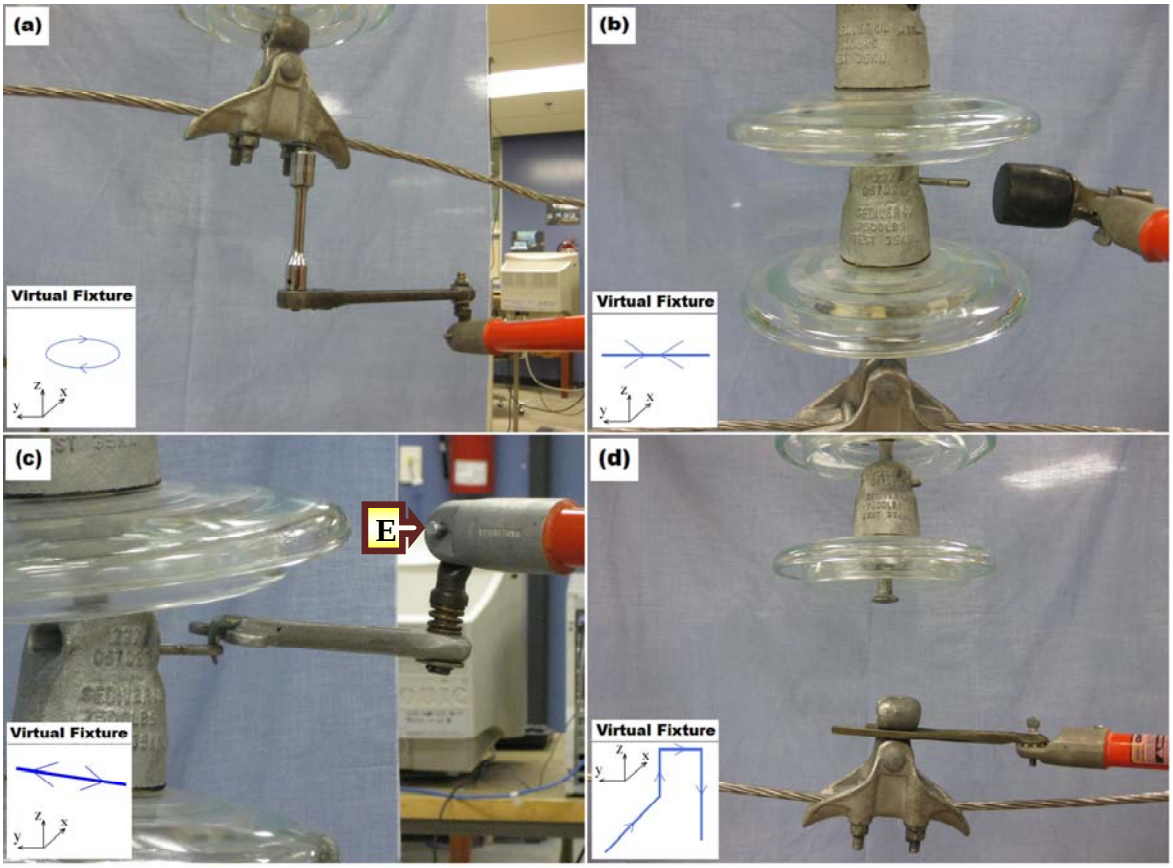

Figure 4.3 Typical live-line maintenance tasks: (a) loosening or tightening a nut; (b) inserting cotter pin; (c) pulling cotter pin out; (d) disconnecting a ball and socket joint. Virtual fixture used for each task is shown as inset.

For a typical task like loosening or tightening a nut, for example, a circle is to be defined as the virtual fixture as shown in (Figure 4.3a). Theoretically, this circle should be defined in horizontal *XY* plane. This is the case when it is assumed that the task environment is stationary and does not have any movements; However, in practice,

because of wear of the maintenance tool and movement of the transmission line that holds the parts when the hot stick applies torque to it, this horizontal circle may be changed. This circle was determined by having the center of circle and a point located at the perimeter to obtain the radius of the circle. All points in the noted tasks are defined by pressing the button on the haptic stylus.

To insert or remove a cotter pin, a straight line should be used as virtual fixture (Figure 4.3b and Figure 4.3c). For inserting the cotter pin, this line is horizontal while for removing the cotter pin, a slightly sloped line is defined to prevent the tool from loosing contact with the cotter pin, which is caused by the movement of the insulator.

For disconnecting or reconnecting a ball-socket joint (Figure 4.3d), a 3D virtual fixture composed of four straight lines must be defined. First, a horizontal straight line is defined for the U-shape tool to approach the ball and socket joint. When the tool holds the socket, a vertical line helps the operator to move it upwards and to make the joint loose. At this point, the operator makes a wobbling movement to disconnect the joint and the horizontal line to the right direction helps the operator to move the socket away from the ball. Finally, a vertical line helps the operator to totally move the socket and the transmission line away from the ball. This line also helps the operator in reconnecting the joint. When the ball and socket joint is disconnected, they have a vertical distance which is caused by the weight of the transmission line and the socket. The mentioned vertical line helps the operator to move the socket close to the ball to be reconnected. For reconnecting the joint, the virtual fixture is the same but this procedure should be performed in the reverse order.

The combination of sub-tasks in a proper sequence can be used in order to do a complete task in the station. For instance, to change a broken insulator which is a common task in line maintenance, the following typical tasks should be performed. Some of these steps are shown in Figure 4.4.

(i) pull out the upper/lower cotter pin (Figure 4.3c and Figure 4.4a),

(ii) disconnect/reconnect the upper/lower ball and socket joint (Figure 4.3d and Figure 4.4b),

(iii) insert the upper/lower cotter pin (Figure 4.3b) and,

(iv) loosen/tighten a nut (Figure 4.3a).

These tasks have been performed experimentally using the test-rig to prove the effectiveness of the system. Six experienced linemen and eight novice operators used the system and performed all tasks successfully.

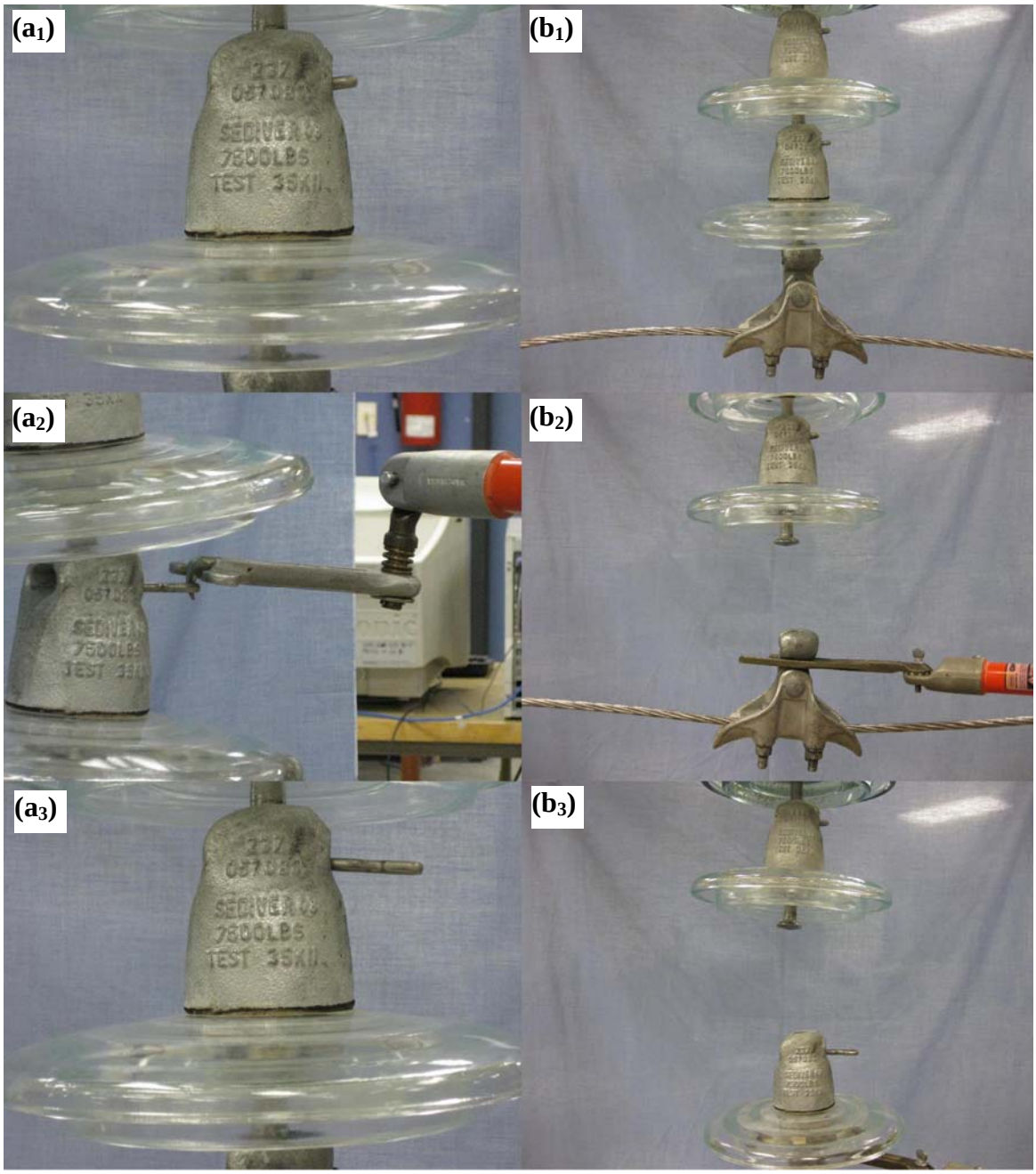

Figure 4.4 Two typical subtasks in changing a broken insulator:

(a) Pulling the pin out; (b) Disconnecting/reconnecting the ball and socket joint.

4.3 Experimental results

The following results of one task (pulling out the cotter pin from the insulator), is presented to show the proof of concept. Plots are shown in Figure 4.5 and Figure 4.6**.**

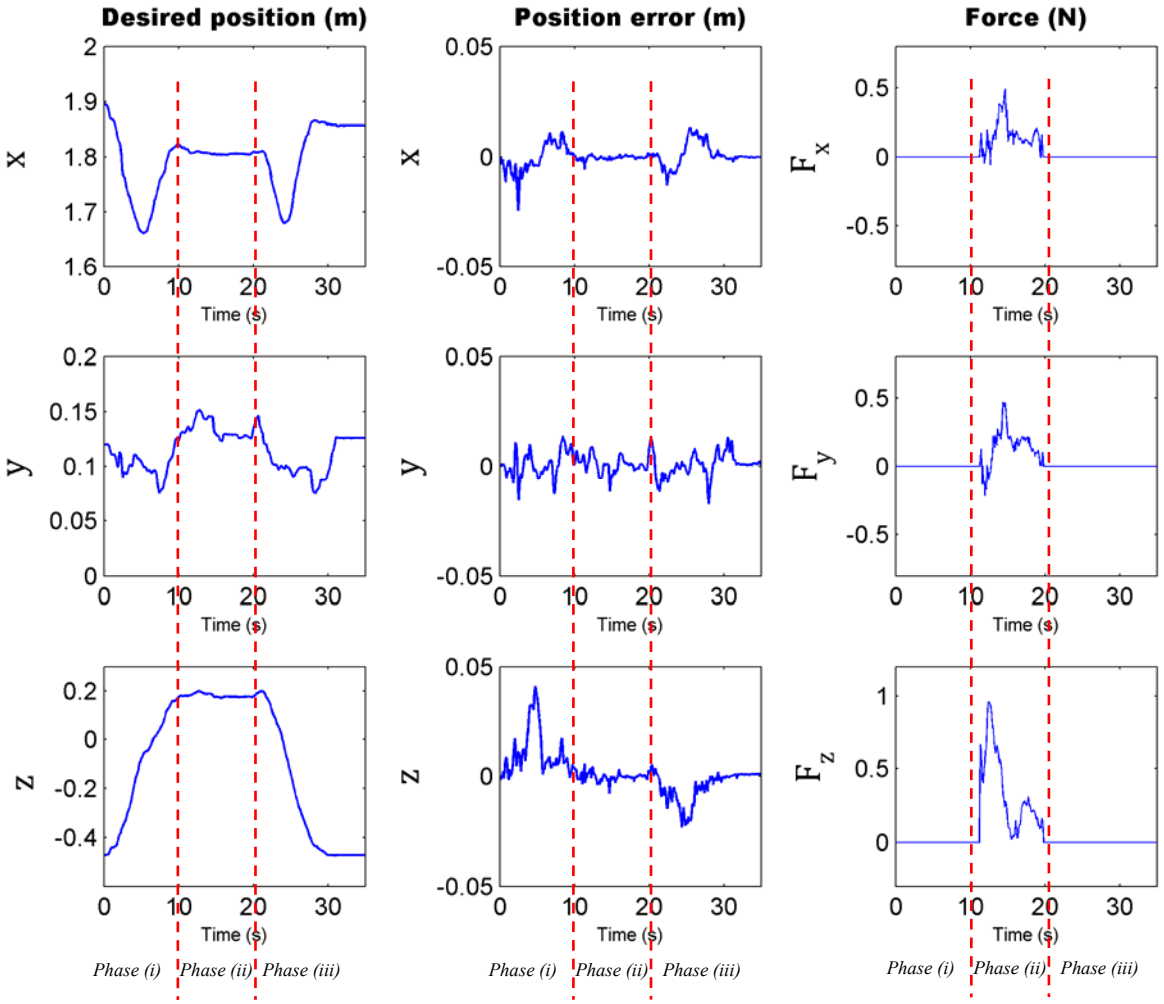

Figure 4.5 Left: desired Cartesian position of end-effector. Middle: error between actual and desired positions. Right: Cartesian forces generated by haptic device.

Figure 4.5(left) shows the desired Cartesian position of the end-effector of the hydraulic manipulator (point **E** in Figure 4.3c). The plots show three phases: (*i*) approaching the

connecting pin from home position, (*ii*) pulling the pin out and (*iii*), returning back to home position. Thus, phase (*ii*) is when the virtual force is generated by the haptic device. The vertical dashed lines on Figure 4.5 separate these phases. Figure 4.5 (middle) shows the error between actual and desired positions of the end-effector of the hydraulic manipulator. Figure 4.5 (right) shows the forces generated by the haptic device when the impedance-type forbidden region virtual fixture is active (phase *ii*). These forces are proportional to the deviation of the end-effector from the desired path (as in Figure 4.2) and are used as feedback to guide the linemen to pull the pin out.

With reference to Figure 4.5, position tracking of the hydraulic manipulator is very good. This is very important in minimizing the position errors caused by the robotic arm's controller. During phase (*ii*), the virtual fixture for pulling the connecting pin out is a straight line almost parallel to the *Y* axis. Thus, both *x* and *z* signals between 10 to 20 seconds, have almost constant values. Actually, this is the effect of the force generated by the haptic device during phase (*ii*) to maintain the straight path (see F_x and F_z in Figure 4.5).

Figure 4.6 shows the desired joint angles of the manipulator (left), joint angle errors (middle), and control signals applied to servo valves (right). All joint angles have good tracking responses. During manipulation, θ_1 has the most variation, because it has direct effect on *y* according to the inverse kinematics. The desired value for θ_5 is zero, but interaction between the hot stick and the environment resulted in torque applied to this joint which in turn caused θ_5 to deviate slightly from its desired value. The controller successfully compensated for this deviation. All control signals are bounded, are not

saturated, and do not have large oscillations.

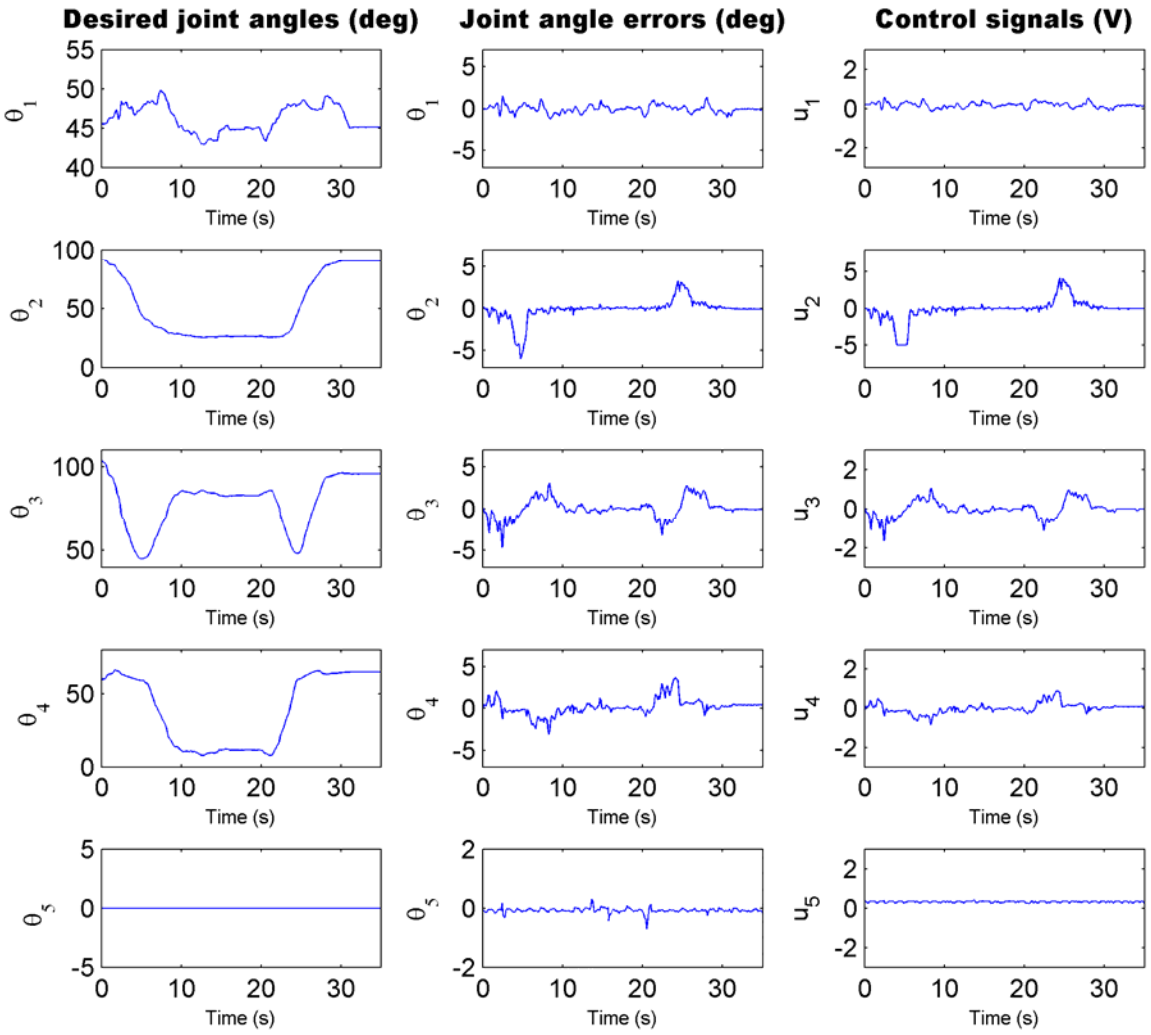

Figure 4.6 Left: desired joint angles. Middle: joint angle errors. Right: control signals applied to servovalves.

4.4 Qualitative study

The system was tested successfully by six experienced linemen from Manitoba Hydro. To better understand the feasibility of the system, a qualitative study is conducted based on the operators' opinions who tried the system experimentally in the laboratory environment.

Results of this study are shown in Figure 4.7. As is shown, all linemen agreed that live line maintenance task can be successfully performed by the system using cameras as indirect visual feedback. In terms of safety there was a broad range of opinions and nothing can be concluded. That is because they believe that their current job as a lineman is already safe and the system does not change their feelings about the safety. The task completion time is the same or more as compared to manual tasks. All linemen stated that the concept of virtual fixtures is easy to understand and it is easy to learn using the system in practice. They found the designed virtual fixtures very helpful in performing the tasks. All linemen also stated that using the system, the physical labor is reduced as compared to the manual tasks. They think the mental load they experienced while using the system was similar to the manual task.

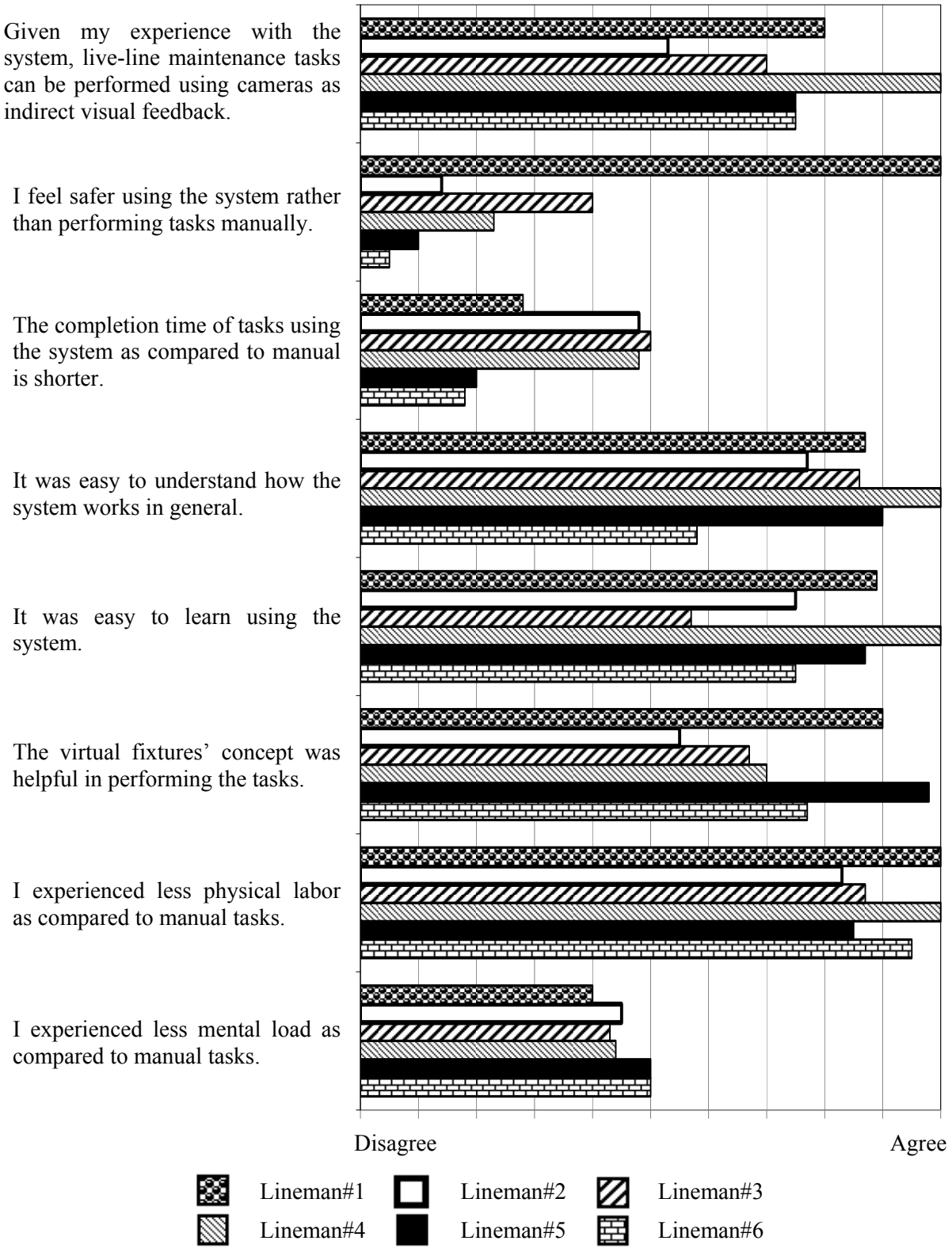

Figure 4.7. Results of qualitative study.

4.5 Summary

Impedance-type Forbidden Region Virtual Fixture (FRVF) was used to control a hydraulic manipulator to perform live-line maintenance tasks. These tasks are currently done manually by operators working in locations high above the ground and near high voltage power lines. The system uses intelligence of the human operator along with the accuracy of the hydraulic manipulator. The control system configures virtual fixtures in the workspace based on the input information regarding the tasks. The effectiveness of the system was shown by performing several live line maintenance tasks encompassing standardized manipulation procedures. As shown, the system was simple to use, and reduced the physical load on linemen, not to mention that it was helpful in harsh climate conditions and did not require to long-term or complicated training.

Chapter 5

5 BILATERAL CONTROL OF HYDRAULIC MANIPULATORS

5.1 Introduction

The objective of this section is to design stable control schemes for bilateral control of hydraulic actuators. Since hydraulic actuators exhibit significant nonlinear characteristics [11], using advanced nonlinear techniques such as Lyapunov stability to design controllers that incorporates nonlinearities and guarantees the stability of the system is preferred [6, 12-14]. Lyapunov stability analysis has been extensively used in controller design for hydraulic actuators. However, none of the previous research studies included haptic force feedback. Specifically, to the best of author's knowledge, no bilateral control scheme has been proposed in the literature based on Lyapunov's stability theory that includes nonlinear characteristics of hydraulic actuation and human operator's dynamics.

In this chapter, three bilateral control schemes are developed, implemented, and experimentally validated. The first one is designed for constrained motion of the hydraulic actuator and the interaction force between the hydraulic actuator and the task environment is used in providing haptic sensation for the human operator. The second controller is then designed for unconstrained (free) motion of the hydraulic actuator. Using this scheme, the position error between displacements of the haptic device and the hydraulic actuator is used at both master and slave sides to maintain good position tracking at the actuator side while providing a feel of performing task at the remote site by coupling the displacement of the haptic device to the displacement of the hydraulic actuator. This controller, therefore, complements the previous controller, in that it allows one to use a haptic device to manipulate a hydraulic actuator in either free motion or constrained control modes. The third controller is designed for combined free and constrained motions of the hydraulic actuator in displacement mode. The control law at the slave side allows the hydraulic actuator to have a stable position tracking in both free and constrained motions. At the master side, the haptic device creates a force that acts like a virtual spring coupling the displacements of the haptic device and the hydraulic actuator. When the actuator moves freely, the virtual spring creates a force indicating to the operator if the slave manipulator is behind/ahead in terms of tracking the master manipulator's displacement. When the actuator is in contact and interacts with an environment, the constraints imposed on its motion are indirectly reflected through this virtual spring force. Instead of making the system transparent, i.e., having direct force feedback on the operator's hand, the haptic device alerts the operator of the reactions as a result of forces acting on the implement. This type of haptic force is most desirable in

applications in which mounting a force sensor on the implement is not practical. In these controllers, at the hydraulic actuator side, both force-mode and displacement-mode controls are investigated. At the haptic side, different force feedbacks are used including interaction force feedback and force feedback based on the position error.

All control laws are obtained during the process of constructing a Lyapunov function to guarantee the stability of the overall closed-loop system. For each control scheme, it is shown that the constructed Lyapunov function guarantees stability of the system considering nonlinear dynamics of hydraulic functions. Due to the discontinuity in the proposed control laws, the control systems are non-smooth. With respect to classical solution theories, a solution cannot even be defined; much less discuss its existence, uniqueness, and stability for such systems. Therefore, Filippov's solution concept is first employed to prove the existence, continuation and uniqueness of the Filippov's solution [86, 87]. Next, the extended Lyapunov's stability theory [88-91] is used for the stability analysis of the resulting bilateral control system. Furthermore, the non-smooth version of LaSalle's theorem [89, 91, 92] is used to prove asymptotic stability where applicable. Simulation and experimental results are provided to validate practicality and performance of the proposed controllers.

5.2 Force-mode control for constrained motion tasks[3]

In this section, a Lyapunov controller for stable haptic manipulation of hydraulic actuators is designed to be used during constrained motion of the hydraulic actuator. Besides stability, the second objective considered in the design of the controller, is transparency. Transparency allows the operator to feel a scaled down version of the force that the actuator is exerting on an object, while mimicking the motion produced by the operator. Two scaling factors are therefore included in the control laws: (*i*) factor to scale the displacement of the haptic to properly map it's workspace to the corresponding workspace of the actuator, and (*ii*) factor to scale the interaction force between the hydraulic actuator and the environment to make it applicable to the human operator's hand by the haptic device.

5.2.1 Description of controller

The model described in Chapter 3 is now employed to design a stable control scheme. The objective is to design a Lyapunov stable feedback controller that is capable of doing the regulating task, i.e. given a constant force by human operator and an arbitrary initial condition, the system should asymptotically approach to an equilibrium point and remain there. The performance of the controller is evaluated by the error between the scaled haptic position, $K_{ps}x_m$, and displacement of the hydraulic actuator, x_s , as well as the error between the force generated by the haptic device, F_m , and the scaled down version of the interaction force between the hydraulic actuator and the environment at the remote

[3] Results of this section have been published in International Journal of Robust and Nonlinear Control [95].

side, $K_{fs}F_l$. This provides a feel of being present at the remote site to the operator [24]. The control laws are constructed during the process of finding the proper Lyapunov function for the system. Here, the control laws are first proposed and then the stability is analyzed using the Lyapunov stability analysis. The following control laws are proposed to determine values for u and F_m:

$$u = -k_p \left(P_L - \frac{k_s}{\alpha A k_h} F_h\right)\sqrt{P_s - sgn(x_{sp})P_L} \tag{5.1}$$

$$F_m = \frac{k_h}{K_{ps}k_s} F_l - \left(\frac{K_{ps}m_m}{\tau} - k_d\right)\dot{x}_m + \left(\frac{m_m}{\tau}\right)\dot{x}_s + \frac{m_m}{K_{ps}}\ddot{x}_s - F_h \tag{5.2}$$

In (5.1), k_p is a positive controller gain, and parameter $\alpha > 0$ is used as a tuning parameter to scale down the interaction force between the hydraulic actuator and the environment for use by the haptic. The manner in which this parameter is determined will be discussed later. Note that the above controller is discontinuous due to term $sgn(x_{sp})$ in (5.1) when $x_{sp} = 0$.

In (5.1), the control signal for the hydraulic actuator, u, is designed to allow the force generated by the hydraulic actuator and the force generated by the operator, follow each other closely. Since the force generated by the operator, F_h, is much less than the hydraulic actuator's force, AP_L, a scaling factor is employed (as will be seen later) for F_h. Similarly, for the force generated by the haptic device in (5.2), the scaled interaction force between the hydraulic actuator and the environment, F_l, is used. The other terms considered in (5.1) and (5.2) are added during the process of constructing a Lyapunov function for the system to make the system stable. For example, the term

$\sqrt{P_s - sgn(x_{sp})P_L}$ is like a multiplier that changes the proportional controller gain, k_p. The other term in (5.2) is "$-\left(\frac{K_{ps}m_m}{\tau} - k_d\right)\dot{x}_m + \left(\frac{m_m}{\tau}\right)\dot{x}_s + \frac{m_m}{K_{ps}}\ddot{x}_s$", which is zero at steady state, and does not change the nature of the controller. This term is added to the control signal to make the derivative of the Lyapunov function always negative for stability purpose.

Using (3.13) and introducing a position scaling parameter, K_{ps} , when the workspace of the haptic (master) device is not the same as the hydraulic actuator's (slave), and replacing the last two states with the error between the scaled master and slave displacements and velocities, the following new states are then defined:

$$\begin{aligned}\vec{x} &= [x_1 \quad x_2 \quad x_3 \quad x_4 \quad x_5 \quad x_6]^T \\ &= \left[x_s \quad \dot{x}_s \quad P_L \quad x_{sp} \quad \left(K_{ps}x_m - x_s\right) \quad \left(K_{ps}\dot{x}_m - \dot{x}_s\right)\right]^T\end{aligned} \tag{5.3}$$

Using the above states, results in the following modified state space model:

$$\begin{cases} \dot{x}_1 = x_2 \\ \dot{x}_2 = \dfrac{A}{m_s}x_3 - \dfrac{d}{m_s}x_2 - \dfrac{k_s}{m_s}x_1 \\ \dot{x}_3 = \dfrac{1}{C}\left(-Ax_2 + \dfrac{c_d}{\sqrt{\rho}}wx_4\sqrt{P_s - sgn(x_4)x_3}\right) \\ \dot{x}_4 = \dfrac{-1}{\tau}x_4 + \dfrac{k_{sp}}{\tau}\,u \\ \dot{x}_5 = x_6 \\ \dot{x}_6 = \dfrac{K_{ps}}{m_m}(F_h + F_m) - \dfrac{k_d}{m_m}x_6 - \dfrac{k_h}{m_m}x_5 - \dfrac{A}{m_s}x_3 + \left(\dfrac{d}{m_s} - \dfrac{k_d}{m_m}\right)x_2 + \left(\dfrac{k_s}{m_s} - \dfrac{k_h}{m_m}\right)x_1 \end{cases} \tag{5.4}$$

Note that in arriving at (5.4), the friction term F_{fr} is neglected. Depending on the type of actuator, this friction can be small or significant [58]. This assumption was necessary to

make the Lyapunov stability analysis manageable. Nevertheless, as will be seen later in the experimental results, the controllers developed here performed well for the real actuator, with friction.

Replacing u and F_m in (5.4) with equations (5.1) and (5.2), results in the following state space equations:

$$\begin{cases} \dot{x}_1 = x_2 \\ \dot{x}_2 = \dfrac{A}{m_s}x_3 - \dfrac{d}{m_s}x_2 - \dfrac{k_s}{m_s}x_1 \\ \dot{x}_3 = \dfrac{1}{C}\left(-Ax_2 + \dfrac{c_d}{\sqrt{\rho}}wx_4\sqrt{P_s - sgn(x_4)x_3}\right) \\ \dot{x}_4 = \dfrac{-1}{\tau}x_4 - k_p\dfrac{k_{sp}}{\tau}(x_3 - \dfrac{k_s}{\alpha A k_h}F_h)\sqrt{P_s - sgn(x_4)x_3} \\ \dot{x}_5 = x_6 \\ \dot{x}_6 = -\dfrac{K_{ps}}{\tau}x_6 - \dfrac{k_h}{m_m}x_5 \end{cases} \tag{5.5}$$

The control system described by (5.5) is non-smooth due to term $sgn(x_4)$ on the right hand side of the equation describing $\dot{x}_4$. These types of systems violate the fundamental assumption of conventional solution theories of ordinary differential equations. With respect to classical solution theories, a solution cannot even be defined; much less discuss its existence, uniqueness and stability. Filippov's solution theory [86, 87] is one of the earliest and most conceptually straightforward approaches developed for analysis of non-smooth systems. Based on the Filippov's solution concept, the conventional Lyapunov stability theory, initially developed for smooth systems, has been extended to non-smooth systems [89-91] and will be used in the next section to study the stability.

5.2.2 Stability analysis

The first step in the stability analysis is the Filippov's solution analysis that establishes a new definition of solutions for differential equations with discontinuous terms. The Filippov's solution provides the required theorems to prove the existence, uniqueness, and continuity of non-smooth systems [86, 87]. The second step is to construct a smooth Lyapunov function for the non-smooth dynamic system of (5.5) and to prove the global asymptotic stability of the system.

5.2.2.1 Existence, uniqueness, and continuation of Filippov's solution

The dynamic system presented by (5.5) consists of nonlinear differential equations with discontinuous right-hand sides. The discontinuity arises from the term $sgn(x_4)$ originated by the control law (5.1). Here, Filippov's solution concept is used for the non-smooth system described by (5.5). The discontinuity surface of the system described in (5.5) is:

$$S := \{\vec{x}: x_4 = 0\} \tag{5.6}$$

The discontinuity surface, *S*, divides the solution region, Ω, into two regions:

$$\Omega_s^+ := \{\vec{x}: x_4 > 0\} \tag{5.7}$$

$$\Omega_s^- := \{\vec{x}: x_4 < 0\} \tag{5.8}$$

The right-hand sides of the equations in (5.5) are piecewise continuous and defined everywhere in Ω. They are also measurable and bounded. Therefore, Equation (5.5) satisfies condition ***B*** of Filippov's solution theory and according to theorems 4 and 5 of Filippov [86], we have the local existence and continuity of a solution. Next, the uniqueness of the solution is proven. Since the right-hand sides of (5.5) are all continuous before and after the discontinuity surface, and the discontinuity surface, *S,* is smooth and independent of time, conditions ***A***, ***B*** and ***C*** of Filippov's solution theory are satisfied [86, 87]. Following the procedure described in [86], the limiting values of the vector function of the right-hand sides of (5.5), when *S* is approached from Ω_s^+ and Ω_s^-, are denoted by f^+ and f^-:

$$f^+ = \begin{cases} x_2 \\ \dfrac{A}{m_s}x_3 - \dfrac{d}{m_s}x_2 - \dfrac{k_s}{m_s}x_1 \\ \dfrac{1}{C}\left(-Ax_2 + \dfrac{c_d}{\sqrt{\rho}}wx_4\sqrt{P_s - x_3}\right) \\ \dfrac{-1}{\tau}x_4 - k_p\,\dfrac{k_{sp}}{\tau}(x_3 - \dfrac{k_s}{\alpha A k_h}F_h)\sqrt{P_s - x_3} \\ x_6 \\ -\dfrac{K_{ps}}{\tau}x_6 - \dfrac{k_h}{m_m}x_5 \end{cases} \tag{5.9}$$

$$f^- = \begin{cases} x_2 \\ \dfrac{A}{m_s}x_3 - \dfrac{d}{m_s}x_2 - \dfrac{k_s}{m_s}x_1 \\ \dfrac{1}{C}\left(-Ax_2 + \dfrac{c_d}{\sqrt{\rho}}wx_4\sqrt{P_s + x_3}\right) \\ \dfrac{-1}{\tau}x_4 - k_p\,\dfrac{k_{sp}}{\tau}(x_3 - \dfrac{k_s}{\alpha A k_h}F_h)\sqrt{P_s + x_3} \\ x_6 \\ -\dfrac{K_{ps}}{\tau}x_6 - \dfrac{k_h}{m_m}x_5 \end{cases} \tag{5.10}$$

The projections of f^+ and f^- along the normal to the discontinuity surface, i.e., $N_s = \{0,0,0,1,0,0\}$ are denoted by f_N^+ and f_N^-:

$$f_N^+ = -k_p\,\frac{k_{sp}}{\tau}(x_3 - \frac{k_s}{\alpha A k_h}F_h)\sqrt{P_s - x_3} \tag{5.11}$$

$$f_N^- = -\,k_p\,\frac{k_{sp}}{\tau}(x_3 - \frac{k_s}{\alpha A k_h}F_h)\sqrt{P_s + x_3} \tag{5.12}$$

From (5.11) and (5.12), f_N^+ and f_N^- have the same sign (note that $\sqrt{P_s \pm x_3}$ is always nonnegative). This satisfies conditions of *Lemma 9* of Filippov's solution [86]. Thus, in the domain $\Omega_s^- + S + \Omega_s^+$ we have uniqueness and continuous dependence of the solution on the initial conditions.

5.2.2.2 Stability proof

For the stability analysis, extension of Lyapunov's second method to non-smooth dynamic systems [89], based on Filippov's solution theory, is used. A smooth Lyapunov function is constructed for the non-smooth dynamic system. The stability of the system is

analyzed for a regulating task in which input F_h is constant. By imposing $\dot{x}_{i\,(i=1..6)} = 0$, the system described by (5.5) is shown to have the following equilibrium point:

$$\begin{aligned}\vec{x}_{eq} &= [x_{1eq} \quad x_{2eq} \quad x_{3eq} \quad x_{4eq} \quad x_{5eq} \quad x_{6eq}]^T \\ &= \left[\frac{F_h}{\alpha k_h} \quad 0 \quad \frac{k_s F_h}{\alpha A k_h} \quad 0 \quad 0 \quad 0\right]^T\end{aligned} \tag{5.13}$$

Defining $\vec{e} = \vec{x} - \vec{x}_{eq}$ the following states are defined:

$$\begin{aligned}\vec{e} &= [e_1 \quad e_2 \quad e_3 \quad e_4 \quad e_5 \quad e_6]^T \\ &= \left[\left(x_1 - \frac{F_h}{\alpha k_h}\right) \quad x_2 \quad \left(x_3 - \frac{k_s F_h}{\alpha A k_h}\right) \quad x_4 \quad x_5 \quad x_6\right]^T\end{aligned} \tag{5.14}$$

and substituting (5.14) into (5.5), the new state-space model having its equilibrium point at the origin, is obtained:

$$\begin{cases} \dot{e}_1 = e_2 \\ \dot{e}_2 = \dfrac{A}{m_s} e_3 - \dfrac{d}{m_s} e_2 - \dfrac{k_s}{m_s} e_1 \\ \dot{e}_3 = \dfrac{1}{C}\left(-Ae_2 + \dfrac{c_d}{\sqrt{\rho}} w e_4 \sqrt{P_s - sgn(e_4)\left(e_3 + \dfrac{k_s}{\alpha A k_h} F_h\right)}\right) \\ \dot{e}_4 = \dfrac{-1}{\tau} e_4 - (k_p)\dfrac{k_{sp}}{\tau} e_3 \sqrt{P_s - sgn(e_4)\left(e_3 + \dfrac{k_s}{\alpha A k_h} F_h\right)} \\ \dot{e}_5 = e_6 \\ \dot{e}_6 = -\dfrac{K_{ps}}{\tau} e_6 - \dfrac{k_h}{m_m} e_5 \end{cases} \tag{5.15}$$

To construct a smooth Lyapunov function for the non-smooth system of (5.15), the procedure described by Wu et al. [89] is used. From (5.15), the discontinuity surface is:

$$S := \{\vec{e}: e_4 = 0\} \tag{5.16}$$

The right-hand sides of (5.15) are discontinuous, but measurable and bounded. The following Lyapunov function is constructed for the system described by (5.15):

$$\begin{aligned} &V(e_1, e_2, e_3, e_4, e_5, e_6) \\ &= k_p \frac{k_s}{2} e_1^2 + k_p \frac{m_s}{2} e_2^2 + k_p \frac{C}{2} e_3^2 + \frac{\tau c_d w}{2k_{sp}\sqrt{\rho}} e_4^2 \\ &+ \left(\frac{k_h}{2m_m} + \frac{K_{ps}^2}{8\tau^2}\right) e_5^2 + \frac{1}{2}\left(\frac{K_{ps}}{2\tau} e_5 + e_6\right)^2 \end{aligned} \tag{5.17}$$

which is continuous, positive and definite. The derivative of V with respect to time is:

$$\dot{V} = \begin{bmatrix} \frac{\partial_V}{\partial_{e_1}} & \frac{\partial_V}{\partial_{e_2}} & \frac{\partial_V}{\partial_{e_3}} & \frac{\partial_V}{\partial_{e_4}} & \frac{\partial_V}{\partial_{e_5}} & \frac{\partial_V}{\partial_{e_6}} \end{bmatrix} \begin{bmatrix} \frac{de_1}{dt} \\ \frac{de_2}{dt} \\ \frac{de_3}{dt} \\ \frac{de_4}{dt} \\ \frac{de_5}{dt} \\ \frac{de_6}{dt} \end{bmatrix} = \nabla V^T \begin{bmatrix} \dot{e}_1 \\ \dot{e}_2 \\ \dot{e}_3 \\ \dot{e}_4 \\ \dot{e}_5 \\ \dot{e}_6 \end{bmatrix} \tag{5.18}$$

where, ∇V is gradient or partial derivative of function V with respect to states $e_{i(i=1..6)}$, and ∇V^T is the transpose of ∇V. Replacing $\dot{e}_{i(i=1..6)}$ in (5.18), with the right-hand sides of (5.15), and taking partial derivatives of (5.17), results in:

$$\nabla V = \begin{bmatrix} k_p k_s e_1 \\ k_p m_s e_2 \\ k_p C e_3 \\ \dfrac{\tau c_d w}{k_{sp}\sqrt{\rho}} e_4 \\ \left(\dfrac{k_h}{m_m} + \dfrac{K_{ps}^2}{4\tau^2}\right) e_5 + \dfrac{K_{ps}}{2\tau}\left(\dfrac{K_{ps}}{2\tau} e_5 + e_6\right) \\ \left(\dfrac{K_{ps}}{2\tau} e_5 + e_6\right) \end{bmatrix} \tag{5.19}$$

and,

$$\dot{V} =$$

$$\begin{bmatrix} k_p k_s e_1 \\ k_p m_s e_2 \\ k_p C e_3 \\ \dfrac{\tau c_d w}{k_{sp}\sqrt{\rho}} e_4 \\ \left(\dfrac{k_h}{m_m} + \dfrac{K_{ps}^2}{4\tau^2}\right) e_5 + \dfrac{K_{ps}}{2\tau}\left(\dfrac{K_{ps}}{2\tau} e_5 + e_6\right) \\ \left(\dfrac{K_{ps}}{2\tau} e_5 + e_6\right) \end{bmatrix}^T \begin{bmatrix} e_2 \\ \dfrac{A}{m_s} e_3 - \dfrac{d}{m_s} e_2 - \dfrac{k_s}{m_s} e_1 \\ \dfrac{1}{C}\left(-A e_2 + \dfrac{c_d}{\sqrt{\rho}} w e_4 \sqrt{P_s - sgn(e_4)\left(e_3 + \dfrac{k_s}{\alpha A k_h} F_h\right)}\right) \\ \dfrac{-1}{\tau} e_4 - (k_p)\dfrac{k_{sp}}{\tau} e_3 \sqrt{P_s - sgn(e_4)\left(e_3 + \dfrac{k_s}{\alpha A k_h} F_h\right)} \\ e_6 \\ -\dfrac{K_{ps}}{\tau} e_6 - \dfrac{k_h}{m_m} e_5 \end{bmatrix}$$

(5.20)

∇V is continuous with respect to states $e_{i(i=1..6)}$. The Lyapunov function V must first be proven smooth. Utilizing the notation described in Section 4.1 of reference [89], $\dot{V}$ can be rewritten in the following form:

$$\dot{V} = W^{(1)}(t,\vec{e}).h^{(1)}(t,\vec{e}) + W^{(2)}(t,\vec{e}).h^{(2)}(t,\vec{e}) \tag{5.21}$$

From (5.18) to (5.21), functions $W^{(1)}(t,\vec{e})$, $W^{(2)}(t,\vec{e})$, $h^{(1)}(t,\vec{e})$ and $h^{(2)}(t,\vec{e})$ are written as follows:

$$W^{(1)}(t,\vec{e}) = \begin{bmatrix} k_p k_s e_1 \\ k_p m_s e_2 \\ k_p C e_3 \\ \dfrac{\tau c_d w}{k_{sp}\sqrt{\rho}} e_4 \\ \left(\dfrac{k_h}{m_m} + \dfrac{K_{ps}^2}{4\tau^2}\right) e_5 + \dfrac{K_{ps}}{2\tau}\left(\dfrac{K_{ps}}{2\tau} e_5 + e_6\right) \\ \left(\dfrac{K_{ps}}{2\tau} e_5 + e_6\right) \end{bmatrix} \tag{5.22}$$

$$W^{(2)}(t,\vec{e}) = \begin{bmatrix} 0 \\ 0 \\ k_p C e_3 \\ \dfrac{\tau c_d w}{k_{sp}\sqrt{\rho}} e_4 \\ 0 \\ 0 \end{bmatrix} \tag{5.23}$$

$$h^{(1)}(t,\vec{e}) = \begin{bmatrix} e_2 \\ \dfrac{A}{m_s} e_3 - \dfrac{d}{m_s} e_2 - \dfrac{k_s}{m_s} e_1 \\ \dfrac{1}{C}(-A e_2) \\ \dfrac{-1}{\tau} e_4 \\ e_6 \\ -\dfrac{K_{ps}}{\tau} e_6 - \dfrac{k_h}{m_m} e_5 \end{bmatrix} \tag{5.24}$$

$$h^{(2)}(t,\vec{e}) = \begin{bmatrix} 0 \\ 0 \\ \frac{1}{C}\left(\frac{c_d}{\sqrt{\rho}} w e_4 \sqrt{P_s - sgn(e_4)\left(e_3 + \frac{k_s}{\alpha A k_h} F_h\right)}\right) \\ -(k_p)\frac{k_{sp}}{\tau} e_3 \sqrt{P_s - sgn(e_4)\left(e_3 + \frac{k_s}{\alpha A k_h} F_h\right)} \\ 0 \\ 0 \end{bmatrix} \tag{5.25}$$

Note that $W^{(1)}(t,\vec{e}), W^{(2)}(t,\vec{e})$ and $h^{(1)}(t,\vec{e})$ are continuous and are related to the gradient of the Lyapunov function V and the continuous part of the rate of the state vector.

$h^{(2)}(t,\vec{e})$ is discontinuous and is related to the discontinuous part of the equations describing the rate of the state vector. Analogous to the established requirements for the construction of smooth Lyapunov function [89], $W^{(2)}(t,\vec{e}).h^{(2)}(t,\vec{e})$ must be continuous and tend to zero as the solution trajectory approaches the discontinuity surface *S* defined by (5.16). Additionally, the set $K\{W^{(2)}(t,\vec{e}).h^{(2)}(t,\vec{e})\}$ must consist of a single value of zero on the discontinuity surface *S.* Since:

$$\begin{aligned} W^{(2)}(t,\vec{e}).h^{(2)}(t,\vec{e}) &= k_p C e_3 \frac{1}{C}\left(\frac{c_d}{\sqrt{\rho}} w e_4 \sqrt{P_s - sgn(e_4)\left(e_3 + \frac{k_s}{\alpha A k_h} F_h\right)}\right) \\ &\quad - \frac{\tau c_d w}{k_{sp}\sqrt{\rho}} e_4\, k_p \frac{k_{sp}}{\tau} e_3 \sqrt{P_s - sgn(e_4)\left(e_3 + \frac{k_s}{\alpha A k_h} F_h\right)} \\ &= 0 \end{aligned} \tag{5.26}$$

Thus, the alternative conditions of the construction of smooth Lyapunov function for a non-smooth system, outlined in [89], are satisfied, and the above Lyapunov function is smooth.

Next, $\dot{V}$ will be proven negative and at least semi-definite. Rewriting (5.20) in the following form:

$$\begin{aligned}\dot{V} = {} & k_p k_s e_1 e_2 + k_p m_s e_2 \left(\frac{A}{m_s} e_3 - \frac{d}{m_s} e_2 - \frac{k_s}{m_s} e_1\right) \\ & + k_p C e_3 \frac{1}{C}\left(-A e_2 + \frac{c_d}{\sqrt{\rho}} w e_4 \sqrt{P_s - sgn(e_4)\left(e_3 + \frac{k_s}{\alpha A k_h} F_h\right)}\right) \\ & + \frac{\tau c_d w}{k_{sp}\sqrt{\rho}} e_4 \left(\frac{-1}{\tau} e_4 - k_p \frac{k_{sp}}{\tau} e_3 \sqrt{P_s - sgn(e_4)\left(e_3 + \frac{k_s}{\alpha A k_h} F_h\right)}\right) \\ & + \left(\frac{k_h}{m_m} + \frac{K_{ps}^2}{4\tau^2}\right) e_5 e_6 + \left(\frac{K_{ps}}{2\tau} e_6 - \frac{K_{ps}}{\tau} e_6 - \frac{k_h}{m_m} e_5\right)\left(\frac{K_{ps}}{2\tau} e_5 + e_6\right) \\ = {} & -k_p d e_2^2 - \frac{c_d w}{k_{sp}\sqrt{\rho}} e_4^2 - \frac{k_h K_{ps}}{2\tau m_m} e_5^2 - \frac{K_{ps}}{2\tau} e_6^2 \end{aligned} \tag{5.27}$$

$\dot{V}$ is continuous and also negative semi-definite (note that all parameters are positive numbers). Thus, V is a smooth Lyapunov function for the non-smooth system described by (5.15). Therefore, the control system is stable in the sense of Lyapunov, according to the theorem outlined in [89]. Further, the asymptotic stability of the system is proven. Here, non-smooth version of *invariant set theorems*, attributed to LaSalle [89, 91, 92] which is a common method to prove asymptotic stability when $\dot{V}$ is negative semi-definite, is used.

Let $\boldsymbol{R}$ be the set of all points within the solution region $\boldsymbol{\Omega}$ where $\dot{V} = 0,$ i.e.

$$\boldsymbol{R} = \left(\{e_1, e_2, e_3, e_4, e_5, e_6\}, \dot{V} = 0\right) \tag{5.28}$$

The largest invariant set $\boldsymbol{M}$, in set $\boldsymbol{R}$, is proven to contain only the equilibrium point, $\vec{e}_{eq} = (0,0,0,0,0,0)^T$. This is proven by contradiction. According to (5.27), $\dot{V} = 0$ requires that for all points in $\boldsymbol{R}$,

$$e_2 = e_4 = e_5 = e_6 = 0 \tag{5.29}$$

Let $\boldsymbol{M}$ be the largest invariant set in $\boldsymbol{R}$ and contain a point where error state e_3 is not zero, i.e. $(e_1, 0, e_3, 0,0,0)$. Note that e_1 can have any value, zero or nonzero. Then, at this point using the following equation from (5.15),

$$\dot{e}_4 = \frac{-1}{\tau} e_4 - (k_p)\frac{k_{sp}}{\tau} e_3 \sqrt{P_s - sgn(e_4)\left(e_3 + \frac{k_s}{\alpha A k_h} F_h\right)} \tag{5.30}$$

applying $e_4 = 0$ from (5.29), and assuming a nonzero e_3, implies that $\dot{e}_4 \neq 0$. This necessitates the solution trajectory to immediately move out of the set $\boldsymbol{R}$ and certainly out of the set $\boldsymbol{M}$, which contradicts the initial assumption that $\boldsymbol{M}$ is the largest invariant set in $\boldsymbol{R}$. Therefore, regardless the values of e_1, all points in set $\boldsymbol{M}$ should also satisfy:

$$e_3 = 0 \tag{5.31}$$

Using the same approach, now assume that $\boldsymbol{M}$ contains a point where error state e_1 is not zero, i.e., $(e_1, 0,0,0,0,0)$. At this point, from (5.15) we have:

$$\dot{e}_2 = \frac{A}{m_s} e_3 - \frac{d}{m_s} e_2 - \frac{k_s}{m_s} e_1 \tag{5.32}$$

applying $e_2 = 0$ from (5.29), $e_3 = 0$ from (5.31), and assuming a nonzero e_1, implies that $\dot{e}_2 \neq 0$. This necessitates the solution trajectory to immediately move out of the set $\boldsymbol{R}$ and certainly out of the set $\boldsymbol{M}$, which contradicts the initial assumption that $\boldsymbol{M}$ is the largest invariant set in $\boldsymbol{R}$. Therefore, all points in set $\boldsymbol{R}$ should also satisfy the following condition:

$$e_1 = 0 \tag{5.33}$$

Thus, using (5.29), (5.31), and (5.33) the largest invariant set $\boldsymbol{M}$ in $\boldsymbol{R}$ can only contain the equilibrium point $e_{eq} = (0,0,0,0,0,0)^T$ and every solution trajectory in $\boldsymbol{\Omega}$ will converge to this point. Therefore, the system described by (5.15) is asymptotically stable. Moreover,

$$V(x) \to \infty \; as \; \|x\| \to \infty \tag{5.34}$$

This implies that the equilibrium at the origin is globally asymptotically stable.

Remark

Rewriting equations (5.2) and (5.13) for the steady-state case (equilibrium point), and using (3.8):

$$F_m = \frac{k_h}{K_{ps} k_s} F_l - F_h \tag{5.35}$$

$$x_s = \frac{F_h}{\alpha k_h} = \frac{F_l}{k_s} \tag{5.36}$$

then replacing F_h in (5.35) by $\frac{\alpha k_h F_l}{k_s}$ from (5.36), the following relationship holds:

$$\alpha = \frac{1}{K_{ps}} - \frac{F_m}{F_l} \cdot \frac{k_s}{k_h} \tag{5.37}$$

Using the following Equation (5.38), one can tune α according to a force scaling coefficient, K_{fs} , that scales down the force range exerted by the actuator to match the force range applied by the haptic (Note: F_m is negative in value given the direction chosen in formulation):

$$\alpha = \frac{1}{K_{ps}} + K_{fs} \frac{k_s}{k_h} \tag{5.38}$$

where

$$K_{fs} = \left| \frac{F_m^{max}}{F_l^{max}} \right| \tag{5.39}$$

F_m^{max} is the maximum force that can be generated by the haptic device, and F_l^{max} is the maximum expected interaction force between the hydraulic actuator and the environment. From (5.38), if sufficient information about the task environment and the human operator is known, i.e., k_s and k_h are known, parameter α can be tuned using proper K_{fs} according to the maximum force of the haptic device. But, if there is not enough information about the environment stiffness k_s and the operator's arm stiffness, k_h, then α should be determined for the worst case scenario, i.e. maximum k_s and minimum k_h. Selecting a large value for α , however, results in increasing the force to be generated by the haptic

device, F_m, in response to force applied by the actuator, F_l. If the force exceeds the device limit it cannot be properly generated.

5.2.3 Performance evaluation

The Performance of the proposed controller is validated by simulation and experimental studies.

5.2.3.1 Simulation results

Simulation studies were conducted first to: (*i*) demonstrate the asymptotic stability of the system and to further study the influence caused by changing the physical parameters in the model, controller parameters, or initial conditions that can be difficult to be implemented experimentally, and (*ii*) confirm that the observations made from the experiments truly reflect the nature of the control laws and not some intrinsic properties (damping due to leakage, fluctuation of pump pressure, measurement noise) inherent to any real-world industrial system.

Equations (5.4), (5.1), and (5.2) were used for numerical simulations, and 4th order Runge-Kutta method was used in C++ as the integration routine. The system parameters used for simulations are provided in Table 3.1. The controller gains were chosen as $k_p = 9.2 \times 10^{-11}\ \mathrm{V/Pa^{3/2}}$, $K_{ps} = 1.0$ representing similar master and slave displacements and $\alpha = 2$, determined from (5.38) given $K_{fs} = \left|\frac{F_m^{max}}{F_l^{max}}\right| = \frac{1}{12500}$.

In the first test, the input F_h was set to a constant value of 0.4N, and the following initial conditions were chosen:

$$\vec{x}_{init} = [x_{1init} \quad x_{2init} \quad x_{3init} \quad x_{4init} \quad x_{5init} \quad x_{6init}]^T$$
$$= [5.0\ \text{mm} \quad 0\ \text{m/s} \quad 98.7 \times 10^4\ \text{Pa} \quad 0\ \text{mm} \quad -5.0\ \text{mm} \quad 0\ \text{m/s}]^T \tag{5.40}$$

The goal of this test was to show that the system can reach an equilibrium point given an arbitrary initial condition. From (5.13), the equilibrium point of the system was determined to be:

$$\vec{x}_{eq} = [x_{1eq} \quad x_{2eq} \quad x_{3eq} \quad x_{4eq} \quad x_{5eq} \quad x_{6eq}]^T$$
$$= [20.0\ \text{mm} \quad 0\ \text{m/s} \quad 39.5 \times 10^5\ \text{Pa} \quad 0\ \text{mm} \quad 0\ \text{mm} \quad 0\ \text{m/s}]^T \tag{5.41}$$

Simulation results are shown in Figure 5.1. With respect to Figure 5.1, all states reach the equilibrium point (5.41). This test confirms the theoretical stability analysis performed earlier, and was then repeated with different initial conditions (results are not shown here).

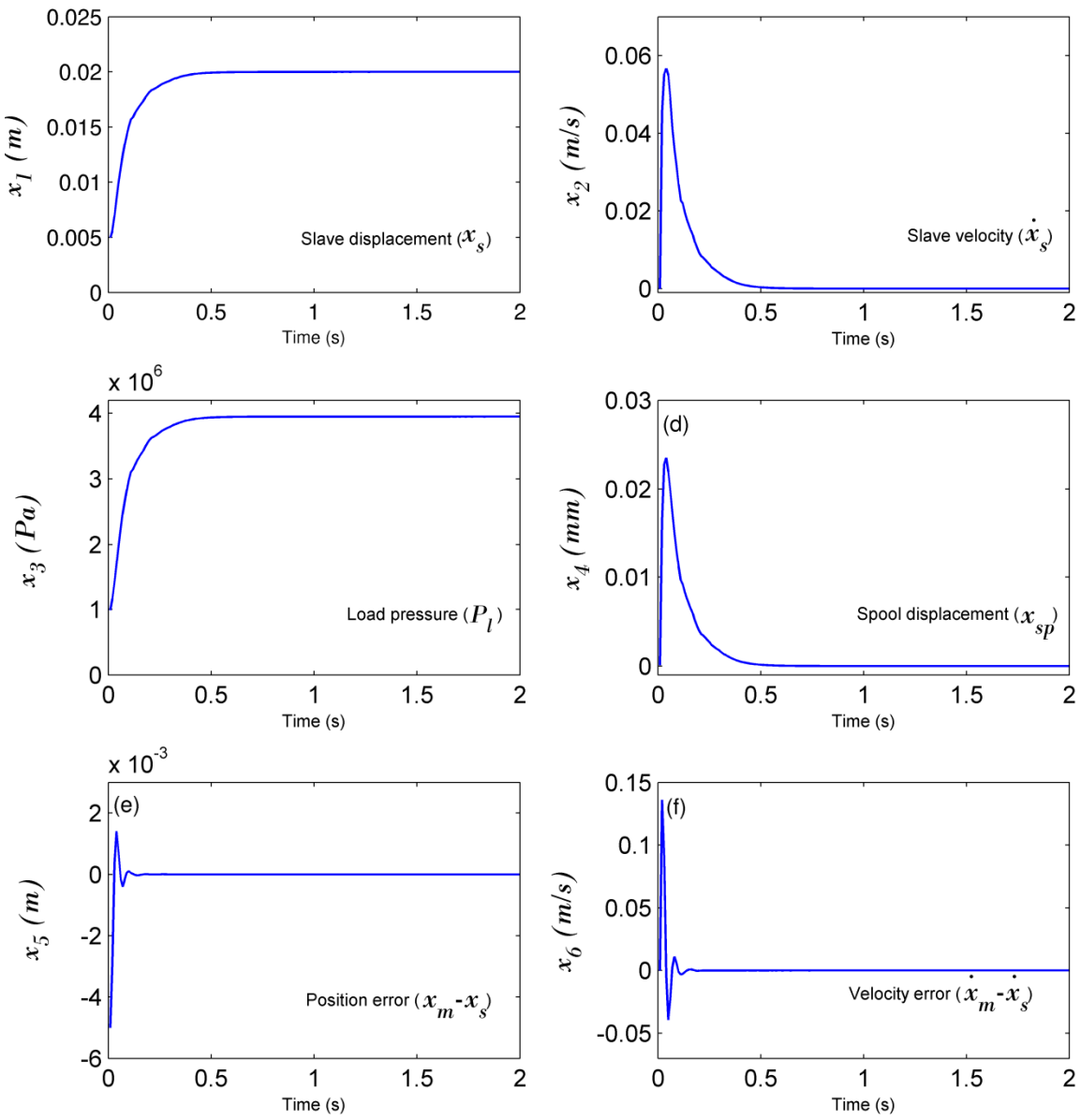

Figure 5.1 Simulation results for a constant operator input and nonzero initial point. Plots of all states are shown.

The next set of simulation studies was designed to observe tracking ability of the control laws resembling the actual experiments to be performed later. In the first test, the operator's force input was gradually increased to the final value of $F_h = 0.4$N. Displacements of the haptic device (x_m) and hydraulic actuator (x_s), the displacement error (x_m-x_s), force generated by the haptic device (F_m) and the scaled force generated by the actuator, $K_{fs}F_l$, the force error ($F_m - K_{fs}F_l$,), and the control signal (u) applied to the actuator are given in Figure 5.2.

In the second test, the operator's input was set to be sinusoidal wave with the frequency of 0.13Hz. The same controller gains as in the previous test were used. Results are shown in Figure 5.3. As is seen, displacements of the haptic and the hydraulic actuator are almost the same (error is within ±0.05mm). In terms of force tracking, the results indicate that the operator is able to feel the scaled version of the force exerted to the environment (error is within ±0.025N). The control signal, as shown in Figure 5.3, is smooth.

To better investigate the effect of uncertainties in the system parameters, the next simulations are conducted. Figure 5.4 shows the force error plots given a step input as in Figure 5.2. With reference to Figure 5.4, it is shown that the controllers are insensitive to the changes in the viscous coefficient of the master, valve time constant, inertia of the master, and the stiffness of the operator's arm. However, they are very sensitive to the values of the environmental stiffness and the piston area. It is not difficult to obtain the accurate value of piston area, *A*. It can be obtained either from manufacturer's data or by direct measurement. The stiffness of the environment can be obtained in implementation by continuously dividing the interaction force, F_l measured by the force sensor at the

slave side, by its displacement measured from the onset of contact. This procedure was adopted during the experiments presented later.

Figure 5.5 shows the extent the controllers developed in this paper respond to inputs of varying frequencies and amplitudes. It should be noted that the system input, F_h, is the force applied by the operator's hand and the frequency of 1.0Hz is adequate for most teleoperation applications when we consider decision making capability of the human brain [93]. With respect to the amplitude of input, 0.8N corresponds to 10000N at the actuator side given the chosen force scale coefficient K_{fs}. This is the maximum force, which can be supplied by the hydraulic actuator having a supply pressure of 17.2MPa. Increasing the controller gain, k_p, can improve the responsiveness at higher frequencies or amplitudes but may promote undesirable oscillations (see Figure 5.5).

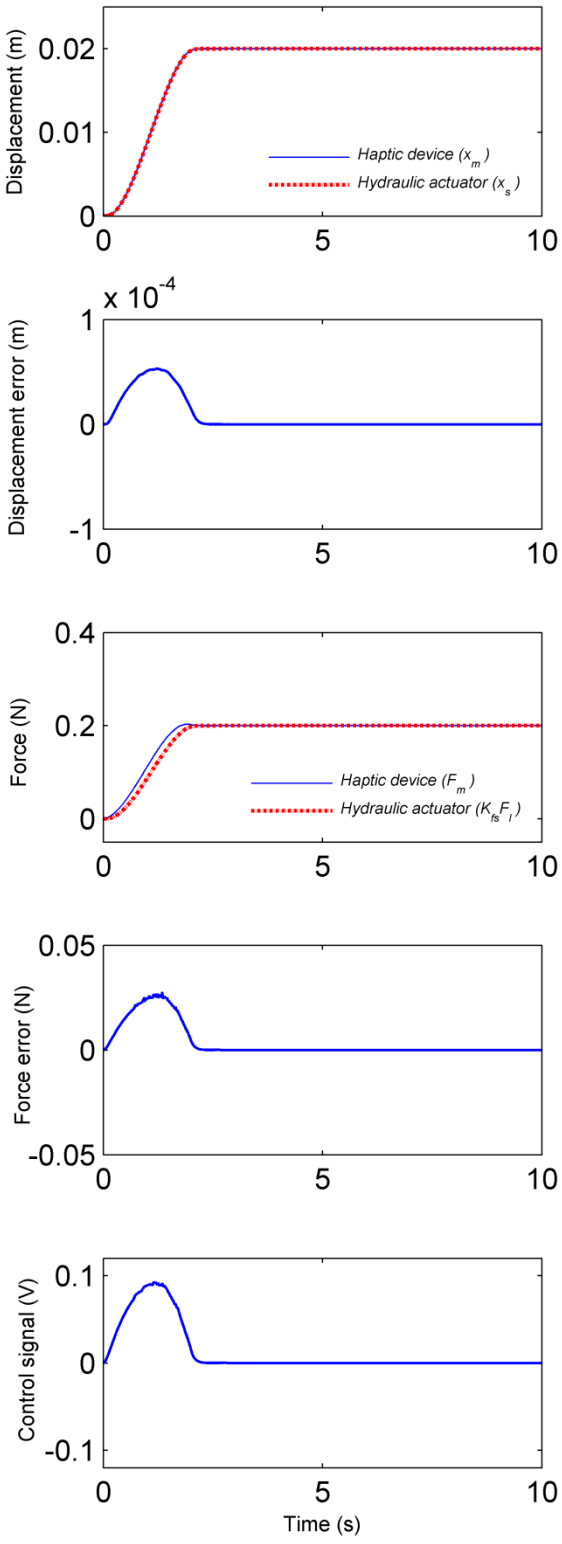

Figure 5.2 Simulation results for positioning task.

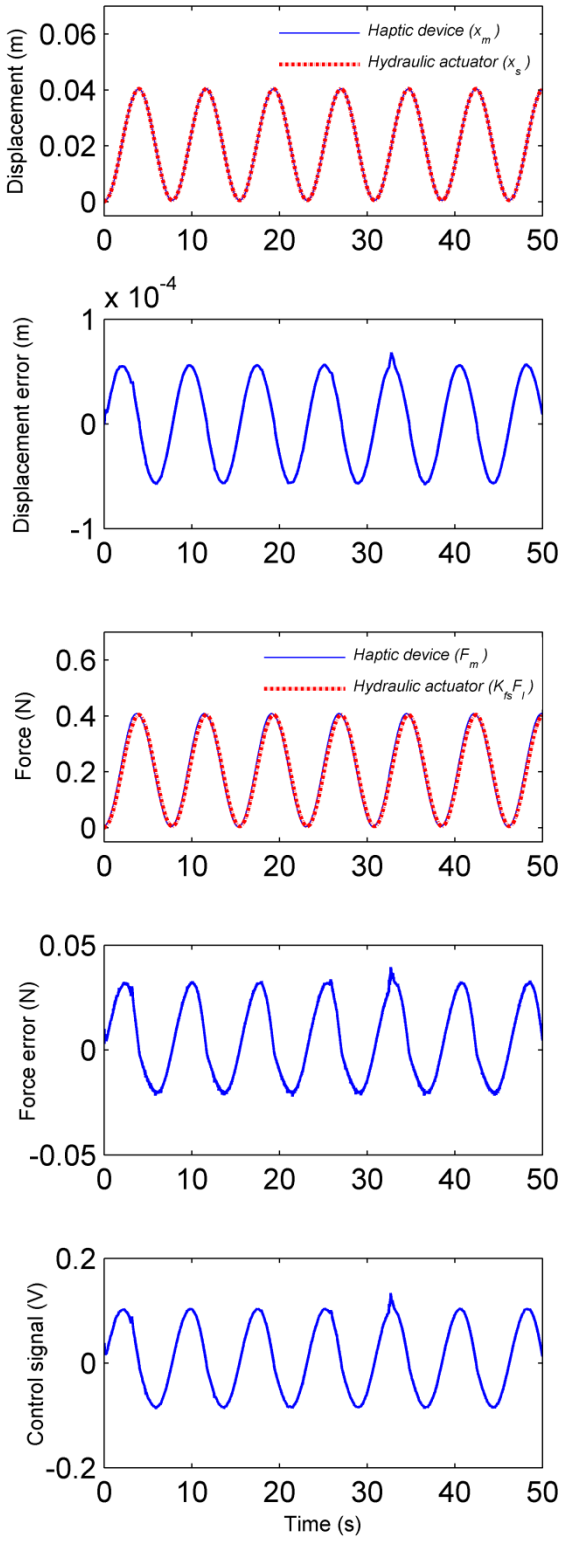

Figure 5.3 Simulation results for tracking task.

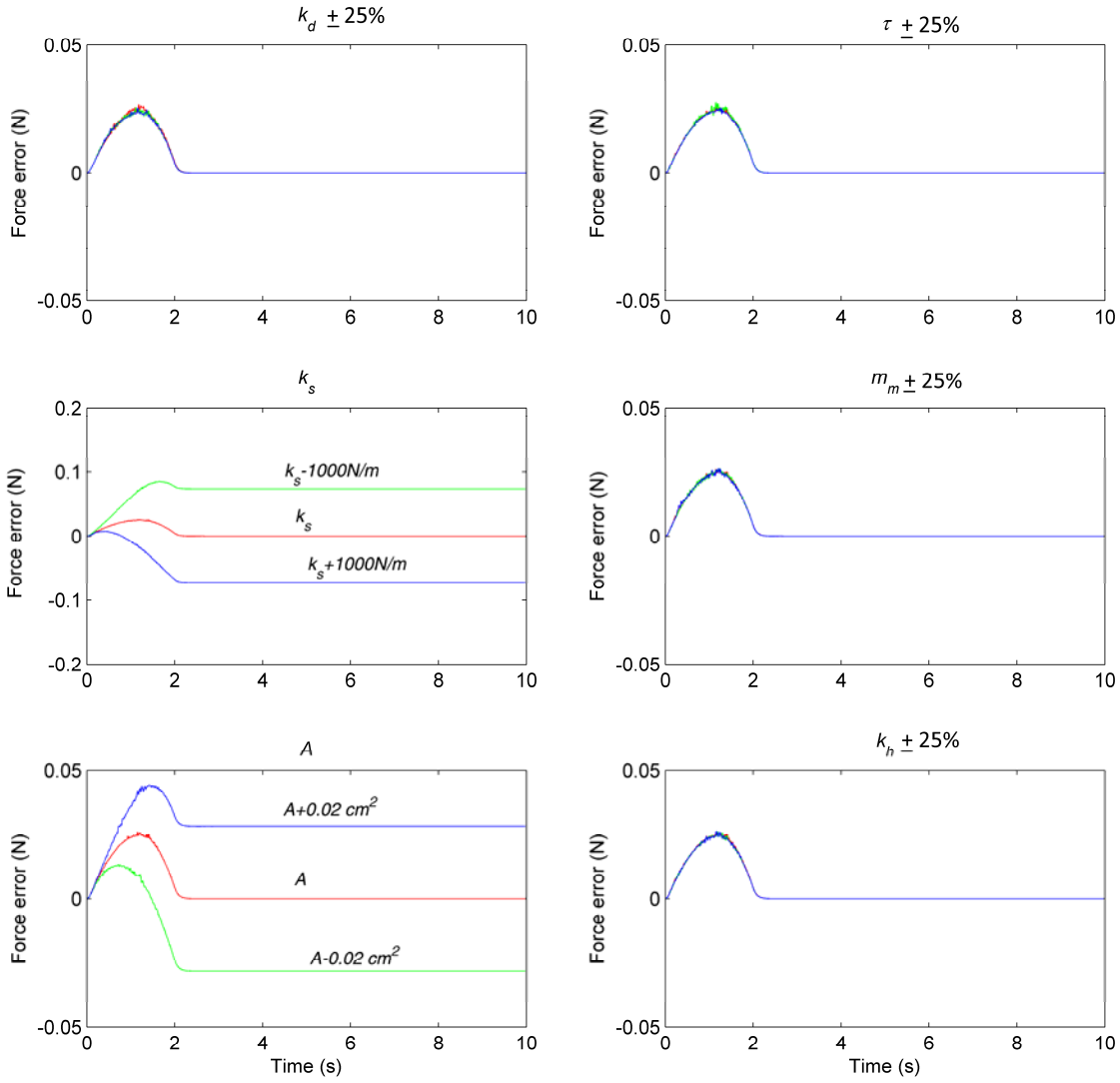

Figure 5.4 Effect of uncertainties in the parameters needed for the controllers on force tracking error.

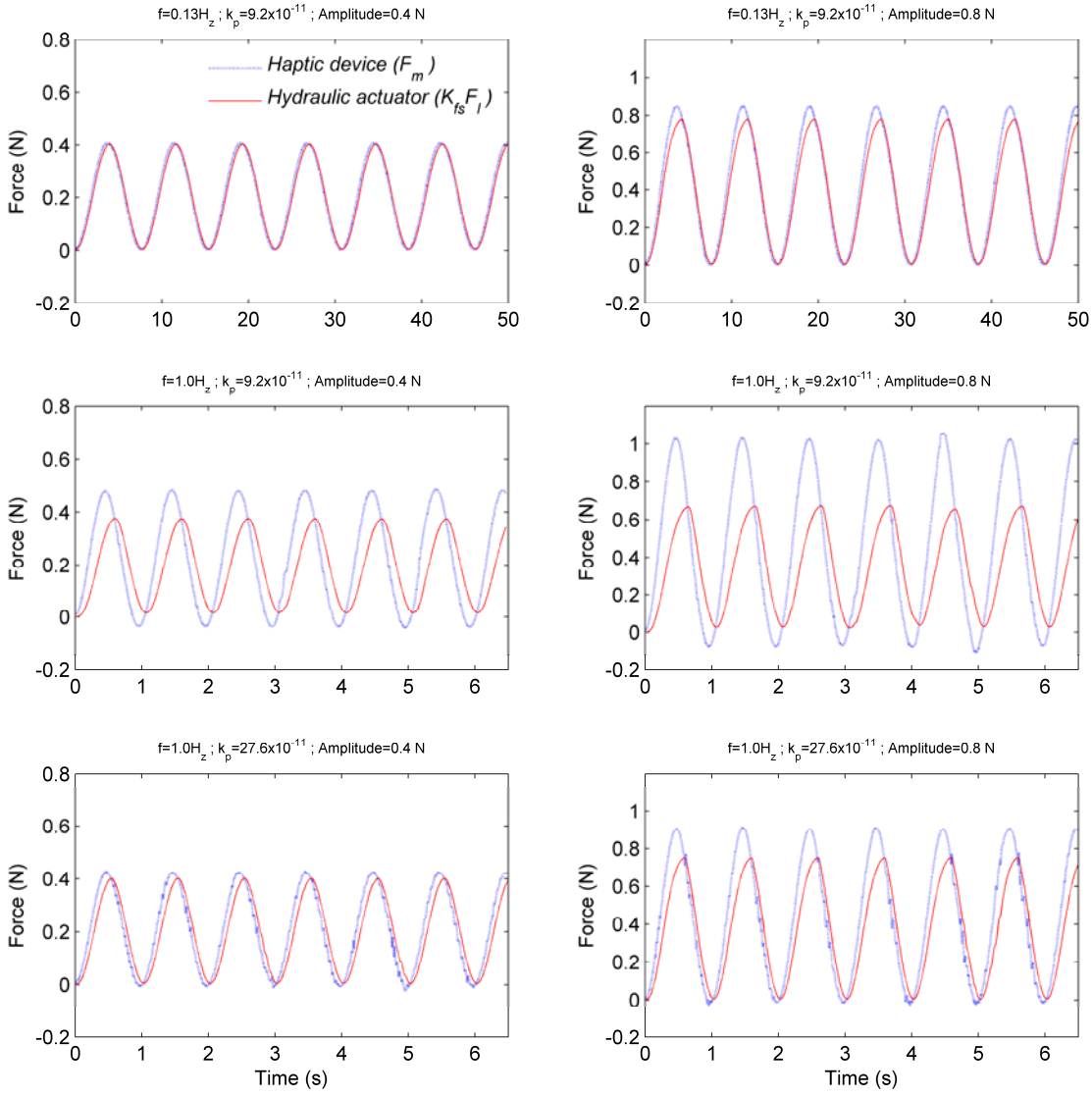

Figure 5.5 Force tracking for input commands with different frequencies ($f = 0.13$Hz and 1.0Hz), amplitudes (0.4N and 0.8N) and controller gains ($k_p = 9.2 \times 10^{-11} V/\text{Pa}^{3/2}$ and $27.6 \times 10^{-11} V/\text{Pa}^{3/2}$).

5.2.3.2 Experimental results

For experiments, the same controller gains as in the simulations were used. The interaction force between hydraulic actuator and the environment, F_l, and the displacement of the hydraulic actuator, x_s, was sent from the slave side to the master. This information from the slave side was then used at the master side to compute the master force, F_m [see (5.2)]. The operator's force, F_h, was needed to compute the control signal, u, for the hydraulic actuator [see (5.1)]. The force F_h is generally a function of x_m [93]. Since the test rig did not have any force sensors to measure the operator's force, it was approximated in this work by its steady-state value, using (5.13), i.e., $F_h = \alpha k_h K_{ps} x_m$. Furthermore, since the hydraulic actuator was not equipped with a tachometer or accelerometer, velocity and acceleration of the hydraulic actuator, $\dot{x}_s$ and $\ddot{x}_s$ respectively, were computed from x_s using a 20-point regression [94]. The nominal stiffness of the spring used in experiments was $k_s = 125\text{kN/m}$, but during experiments, it was obtained by continuously dividing the interaction force measured by the force sensor at the slave side divided by its displacement measured by encoder. The spring used in the experiments could not travel more than 20mm. Thus, during the experiments, the operator was restricted not to push beyond this limit. Other variables needed by the controllers were pump pressure, P_s, and differential pressures, P_L, and were easily obtained via online measurements.

Figure 5.6 and Figure 5.7 show the experimental results of using the control laws developed in this section, based on the Lyapunov stability control technique. These figures show that the system is stable and exhibits good responses in terms of position

and force tracking capabilities. The displacement error is within ±2.0mm and force error is within ± 0.1N for both experiments.

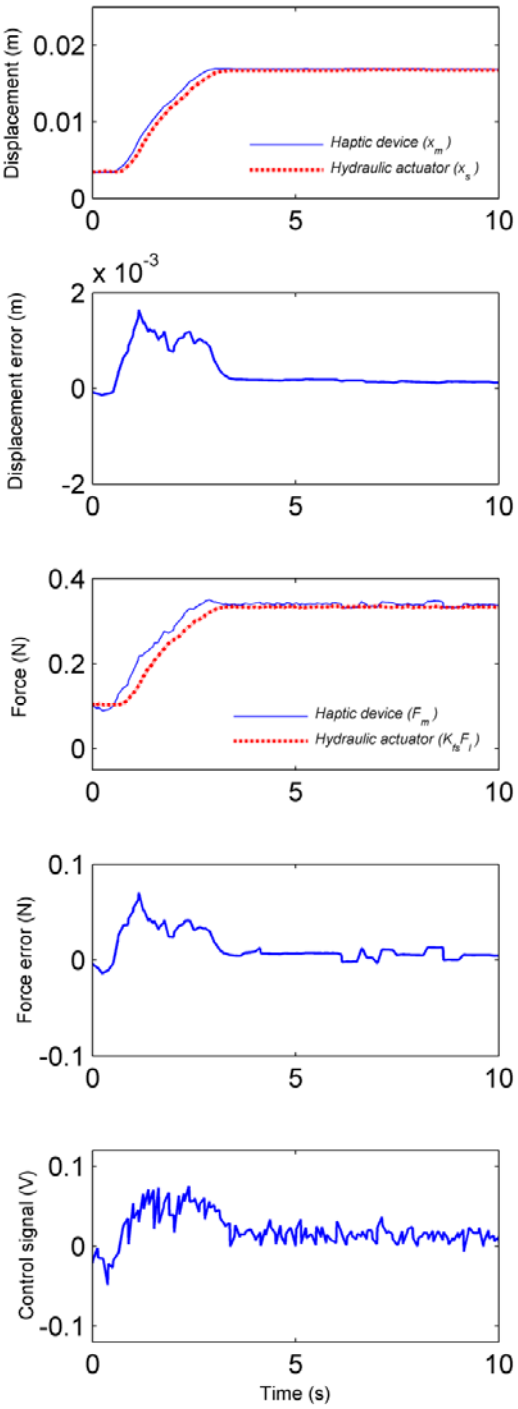

Figure 5.6 Experimental results for positioning task.

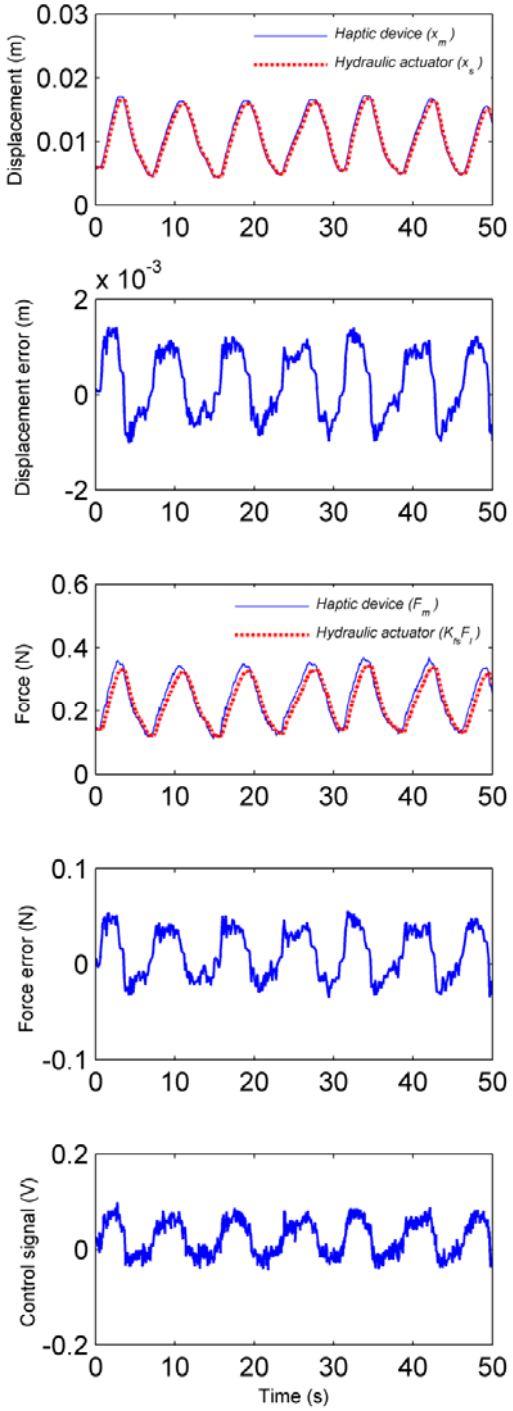

Figure 5.7 Experimental results for tracking task.

5.3 Displacement-mode control for free motion tasks[4]

Section 5.2 presented a bilateral control scheme based on Lyapunov's stability theory that includes nonlinear characteristics of hydraulic actuation and human operator dynamics. However, the force-mode bilateral controller presented in Section 5.2 was developed for constrained motion of a manipulator interacting with an environment. In this section, a position-mode bilateral control scheme is presented that can be used during unconstrained (free) motion. Using this scheme, the position error between displacements of the haptic device and the hydraulic actuator is used at both master and slave sides to maintain good position tracking at the actuator side while providing a feel of performing task at the remote site by coupling the displacement of the haptic device to the displacement of the hydraulic actuator. The work presented in this section, therefore, complements the previous work (Section 5.2), in that it allows the operator to use a haptic device to manipulate a hydraulic actuator in either free motion or constrained control modes.

5.3.1 Description of controller

The model described in Chapter 3 is employed to design a control scheme capable of regulating the actuator's position, i.e., given a constant force by human operator and an arbitrary initial condition, the system should asymptotically approach to an equilibrium point and remain there. The following control laws are proposed to determine values for u and F_m:

[4] Results of this section was presented and published in proceedings of 4th annual ASME Dynamic Systems and Control Conference, and Bath/ASME Symposium on Fluid Power and Motion Control, October 31-November 2, 2011, Arlington, VA, USA.

$$u = \left[-K_{p1}(x_s - x_m) - K_{p2}(P_L)\right]\sqrt{P_s - sgn(x_{sp})P_L} \tag{5.42}$$

$$F_m = K_{p3}(x_s - x_m) + K_{p4}(P_L) \tag{5.43}$$

In (5.42) and (5.43), K_{p1}, K_{p2}, K_{p3}, and K_{p4} are all real positive gains. For the force generated by the haptic device, F_m, two terms are included. The first term in Equation (5.43) is proportional to the position error between the haptic device and hydraulic actuator's positions. This term contributes to producing a feedback to the human operator proportional to the position error between master and slave manipulators. This type of force feedback is like a virtual spring which couples the displacement of the haptic device to the displacement of the hydraulic actuator [7]. This force feedback notifies the human operator about the position error between master and slave devices and constrains the operator's hand to move very fast when the slave manipulator is behind/ahead in tracking master manipulator's displacement. The second term relates to the load pressure, P_L, of the hydraulic actuator and added for stabilizing the entire control system. The same terms, but scaled by term $\sqrt{P_s - sgn(x_{sp})P_L}$, have been used in the calculation of the control signal u with different controller gains, which helps to stabilize the position tracking ability of the hydraulic actuator. The proposed controller here only needs system's pressures and displacements that are easy to obtain via on-line measurements. Additionally, the controller does not need any information about the parameters of the system. These characteristics make the controller very attractive from the implementation view point.

Using states defined in (3.12) and replacing u and F_m in (3.13) with (5.42) and (5.43), and ignoring F_{fr} for the sake of simplicity, results in the following state space equations:

$$\begin{cases} \dot{x}_1 = x_2 \\ \dot{x}_2 = \dfrac{A}{m_s}x_3 - \dfrac{d}{m_s}x_2 \\ \dot{x}_3 = \dfrac{-A}{C}x_2 + \dfrac{c_d w}{C\sqrt{\rho}}x_4\sqrt{P_s - sgn(x_4)x_3} \\ \dot{x}_4 = \dfrac{-1}{\tau}x_4 + \dfrac{k_{sp}}{\tau}\left[-K_{p1}(x_1 - x_5) - K_{p2}(x_3)\right]\sqrt{P_s - sgn(x_4)x_3} \\ \dot{x}_5 = x_6 \\ \dot{x}_6 = \dfrac{1}{m_m}\left(F_h + K_{p3}(x_1 - x_5) + K_{p4}(x_3) - k_d x_6 - k_h x_5\right) \end{cases} \tag{5.44}$$

The control system described by (5.44) is non-smooth due to term $sgn(x_4)$ on the right hand side of the equation describing $\dot{x}_4$ originating from control law (5.42). Filippov's solution theory [86, 87] and extension of Lyapunov's second method to non-smooth dynamic systems [89-91] will be used in the next section to study the stability.

5.3.2 Stability analysis

5.3.2.1 Existence, uniqueness, and continuation of Filippov's solution

The dynamic system presented by (5.44) consists of nonlinear differential equations with discontinuous right-hand sides. Here, Filippov's solution concept is used for the non-smooth system described by (5.44). The discontinuity surface of the system described in (5.44) is:

$$S := \{\vec{x}: x_4 = 0\} \tag{5.45}$$

The discontinuity surface, S, divides the solution region, Ω, into two regions:

$$\Omega_s^+ := \{\vec{x}: x_4 > 0\} \tag{5.46}$$

$$\Omega_s^- := \{\vec{x}: x_4 < 0\} \tag{5.47}$$

The right-hand sides of the equations in (5.44) are piecewise continuous and defined everywhere in Ω. They are also measurable and bounded. Therefore, equation (5.44) satisfies condition ***B*** of Filippov's solution theory and according to theorems 4 and 5 of Filippov [86], we have the local existence and continuity of a solution. Next, the uniqueness of the solution is proven. Since the right-hand sides of (5.44) are all continuous before and after the discontinuity surface, and the discontinuity surface, S, is smooth and independent of time, conditions ***A***, ***B*** and ***C*** of Filippov's solution theory are satisfied [86, 87]. Following the procedure described in [86], the limiting values of the vector function of the right-hand sides of (5.44), i.e. f^+ and f^- when S is approached from Ω_s^+ and Ω_s^-, are:

$$f^+ = \begin{cases} x_2 \\ \dfrac{A}{m_s}x_3 - \dfrac{d}{m_s}x_2 \\ \dfrac{-A}{C}x_2 + \dfrac{c_d w}{C\sqrt{\rho}}x_4\sqrt{P_s - x_3} \\ \dfrac{-1}{\tau}x_4 + \dfrac{k_{sp}}{\tau}\left[-K_{p1}(x_1 - x_5) - K_{p2}(x_3)\right]\sqrt{P_s - x_3} \\ x_6 \\ \dfrac{1}{m_m}\left(F_h + K_{p3}(x_1 - x_5) + K_{p4}(x_3) - k_d x_6 - k_h x_5\right) \end{cases} \tag{5.48}$$

$$f^- = \begin{cases} x_2 \\ \dfrac{A}{m_s}x_3 - \dfrac{d}{m_s}x_2 \\ \dfrac{-A}{C}x_2 + \dfrac{c_d w}{C\sqrt{\rho}}x_4\sqrt{P_s + x_3} \\ \dfrac{-1}{\tau}x_4 + \dfrac{k_{sp}}{\tau}\left[-K_{p1}(x_1 - x_5) - K_{p2}(x_3)\right]\sqrt{P_s + x_3} \\ x_6 \\ \dfrac{1}{m_m}\left(F_h + K_{p3}(x_1 - x_5) + K_{p4}(x_3) - k_d x_6 - k_h x_5\right) \end{cases} \tag{5.49}$$

The projections of f^+ and f^- along the normal to the discontinuity surface, i.e., $N_s = \{0,0,0,1,0,0\}$ are denoted by f_N^+ and f_N^-:

$$f_N^+ = + \frac{k_{sp}}{\tau}\left[-K_{p1}(x_1 - x_5) - K_{p2}(x_3)\right]\sqrt{P_s - x_3} \tag{5.50}$$

$$f_N^- = + \frac{k_{sp}}{\tau}\left[-K_{p1}(x_1 - x_5) - K_{p2}(x_3)\right]\sqrt{P_s + x_3} \tag{5.51}$$

From (5.50) and (5.51), f_N^+ and f_N^- have the same sign (note that $\sqrt{P_s \pm x_3}$ is always nonnegative). This satisfies conditions of *Lemma 9* of Filippov's solution [86]. Thus, in the domain $\Omega_s^- + S + \Omega_s^+$ we have uniqueness and continuous dependence of the solution on the initial conditions.

5.3.2.2 Stability proof

For the stability proof, extension of Lyapunov's second method to non-smooth dynamic systems [89], based on Filippov's solution theory, is used. The stability of the system is analyzed for a regulating task in which input F_h is constant. By imposing $\dot{x}_{i\ (i=1..6)} = 0$, the system described by (5.44) is shown to have the following equilibrium point:

$$\vec{x}_{eq} = [x_{1eq} \quad x_{2eq} \quad x_{3eq} \quad x_{4eq} \quad x_{5eq} \quad x_{6eq}]^T = \left[\frac{F_h}{k_h} \quad 0 \quad 0 \quad 0 \quad \frac{F_h}{k_h} \quad 0\right]^T \tag{5.52}$$

Defining $\vec{e} = \vec{x} - \vec{x}_{eq}$ the following states are defined:

$$\begin{aligned}\vec{e} &= [e_1 \quad e_2 \quad e_3 \quad e_4 \quad e_5 \quad e_6]^T \\ &= \left[\left(x_1 - \frac{F_h}{k_h}\right) \quad x_2 \quad x_3 \quad x_4 \quad \left(x_5 - \frac{F_h}{k_h}\right) \quad x_6\right]^T\end{aligned} \tag{5.53}$$

And substituting (5.53) into (5.44), the new state-space model having its equilibrium point at the origin, is obtained:

$$\begin{cases} \dot{e}_1 = e_2 \\ \dot{e}_2 = \dfrac{A}{m_s} e_3 - \dfrac{d}{m_s} e_2 \\ \dot{e}_3 = \dfrac{-A}{C} e_2 + \dfrac{c_d w}{C\sqrt{\rho}} e_4 \sqrt{P_s - sgn(e_4) e_3} \\ \dot{e}_4 = \dfrac{-1}{\tau} e_4 + \dfrac{k_{sp}}{\tau}\left[-K_{p1}(e_1 - e_5) - K_{p2}(e_3)\right]\sqrt{P_s - sgn(e_4) e_3} \\ \dot{e}_5 = e_6 \\ \dot{e}_6 = \dfrac{1}{m_m}\left(K_{p3}(e_1 - e_5) + K_{p4} e_3 - k_d e_6 - k_h e_5\right) \end{cases} \tag{5.54}$$

To construct a smooth Lyapunov function for the non-smooth system of (5.54), the procedure described by Wu et al. [89] is used. From (5.54), the discontinuity surface is:

$$S := \{\vec{e} : e_4 = 0\} \tag{5.55}$$

The right-hand sides of (5.54) are discontinuous, but measurable and bounded. The following Lyapunov function is constructed for the system described by (5.54):

$$
\begin{aligned}
&V(e_1, e_2, e_3, e_4, e_5, e_6) \\
&= \frac{A\left(K_{p1}A - K_{p2}C\right) + K_{p1}C^2}{2C(K_{p2}A - K_{p1}C)} e_1^2 + \frac{2K_{p1}C + (K_{p2}A - K_{p1}C)}{4(K_{p2}A - K_{p1}C)} e_3^2 \\
&+ \frac{K_{p1}A}{(K_{p2}A - K_{p1}C)} e_1 e_3 + \frac{m_s}{2C} e_2^2 + \frac{Ac_d w\tau}{2k_{sp}C\sqrt{\rho}(K_{p2}A - K_{p1}C)} e_4^2 \\
&+ \frac{1}{2}\left(e_1 - \frac{K_{p1}A^2}{C(K_{p2}A - K_{p1}C)} e_5\right)^2 + \frac{1}{4}\left(e_3 - \frac{2K_{p1}A}{(K_{p2}A - K_{p1}C)} e_5\right)^2 \\
&+ \frac{\left(K_{p1}A^2CK_{p3} + K_{p1}A^2k_hC\right)\left(K_{p2}A - K_{p1}C\right) - 2K_{p1}^2A^2C^2K_{p3} - K_{p1}^2A^4K_{p3}}{2C^2K_{p3}(K_{p2}A - K_{p1}C)^2} e_5^2 \\
&+ \frac{K_{p1}A^2m_m}{2CK_{p3}(K_{p2}A - K_{p1}C)} e_6^2
\end{aligned}
\tag{5.56}
$$

Function V is continuous. Next, V is proven to be positive and definite. During this process, some conditions should be applied to controller gains. Rewriting V as follows:

$$V = V_1 + V_2 \tag{5.57}$$

where:

$$V_1 =$$

$$\frac{A\left(K_{p1}A - K_{p2}C\right) + K_{p1}C^2}{2C(K_{p2}A - K_{p1}C)}e_1^2 + \frac{2K_{p1}C + (K_{p2}A - K_{p1}C)}{4(K_{p2}A - K_{p1}C)}e_3^2 + \frac{K_{p1}A}{(K_{p2}A - K_{p1}C)}e_1e_3 \tag{5.58}$$

and,

$$V_2 =$$

$$\frac{m_s}{2C}e_2^2 + \frac{Ac_dw\tau}{2k_{sp}C\sqrt{\rho}\left(K_{p2}A - K_{p1}C\right)}e_4^2 + \frac{1}{2}\left(e_1 - \frac{K_{p1}A^2}{C(K_{p2}A - K_{p1}C)}e_5\right)^2 + \frac{1}{4}\left(e_3 - \frac{2K_{p1}A}{(K_{p2}A - K_{p1}C)}e_5\right)^2 + \frac{\left(K_{p1}A^2CK_{p3} + K_{p1}A^2k_hC\right)\left(K_{p2}A - K_{p1}C\right) - 2K_{p1}^2A^2C^2K_{p3} - K_{p1}^2A^4K_{p3}}{2C^2K_{p3}(K_{p2}A - K_{p1}C)^2}e_5^2 + \frac{K_{p1}A^2m_m}{2CK_{p3}(K_{p2}A - K_{p1}C)}e_6^2 \tag{5.59}$$

V_1 can be re-written in the following form:

$$V_1 = \begin{bmatrix} e_1 & e_2 \end{bmatrix} Q \begin{bmatrix} e_1 \\ e_2 \end{bmatrix} \tag{5.60}$$

where matrix Q is:

$$Q = \begin{bmatrix} \frac{A(K_{p1}A - K_{p2}C) + K_{p1}C^2}{2C(K_{p2}A - K_{p1}C)} & \frac{K_{p1}A}{2(K_{p2}A - K_{p1}C)} \\ \frac{K_{p1}A}{2(K_{p2}A - K_{p1}C)} & \frac{2K_{p1}C + (K_{p2}A - K_{p1}C)}{4(K_{p2}A - K_{p1}C)} \end{bmatrix} \tag{5.61}$$

According to the Sylvester's theorem [92], for V_1 to be positive definite, a necessary and sufficient condition for the symmetric matrix Q is that its principal minors, i.e., Q_{11} and $(Q_{11}Q_{22} - Q_{12}Q_{21})$ must be strictly positive. Q_{11} is shown below:

$$Q_{11} = \frac{A(K_{p1}A - K_{p2}C) + K_{p1}C^2}{2C(K_{p2}A - K_{p1}C)} \tag{5.62}$$

For Q_{11} to be positive, we need to ensure the following condition holds for the controller gains $K_{p1}$and K_{p2}:

$$\frac{C}{A} < \frac{K_{p2}}{K_{p1}} < \frac{A}{C} \tag{5.63}$$

Given condition (5.63), terms shown within parentheses in (5.62) are positive. Thus, Q_{11} is strictly positive. Term $(Q_{11}Q_{22} - Q_{12}Q_{21})$ is given below:

$$\begin{aligned} &(Q_{11}Q_{22} - Q_{12}Q_{21}) \\ &= \left(\frac{A(K_{p1}A - K_{p2}C) + K_{p1}C^2}{2C(K_{p2}A - K_{p1}C)}\right)\left(\frac{2K_{p1}C + (K_{p2}A - K_{p1}C)}{4(K_{p2}A - K_{p1}C)}\right) \\ &- \left(\frac{K_{p1}A}{2(K_{p2}A - K_{p1}C)}\right)\left(\frac{K_{p1}A}{2(K_{p2}A - K_{p1}C)}\right) \end{aligned} \tag{5.64}$$

which can be rewritten as follows:

$$(Q_{11}Q_{22} - Q_{12}Q_{21}) = \frac{A(K_{p1}A - 2K_{p2}C) + C(K_{p2}A - K_{p1}C)}{8C(K_{p2}A - K_{p1}C)} \tag{5.65}$$

To ensure $(Q_{11}Q_{22} - Q_{12}Q_{21})$ is strictly positive the following condition must hold:

$$\frac{C}{A} < \frac{K_{p2}}{K_{p1}} < \frac{A}{2C} \tag{5.66}$$

For V_2, all terms are positive subject to satisfying condition (5.63) only, except for term pertaining to e_5^2 which is positive subject to satisfying the following condition:

$$\left(K_{p1}A^2CK_{p3} + K_{p1}A^2k_hC\right)\left(K_{p2}A - K_{p1}C\right) - 2K_{p1}^2A^2C^2K_{p3} - K_{p1}^2A^4K_{p3} > 0 \tag{5.67}$$

Condition (5.67) leads to the following relation:

$$K_{p3} < \frac{k_hC\left(K_{p2}A - K_{p1}C\right)}{3K_{p1}C^2 + A\left(K_{p1}A - K_{p2}C\right)} \tag{5.68}$$

Note that using (5.63), the right hand side of (5.68) is positive. Thus, subject to satisfying conditions (5.63), (5.66) and (5.68), function V is positive definite.

V is now proven to be a smooth Lyapunov function and $\dot{V}$ is negative and at least semi-definite. The derivative of V with respect to time is:

$$\dot{V} = \frac{A\left(K_{p1}A - K_{p2}C\right) + K_{p1}C^2}{C\left(K_{p2}A - K_{p1}C\right)} e_1\dot{e}_1 + \frac{2K_{p1}C + \left(K_{p2}A - K_{p1}C\right)}{2\left(K_{p2}A - K_{p1}C\right)} e_3\dot{e}_3$$

$$+ \frac{K_{p1}A}{(K_{p2}A - K_{p1}C)} \dot{e}_1 e_3 + \frac{K_{p1}A}{(K_{p2}A - K_{p1}C)} e_1\dot{e}_3 + \frac{m_s}{C} e_2\dot{e}_2$$

$$+ \frac{Ac_d w\tau}{k_{sp}C\sqrt{\rho}(K_{p2}A - K_{p1}C)} e_4\dot{e}_4$$

$$+ \left(e_1 - \frac{K_{p1}A^2}{C(K_{p2}A - K_{p1}C)} e_5\right)\left(\dot{e}_1 - \frac{K_{p1}A^2}{C(K_{p2}A - K_{p1}C)} \dot{e}_5\right) \tag{5.69}$$

$$+ \frac{1}{2}\left(e_3 - \frac{2K_{p1}A}{(K_{p2}A - K_{p1}C)} e_5\right)\left(\dot{e}_3 - \frac{2K_{p1}A}{(K_{p2}A - K_{p1}C)} \dot{e}_5\right)$$

$$+ \frac{\left(K_{p1}A^2CK_{p3} + K_{p1}A^2k_hC\right)\left(K_{p2}A - K_{p1}C\right) - 2K_{p1}^2A^2C^2K_{p3} - K_{p1}^2A^4K_{p3}}{C^2K_{p3}(K_{p2}A - K_{p1}C)^2} e_5\dot{e}_5$$

$$+ \frac{K_{p1}A^2m_m}{CK_{p3}(K_{p2}A - K_{p1}C)} e_6\dot{e}_6$$

Rewriting $\dot{V}$ in the following form:

$$\dot{V} = \begin{bmatrix} \frac{\partial_V}{\partial_{e_1}} & \frac{\partial_V}{\partial_{e_2}} & \frac{\partial_V}{\partial_{e_3}} & \frac{\partial_V}{\partial_{e_4}} & \frac{\partial_V}{\partial_{e_5}} & \frac{\partial_V}{\partial_{e_6}} \end{bmatrix} \begin{bmatrix} \frac{de_1}{dt} \\ \frac{de_2}{dt} \\ \frac{de_3}{dt} \\ \frac{de_4}{dt} \\ \frac{de_5}{dt} \\ \frac{de_6}{dt} \end{bmatrix} = \nabla V^T \begin{bmatrix} \dot{e}_1 \\ \dot{e}_2 \\ \dot{e}_3 \\ \dot{e}_4 \\ \dot{e}_5 \\ \dot{e}_6 \end{bmatrix} \tag{5.70}$$

where elements of ∇V are given below,

$$\frac{\partial_V}{\partial_{e_1}} = \frac{A\left(K_{p1}A - K_{p2}C\right) + K_{p1}C^2}{C\left(K_{p2}A - K_{p1}C\right)} e_1 + \frac{K_{p1}A}{\left(K_{p2}A - K_{p1}C\right)} e_3 + e_1 - \frac{K_{p1}A^2}{C\left(K_{p2}A - K_{p1}C\right)} e_5 \tag{5.71}$$

$$\frac{\partial_V}{\partial_{e_2}} = \frac{m_s}{C} e_2 \tag{5.72}$$

$$\frac{\partial_V}{\partial_{e_3}} = \frac{2K_{p1}C + \left(K_{p2}A - K_{p1}C\right)}{2\left(K_{p2}A - K_{p1}C\right)} e_3 + \frac{K_{p1}A}{\left(K_{p2}A - K_{p1}C\right)} e_1 + \frac{1}{2} e_3 - \frac{K_{p1}A}{\left(K_{p2}A - K_{p1}C\right)} e_5 \tag{5.73}$$

$$\frac{\partial_V}{\partial_{e_4}} = \frac{Ac_d w\tau}{k_{sp}C\sqrt{\rho}\left(K_{p2}A - K_{p1}C\right)} e_4 \tag{5.74}$$

$$\frac{\partial_V}{\partial_{e_5}} = -\frac{K_{p1}A^2}{C\left(K_{p2}A - K_{p1}C\right)} e_1 + \left(\frac{K_{p1}A^2}{C\left(K_{p2}A - K_{p1}C\right)}\right)^2 e_5 - \frac{K_{p1}A}{\left(K_{p2}A - K_{p1}C\right)} e_3 + \frac{1}{2}\left(\frac{2K_{p1}A}{\left(K_{p2}A - K_{p1}C\right)}\right)^2 e_5 + \frac{\left(K_{p1}A^2CK_{p3} + K_{p1}A^2k_hC\right)\left(K_{p2}A - K_{p1}C\right) - 2K_{p1}^2A^2C^2K_{p3} - K_{p1}^2A^4K_{p3}}{C^2K_{p3}\left(K_{p2}A - K_{p1}C\right)^2} e_5 \tag{5.75}$$

$$\frac{\partial_V}{\partial_{e_6}} = \frac{K_{p1}A^2m_m}{CK_{p3}\left(K_{p2}A - K_{p1}C\right)} e_6 \tag{5.76}$$

and using (5.54), results in,

$$\begin{bmatrix}\dot{e}_1\\ \dot{e}_2\\ \dot{e}_3\\ \dot{e}_4\\ \dot{e}_5\\ \dot{e}_6\end{bmatrix} = \begin{bmatrix} e_2 \\ \frac{A}{m_s}e_3 - \frac{d}{m_s}e_2 \\ \frac{-A}{C}e_2 + \frac{c_d w}{C\sqrt{\rho}}e_4\sqrt{P_s - sgn(e_4)e_3} \\ \frac{-1}{\tau}e_4 + \frac{k_{sp}}{\tau}\left[-K_{p1}(e_1 - e_5) - K_{p2}(e_3)\right]\sqrt{P_s - sgn(e_4)e_3} \\ e_6 \\ \frac{1}{m_m}\left(K_{p3}(e_1 - e_5) + K_{p4}e_3 - k_d e_6 - k_h e_5\right) \end{bmatrix} \tag{5.77}$$

∇V is the gradient of function V and is continuous with respect to states $e_{i(i=1..6)}$. V should be first proven a smooth Lyapunov function. Utilizing the notation described in Section 4.1 of reference [89], one can rewrite $\dot{V}$ in the following form:

$$\dot{V} = W^{(1)}(t,\vec{e}).h^{(1)}(t,\vec{e}) + W^{(2)}(t,\vec{e}).h^{(2)}(t,\vec{e}) \tag{5.78}$$

Using (5.70) to (5.78), functions $W^{(1)}(t,\vec{e})$, $h^{(1)}(t,\vec{e})$, $W^{(2)}(t,\vec{e})$, and $h^{(2)}(t,\vec{e})$ are written as follows:

$$W^{(1)}(t,\vec{e}) = \nabla V \tag{5.79}$$

$$h^{(1)}(t,\vec{e}) = \begin{bmatrix} e_2 \\ \frac{A}{m_s}e_3 - \frac{d}{m_s}e_2 \\ \frac{-A}{C}e_2 \\ \frac{-1}{\tau}e_4 \\ e_6 \\ \frac{1}{m_m}\left(K_{p3}(e_1 - e_5) + K_{p4}e_3 - k_d e_6 - k_h e_5\right) \end{bmatrix} \tag{5.80}$$

$$W^{(2)}(t,\vec{e}) =$$

$$\begin{bmatrix} 0 \\ 0 \\ \frac{2K_{p1}C + \left(K_{p2}A - K_{p1}C\right)}{2\left(K_{p2}A - K_{p1}C\right)}e_3 + \frac{K_{p1}A}{(K_{p2}A - K_{p1}C)}e_1 + \frac{1}{2}e_3 - \frac{K_{p1}A}{(K_{p2}A - K_{p1}C)}e_5 \\ \frac{Ac_d w\tau}{k_{sp}C\sqrt{\rho}(K_{p2}A - K_{p1}C)}e_4 \\ 0 \\ 0 \end{bmatrix} \tag{5.81}$$

$$h^{(2)}(t,\vec{e}) = \begin{bmatrix} 0 \\ 0 \\ \frac{c_d w}{C\sqrt{\rho}}e_4\sqrt{P_s - sgn(e_4)e_3} \\ \frac{k_{sp}}{\tau}\left[-K_{p1}(e_1 - e_5) - K_{p2}(e_3)\right]\sqrt{P_s - sgn(e_4)e_3} \\ 0 \\ 0 \end{bmatrix} \tag{5.82}$$

Note that $W^{(1)}(t,\vec{e}), W^{(2)}(t,\vec{e})$ and $h^{(1)}(t,\vec{e})$ are continuous and are related to the gradient of the Lyapunov function V and the continuous part of the rate of the state vector.

$h^{(2)}(t,\vec{e})$ is discontinuous and related to the discontinuous part of the equations describing the rate of the state vector. According to the established requirements for the construction of smooth Lyapunov function [89], $W^{(2)}(t,\vec{e}).h^{(2)}(t,\vec{e})$ must be continuous and tend to zero as the solution trajectory approaches the discontinuity surface *S* defined by (5.55). Additionally, the set $K\{W^{(2)}(t,\vec{e}).h^{(2)}(t,\vec{e})\}$ must consist of a single value of zero on the discontinuity surface *S.* Since:

$$
\begin{aligned}
W^{(2)}(t,\vec{e}).h^{(2)}(t,\vec{e}) &= \left[\frac{2K_{p1}C+\left(K_{p2}A-K_{p1}C\right)}{2\left(K_{p2}A-K_{p1}C\right)}e_3+\frac{K_{p1}A}{(K_{p2}A-K_{p1}C)}e_1+\frac{1}{2}e_3\right.\\
&\left.-\frac{K_{p1}A}{(K_{p2}A-K_{p1}C)}e_5\right]\left[\frac{c_d w}{C\sqrt{\rho}}e_4\sqrt{P_s-sgn(e_4)e_3}\right]\\
&+\left[\frac{Ac_d w\tau}{k_{sp}C\sqrt{\rho}(K_{p2}A-K_{p1}C)}e_4\right]\left[\frac{k_{sp}}{\tau}\left[-K_{p1}(e_1-e_5)\right.\right.\\
&\left.\left.-K_{p2}(e_3)\right]\sqrt{P_s-sgn(e_4)e_3}\right] \qquad (5.83)\\
&= 0
\end{aligned}
$$

Thus, the alternative conditions of the construction of smooth Lyapunov function for a non-smooth system, outlined in [89], are satisfied, and the above Lyapunov function is smooth.

$\dot{V}$ is now proven negative and at least semi-definite. From (5.69) to (5.77), and subject to the following condition:

$$K_{p4} = K_{p3}\frac{C}{A} \tag{5.84}$$

It can be shown that (details are not included for the sake of brevity):

$$\dot{V} = -\frac{d}{C}e_2^2 - \frac{Ac_d w}{k_{sp}C\sqrt{\rho}(K_{p2}A - K_{p1}C)}e_4^2 - \frac{k_d K_{p1}A^2}{CK_{p3}(K_{p2}A - K_{p1}C)}e_6^2 \tag{5.85}$$

Therefore, $\dot{V}$ is continuous and negative semi-definite. Note that all parameters are positive numbers. Thus, V is a smooth Lyapunov function for the non-smooth system described by (5.54). Therefore, the control system is Lyapunov stable, according to the theorem outlined in [89].

The asymptotic stability of the system is now proven. Here, non-smooth version of *invariant set theorems*, attributed to LaSalle [89, 91, 92] is used, which is a common method to prove asymptotic stability when $\dot{V}$ is negative semi-definite.

Let $\boldsymbol{R}$ be the set of all points within the solution region $\boldsymbol{\Omega}$ where $\dot{V} = 0,$ i.e.

$$\boldsymbol{R} = \left(\{e_1, e_2, e_3, e_4, e_5, e_6\}, \dot{V} = 0\right) \tag{5.86}$$

The largest invariant set $\boldsymbol{M}$, in set $\boldsymbol{R}$, is now proven to contain only the equilibrium point, $\vec{e}_{eq} = (0,0,0,0,0,0)^T$. This is proven by contradiction. According to (5.85), $\dot{V} = 0$ requires that for all points in $\boldsymbol{R}$,

$$e_2 = e_4 = e_6 = 0 \tag{5.87}$$

Now, let $\boldsymbol{M}$ be the largest invariant set in $\boldsymbol{R}$ and contains a point where error state e_3 is not zero, i.e., $(e_1, 0, e_3, 0, e_5, 0)$. Note that e_1 and e_5 can have any value, zero or nonzero. At this point, using the following equation from (5.54), we have:

$$\dot{e}_2 = \frac{A}{m_s} e_3 - \frac{d}{m_s} e_2 \tag{5.88}$$

applying $e_2 = 0$ from (5.87), and assuming a nonzero e_3, implies that $\dot{e}_2 \neq 0$. This necessitates the solution trajectory to immediately move out of the set $\boldsymbol{R}$ and certainly out of the set $\boldsymbol{M}$, which contradicts the initial assumption that $\boldsymbol{M}$ is the largest invariant set in $\boldsymbol{R}$. Therefore, regardless the values of e_1 and e_5, all points in set $\boldsymbol{M}$ should also satisfy:

$$e_3 = 0 \tag{5.89}$$

For every point in $\boldsymbol{M}$, it is now proven $e_1 = e_5$. This is proven by contradiction. Assume that $\boldsymbol{M}$ contains a point where $e_1 \neq e_5$. Note that e_1 and e_5 can have any value, zero or nonzero, but all other states are zero according to (5.87) and (5.89). At this point using the following equation from (5.54):

$$\dot{e}_4 = \frac{-1}{\tau} e_4 + \frac{k_{sp}}{\tau} \left[-K_{p1}(e_1 - e_5) - K_{p2}(e_3) \right] \sqrt{P_s - sgn(e_4) e_3} \tag{5.90}$$

and applying $e_3 = 0$ from (5.89) and $e_4 = 0$ from (5.87), implies that, unless $e_1 = e_5$, $\dot{e}_4 \neq 0$. This necessitates the solution trajectory to immediately move out of the set $\boldsymbol{R}$ and certainly out of the set $\boldsymbol{M}$, which contradicts the initial assumption that $\boldsymbol{M}$ is the largest invariant set in $\boldsymbol{R}$. Therefore, all points in set $\boldsymbol{R}$ must also satisfy the following condition:

$$e_1 = e_5 \tag{5.91}$$

Now, assume that $\boldsymbol{M}$ contains a point where error states e_1 and e_5 are not zero, i.e. $(e_1, 0,0,0, e_5, 0)$. Note that all other states are zero according to (5.87) and (5.89). At this point using the last equation of (5.54) we have:

$$\dot{e}_6 = \frac{1}{m_m}\left(K_{p3}(e_1 - e_5) + K_{p4}e_3 - k_d e_6 - k_h e_5\right) \tag{5.92}$$

applying $e_3 = 0$ from (5.89), $e_6 = 0$ from (5.87), and $e_1 = e_5$ from (5.91), having a nonzero e_5 implies that $\dot{e}_6 \neq 0$. This necessitates the solution trajectory to immediately move out of the set $\boldsymbol{R}$ and certainly out of the set $\boldsymbol{M}$, which contradicts the initial assumption that $\boldsymbol{M}$ is the largest invariant set in $\boldsymbol{R}$. Therefore, all points in set $\boldsymbol{R}$ should also satisfy the following condition:

$$e_5 = 0 \tag{5.93}$$

Thus, using (5.87), (5.89), (5.91), and (5.93) the largest invariant set $\boldsymbol{M}$ in $\boldsymbol{R}$ can only contain the equilibrium point $\vec{e}_{eq} = (0,0,0,0,0,0)^T$ and every solution trajectory in $\boldsymbol{\Omega}$ will

converge to this point. Therefore, the system described by (5.54) is asymptotically stable. Moreover:

$$V(x) \to \infty \; as \; \|x\| \to \infty \tag{5.94}$$

This implies that the equilibrium at the origin is globally asymptotically stable.

Conditions needed to prove the asymptotic stability are summarized again for future reference:

$$\frac{C}{A} < \frac{K_{p2}}{K_{p1}} < \frac{A}{2C} \tag{5.95}$$

$$K_{p3} < \frac{k_h C\left(K_{p2}A - K_{p1}C\right)}{3K_{p1}C^2 + A\left(K_{p1}A - K_{p2}C\right)} \tag{5.96}$$

$$K_{p4} = K_{p3}\frac{C}{A} \tag{5.97}$$

5.3.3 Performance evaluation

The performance of proposed controller in this section is now validated by simulation and experimental studies.

5.3.3.1 Simulation results

Equation (3.13) was used as the system and equations (5.42) and (5.43) were used as controllers. For numerical simulations, 4th order Runge-Kutta method was used in C++ as the integration routine. The parameters used for the simulations are given in Table 3.1.

The controller gains were chosen as $K_{p1} = 0.125$, $K_{p2} = 4.0 \times 10^{-11}$, $K_{p3} = 50$, and $K_{p4} = 1.5798 \times 10^{-8}$ which satisfy conditions (5.95), (5.96), and (5.97).

In the first test, the input F_h was set to a constant value of 0.4N, and zero initial conditions for all states were chosen, i.e.

$$\begin{aligned}\vec{x}_{init} &= [x_{1init} \quad x_{2init} \quad x_{3init} \quad x_{4init} \quad x_{5init} \quad x_{6init}]^T \\ &= [0.0 \text{ mm} \quad 0.0 \text{ m/s} \quad 0.0 \text{ Pa} \quad 0.0 \text{ mm} \quad 0.0 \text{ mm} \quad 0.0 \text{ m/s}]^T\end{aligned} \tag{5.98}$$

The goal of this test was to show that the system can reach the equilibrium point given a constant input. From (5.52), the equilibrium point of the system can be determined to be:

$$\begin{aligned}\vec{x}_{eq} &= [x_{1\text{eq}} \quad x_{2\text{eq}} \quad x_{3\text{eq}} \quad x_{4\text{eq}} \quad x_{5\text{eq}} \quad x_{6\text{eq}}]^T \\ &= [40.0 \text{ mm} \quad 0.0 \text{ m/s} \quad 0.0 \text{ Pa} \quad 0.0 \text{ mm} \quad 40.0 \text{ mm} \quad 0.0 \text{ m/s}]^T\end{aligned} \tag{5.99}$$

Figure 5.8 shows simulation results for all states. All states, as can be seen from Figure 5.8 to reach the equilibrium point given by (5.99). This test confirms the theoretical stability analysis performed earlier.

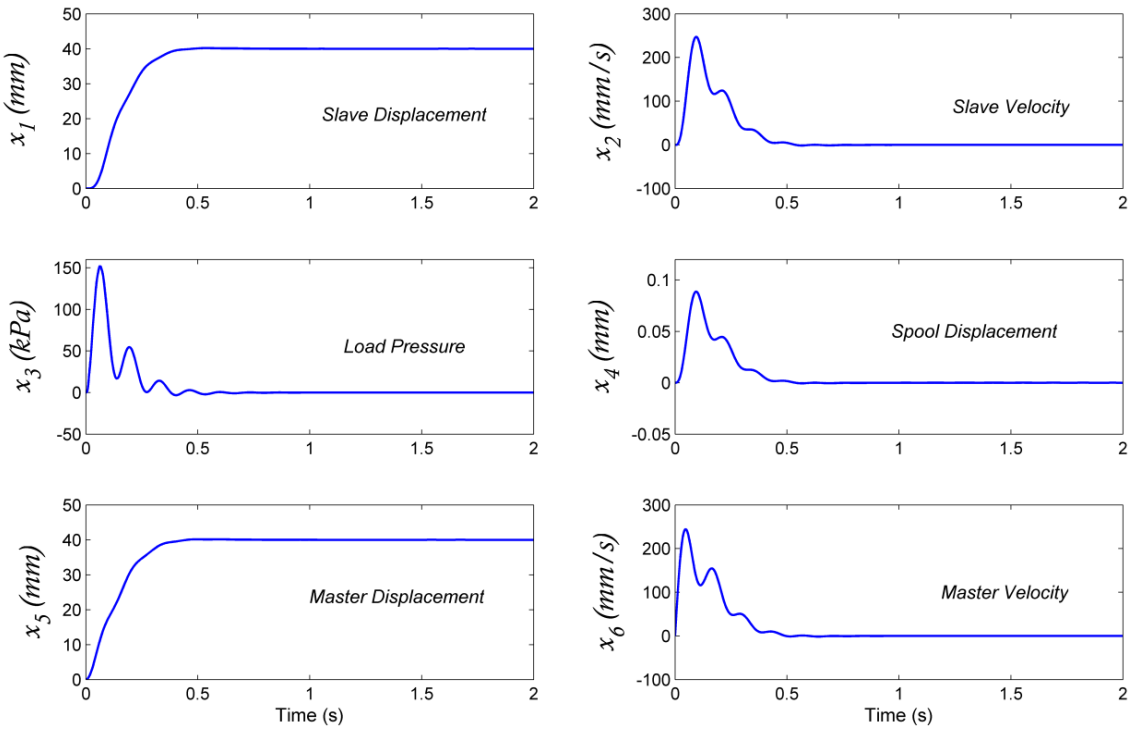

Figure 5.8 Simulation results for a constant operator input ($F_h = 0.4$N).

5.3.3.2 Experimental results

For experiments, the same controller gains as in the simulations were used. The load pressure, P_L, and the displacement of the hydraulic actuator, x_s, were sent from the slave side to the master. This data was used on the master side to compute the master force, F_m [see (5.43)]. The displacement of the haptic device, x_m , was sent from the master side to the slave to determine the control signal of the hydraulic actuator, u [see (5.42)]. Other variables needed by the controllers were pump pressure, P_s, and differential pressures, P_L, which were easily obtained via on-line measurements.

Figure 5.9 and Figure 5.10 shows the experimental results of using the control laws developed in this paper. In Figure 5.9, the operator applied constant input commands to the haptic device. As is seen, the system was stable and exhibited acceptable responses in term of position tracking. The experimental results confirm that even though actuator dry friction was not explicitly considered as part of the controllers design, the experimental system performed well.

For the next experiment, the operator moved the haptic device back and forth. From Figure 5.10, displacement error between the haptic device and the hydraulic actuator is within ±5mm. As is seen, the system was stable and exhibited good tracking response while providing haptic force feedback to the operator. Note that plots show only a 20-second period while the actual test was conducted for much longer. In all experiments, control signals were within the range and not saturated.

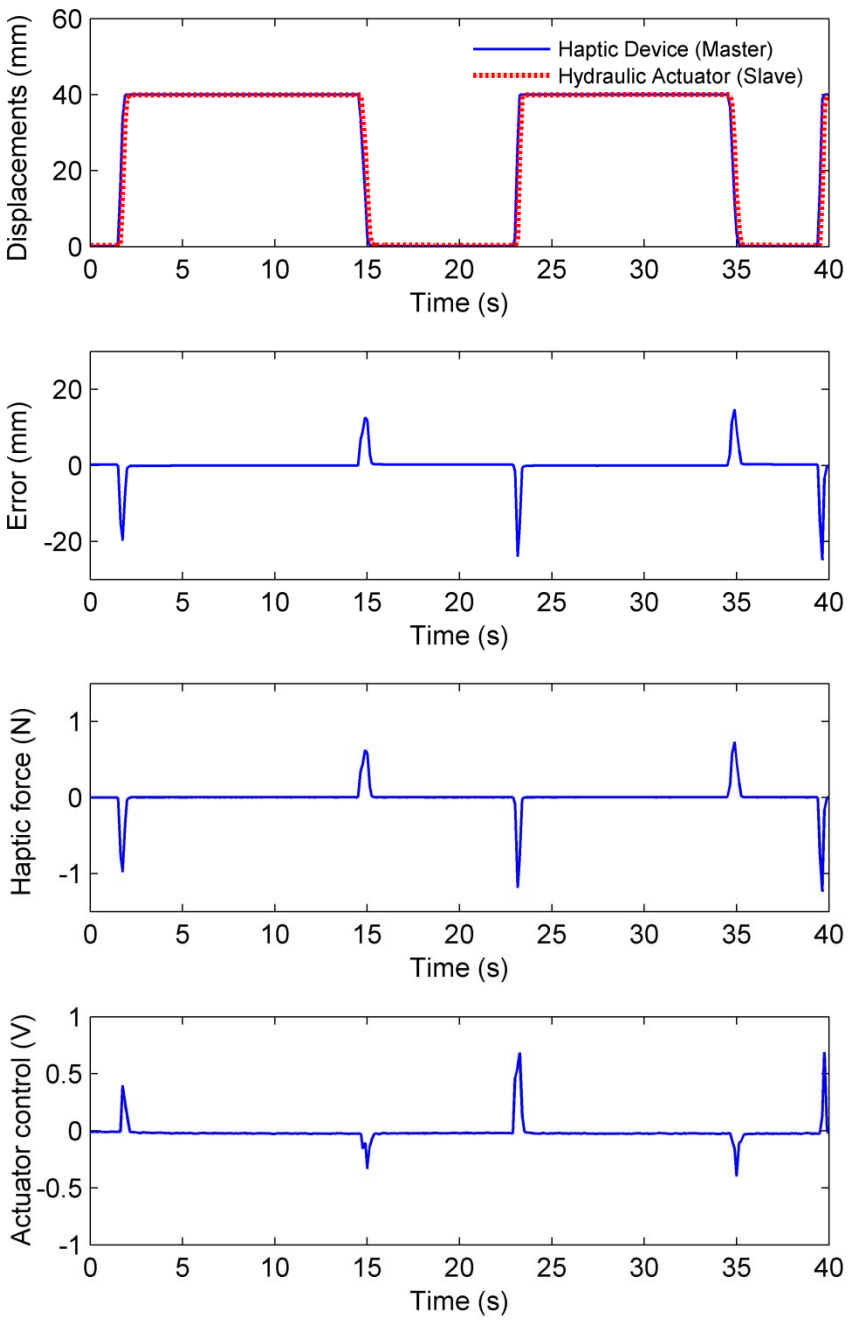

Figure 5.9 Experimental results given step-like operator input.

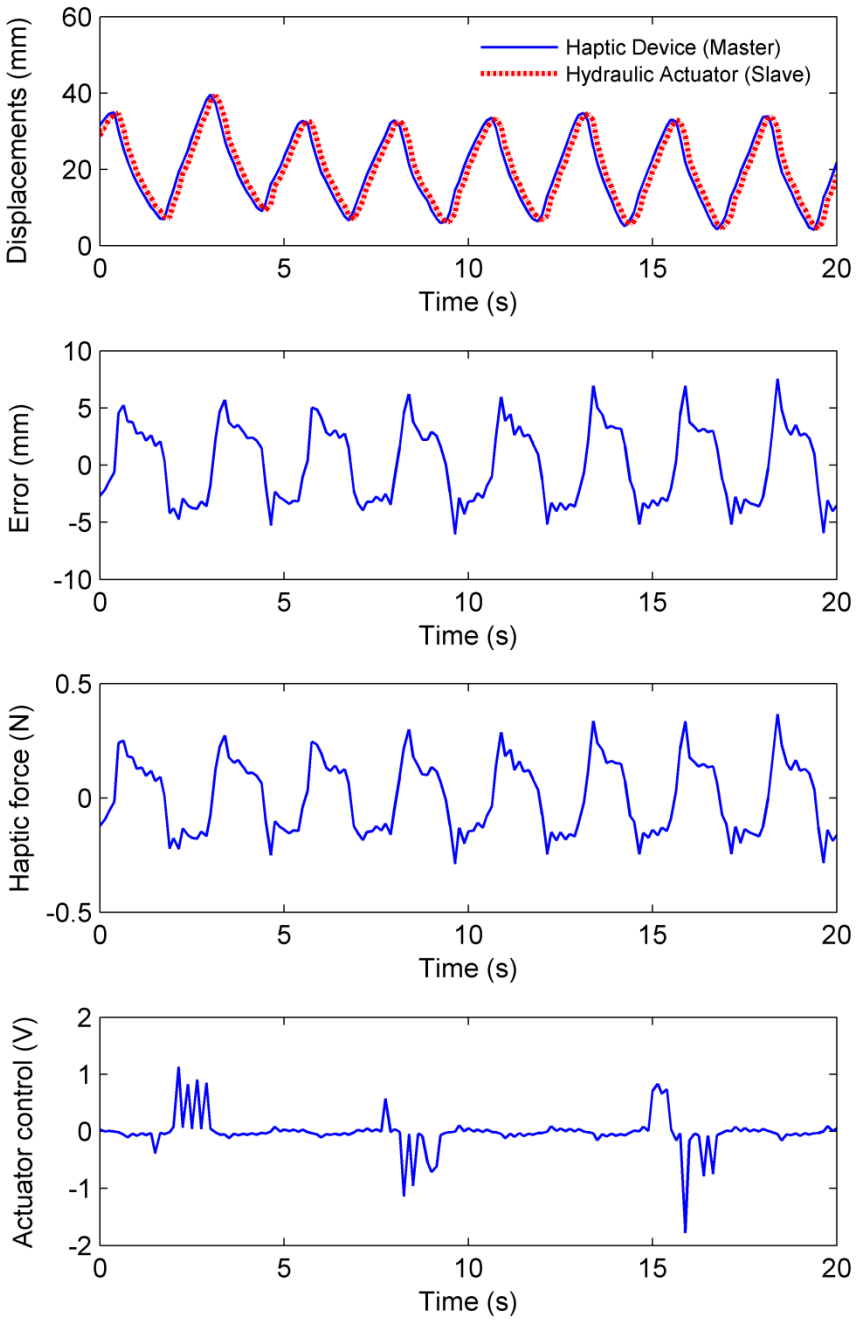

Figure 5.10 Experimental results given sinusoid-like operator input.

5.4 Displacement-mode control for combined free and constrained motions tasks[5]

There are many methods of generating and applying haptic force to the operator's hand in teleoperation systems [15]. One way to generate and apply haptic sensation is to use the interaction force between the slave manipulator and the task environment [26]. This method was used in Section 5.2 [95] to develop a control scheme in which the force applied to the operator's hand by the haptic device was a scaled version of the interaction force between the hydraulic actuator and the environment. However, in certain applications as in controlling backhoes and excavators, providing haptic force feedback based on measurement of interaction force, introduces many challenges [6]. When interaction force information is not readily available, position information can potentially be used to generate haptic feedback [6]. In this context, different approaches have been introduced. The concept of virtual fixtures is one of them [45], which is used in Chapter 4 [96] in controlling a hydraulic manipulator to perform live power transmission line maintenance tasks.

The second approach in using position information for providing haptic feedback is to use the positions of master and slave manipulators [6, 7, 97, 98]. Instead of making the system transparent, i.e., having direct force feedback on the operator's hand, the haptic device alerts the operator of the reactions as a result of forces acting on the implement. This type of approach in producing haptic feedback, was experimentally shown to be quite useful in providing a "feel" of telepresence to operators by human-in-the-loop

[5] Results of this section was submitted to Journal.

testing of a teleoperated excavator [7] and controlling a hydraulically-actuated lifter [6]. None of the above studies investigated stability of the entire control system considering combined operator-haptic-actuator dynamics. This section describes a design of stable control scheme for telemanipulation of hydraulic actuators in displacement mode. Lyapunov stability control design method is adopted in this work to deal with hydraulic nonlinearities and guarantee the stability [13, 14].

The proposed control scheme consists of two control laws. The control law at the slave side allows the hydraulic actuator to have a stable position tracking in both free and constrained motions. At the master side, the haptic device creates a force that acts like a virtual spring coupling the displacements of the haptic device and the hydraulic actuator. When the actuator moves freely, the virtual spring creates a force indicating to the operator if the slave manipulator is behind/ahead in terms of tracking the master manipulator's displacement. When the actuator is in contact and interacts with an environment, the constraints imposed on its motion are indirectly reflected through this virtual spring force.

5.4.1 Description of controller

The model described in Chapter 3 is employed to design a control scheme capable of regulating the actuator's position, i.e., given a force by the operator and an arbitrary initial condition, the system should approach to an equilibrium point and remain there. The following control laws are proposed to determine values for u and F_m:

$$u = \left[-K_{p1}(x_s - x_m) - K_{p2}(P_L)\right]\sqrt{P_s - sgn(x_{sp})P_L} \tag{5.100}$$

$$F_m = K_{p3}(x_s - x_m) + K_{p4}(P_L) \tag{5.101}$$

In (5.100) and (5.101), K_{p1}, K_{p2}, K_{p3}, and K_{p4} are real positive gains. The first term in Equation (5.101) contributes to producing a feedback to the operator proportional to the position error between master and slave manipulators. This first term notifies the operator about the position error between master and slave devices and constrains the operator's hand to move very fast when the slave manipulator is behind/ahead in tracking master manipulator's displacement. The second term relates to the load pressure, P_L, of the hydraulic actuator. The entire control law helps the operator to feel as if she/he is directly manipulating the hydraulic actuator creating the level of telepresence, or "feel" of the remote site [24]. Similar terms, but scaled by term $\sqrt{P_s - sgn(x_{sp})P_L}$ to ensure stability, are used in calculation of the control signal u, which help the hydraulic actuator to have a stable position tracking.

Using states defined in (3.12) and replacing u and F_m in (3.13) with (5.100) and (5.101), and ignoring F_{fr} for the sake of simplicity, results in the following state space equations:

$$\begin{cases} \dot{x}_1 = x_2 \\ \dot{x}_2 = \dfrac{A}{m_s}x_3 - \dfrac{d}{m_s}x_2 - \dfrac{k_s}{m_s}x_1 \\ \dot{x}_3 = \dfrac{-A}{C}x_2 + \dfrac{c_d w}{C\sqrt{\rho}}x_4\sqrt{P_s - sgn(x_4)x_3} \\ \dot{x}_4 = \dfrac{-1}{\tau}x_4 + \dfrac{k_{sp}}{\tau}\left[-K_{p1}(x_1 - x_5) - K_{p2}(x_3)\right]\sqrt{P_s - sgn(x_4)x_3} \\ \dot{x}_5 = x_6 \\ \dot{x}_6 = \dfrac{1}{m_m}\left(F_h + K_{p3}(x_1 - x_5) + K_{p4}(x_3) - k_d x_6 - k_h x_5\right) \end{cases} \quad (5.102)$$

The control system described by (5.102) is non-smooth. Filippov's solution theory [86, 87] and extension of Lyapunov's second method to non-smooth dynamic systems [89-91] will be used in the next section to study the stability.

5.4.2 Stability analysis

First, Filippov's solution concept is used to cope with the non-smoothness in the system. Then, extended Lyapunov's method is used for stability analysis.

5.4.2.1 Existence, uniqueness, and continuation of Filippov's solution

The dynamic system presented by (5.102) consists of nonlinear differential equations with discontinuous right-hand sides. Here, Filippov's solution concept is used for the non-smooth system described by (5.102). The discontinuity surface of the system described in (5.102) for either non-contact or contact phase is:

$$S_1 := \{\vec{x}: x_1 \neq 0 \; and \; x_4 = 0\} \quad (5.103)$$

The discontinuity surface, S_1, divides the solution region, Ω_{S_1}, into two regions:

$$\Omega_{S_1}^{+} := \{\vec{x}: x_1 \neq 0 \; and \; x_4 > 0\} \tag{5.104}$$

$$\Omega_{S_1}^{-} := \{\vec{x}: x_1 \neq 0 \; and \; x_4 < 0\} \tag{5.105}$$

The right-hand sides of equations in (5.102) are piecewise continuous and defined everywhere in Ω_{S_1}. They are also measurable and bounded. Therefore, equation (5.102) satisfies condition ***B*** of Filippov's solution theory and according to theorems 4 and 5 of Filippov [86], the local existence and continuity of a solution is guaranteed. Next, the uniqueness of the solution is proven. Since the right-hand sides of (5.102) are all continuous before and after the discontinuity surface, and the discontinuity surface, S_1, is smooth and independent of time, conditions ***A***, ***B*** and ***C*** of Filippov's solution theory are satisfied [86, 87]. Following the procedure described in [86], the limiting values of the vector function of the right-hand sides of (5.102), i.e. $f^{+}$and f^{-} when S_1 is approached from $\Omega_{S_1}^{+}$ and $\Omega_{S_1}^{-}$, are:

$$f^{+} = \begin{cases} x_2 \\ \dfrac{A}{m_s}x_3 - \dfrac{d}{m_s}x_2 - \dfrac{k_s}{m_s}x_1 \\ \dfrac{-A}{C}x_2 + \dfrac{c_d w}{C\sqrt{\rho}}x_4\sqrt{P_s - x_3} \\ \dfrac{-1}{\tau}x_4 + \dfrac{k_{sp}}{\tau}\left[-K_{p1}(x_1 - x_5) - K_{p2}(x_3)\right]\sqrt{P_s - x_3} \\ x_6 \\ \dfrac{1}{m_m}\left(F_h + K_{p3}(x_1 - x_5) + K_{p4}(x_3) - k_d x_6 - k_h x_5\right) \end{cases} \tag{5.106}$$

$$f^- = \begin{cases} x_2 \\ \frac{A}{m_s}x_3 - \frac{d}{m_s}x_2 - \frac{k_s}{m_s}x_1 \\ \frac{-A}{C}x_2 + \frac{c_d w}{C\sqrt{\rho}}x_4\sqrt{P_s + x_3} \\ \frac{-1}{\tau}x_4 + \frac{k_{sp}}{\tau}\left[-K_{p1}(x_1 - x_5) - K_{p2}(x_3)\right]\sqrt{P_s + x_3} \\ x_6 \\ \frac{1}{m_m}\left(F_h + K_{p3}(x_1 - x_5) + K_{p4}(x_3) - k_d x_6 - k_h x_5\right) \end{cases} \tag{5.107}$$

The projections of f^+ and f^- along the normal to the discontinuity surface, i.e., $N_{S_1} = \{0,0,0,1,0,0\}$ are denoted by f_N^+ and f_N^-:

$$f_N^+ = + \frac{k_{sp}}{\tau}\left[-K_{p1}(x_1 - x_5) - K_{p2}(x_3)\right]\sqrt{P_s - x_3} \tag{5.108}$$

$$f_N^- = + \frac{k_{sp}}{\tau}\left[-K_{p1}(x_1 - x_5) - K_{p2}(x_3)\right]\sqrt{P_s + x_3} \tag{5.109}$$

From (5.108) and (5.109), f_N^+ and f_N^- have the same sign (note that $\sqrt{P_s \pm x_3}$ is always non-negative). This satisfies conditions of *Lemma 9* of Filippov's solution [86]. Thus, in the domain $\Omega_{S_1}^- + S_1 + \Omega_{S_1}^+$, uniqueness and continuous dependence of the solution on the initial conditions is guaranteed. Note that this proof is valid for both contact and non-contact phases, since k_s only appears in second equation of (5.102) and does not have any effect on f_N^+ and f_N^- in (5.108) and (5.109). For transition phase, however, two different discontinuity surfaces are possible:

$$S_2 := \{\vec{x}: x_1 = 0 \; and \; x_4 \neq 0\} \tag{5.110}$$

$$S_3 := \{\vec{x}: x_1 = 0 \; and \; x_4 = 0\} \tag{5.111}$$

Note that S_3 is the intersection of S_1 and S_2. Uniqueness of Filippov's solution analysis for S_2 can be done in a similar way. Uniqueness analysis of S_3 requires heavier mathematical machinery and is not provided here.

5.4.2.2 Stability proof

For the stability proof, extension of Lyapunov's second method to non-smooth dynamic systems [89], based on Filippov's solution theory, is used. The stability of the system is analyzed for a regulating task in which input F_h is constant. By imposing $\dot{x}_{i\,(i=1..6)} = 0$, the system described by (5.102) is shown to have the following equilibrium point:

$$\vec{x}_{eq} = [x_{1eq} \quad x_{2eq} \quad x_{3eq} \quad x_{4eq} \quad x_{5eq} \quad x_{6eq}]^T = [x_{1ss} \quad 0 \quad x_{3ss} \quad 0 \quad x_{5ss} \quad 0]^T \tag{5.112}$$

where,

$$x_{1ss} = \frac{F_h K_{p1} A}{K_{p2} K_{p3} k_s - K_{p1} K_{p4} k_s + K_{p1} k_h A + K_{p2} k_h k_s} \tag{5.113}$$

$$x_{3ss} = \frac{F_h K_{p1} k_s}{K_{p2} K_{p3} k_s - K_{p1} K_{p4} k_s + K_{p1} k_h A + K_{p2} k_h k_s} \tag{5.114}$$

$$x_{5ss} = \frac{F_h K_{p1} A + F_h K_{p2} k_s}{K_{p2} K_{p3} k_s - K_{p1} K_{p4} k_s + K_{p1} k_h A + K_{p2} k_h k_s} \tag{5.115}$$

Defining $\vec{e} = \vec{x} - \vec{x}_{eq}$ the following error states are then defined:

$$\begin{aligned} \vec{e} &= [e_1 \quad e_2 \quad e_3 \quad e_4 \quad e_5 \quad e_6]^T \\ &= [(x_1 - x_{1ss}) \quad x_2 \quad (x_3 - x_{3ss}) \quad x_4 \quad (x_5 - x_{5ss}) \quad x_6]^T \end{aligned} \tag{5.116}$$

Substituting (5.116) into (5.102), the new state-space model having its equilibrium point at the origin, is obtained:

$$\begin{cases} \dot{e}_1 = e_2 \\ \dot{e}_2 = \dfrac{A}{m_s} e_3 - \dfrac{d}{m_s} e_2 - \dfrac{k_s}{m_s} e_1 \\ \dot{e}_3 = \dfrac{-A}{C} e_2 + \dfrac{c_d w}{C\sqrt{\rho}} e_4 \sqrt{P_s - sgn(e_4)(e_3 + x_{3ss})} \\ \dot{e}_4 = \dfrac{-1}{\tau} e_4 + \dfrac{k_{sp}}{\tau} \left[-K_{p1}(e_1 - e_5) - K_{p2}(e_3)\right] \sqrt{P_s - sgn(e_4)(e_3 + x_{3ss})} \\ \dot{e}_5 = e_6 \\ \dot{e}_6 = \dfrac{1}{m_m} \left(K_{p3}(e_1 - e_5) + K_{p4} e_3 - k_d e_6 - k_h e_5\right) \end{cases} \tag{5.117}$$

Remarks:

Remark 1: The steady-state displacement of the hydraulic actuator is different from the haptic device, by a factor of $(K_{p2}/K_{p1})(k_s/A)$. This is not a problem when there is the human-in-the-loop in the teleoperation system; because operator can always apply more input to allow the slave actuator reaches the desired position. Alternatively to decrease this difference, controller gains can be tuned in such a way to minimize $\left(K_{p2}/K_{p1}\right)$.

Remark 2: During the steady-state, force generated by the haptic device, F_{mss}, is related to the interaction force between the hydraulic actuator and the environment, as follows:

$$F_{mss} = \frac{K_{p1}K_{p4} - K_{p3}K_{p2}}{AK_{p1}} F_{lss} \tag{5.118}$$

From (5.118), it is observed that even though the interaction force is not directly measured, the force generated by the haptic device is proportional to the interaction force. The proportionality gain can be adjusted via controller gains.

To construct a smooth Lyapunov function for the non-smooth system of (5.117), the procedure described by Wu et al. [89] is used. The right-hand sides of (5.117) are discontinuous, but measurable and bounded. The following Lyapunov function is constructed for the system described by (5.117):

$$
\begin{aligned}
&V(e_1, e_2, e_3, e_4, e_5, e_6) \\
&= \left(\frac{7K_{p1}A^2}{16C(K_{p2}A - K_{p1}C)} + \frac{k_s}{2C}\right) e_1^2 \\
&+ \frac{2K_{p1}C + (K_{p2}A - K_{p1}C)}{4(K_{p2}A - K_{p1}C)} e_3^2 + \frac{K_{p1}A}{(K_{p2}A - K_{p1}C)} e_1 e_3 + \frac{m_s}{2C} e_2^2 \\
&+ \frac{Ac_d w\tau}{2k_{sp}C\sqrt{\rho}(K_{p2}A - K_{p1}C)} e_4^2 \\
&+ \frac{K_{p1}A^2}{16C(K_{p2}A - K_{p1}C)} (e_1 - 8e_5)^2 \\
&+ \frac{1}{4}\left(e_3 - \frac{2K_{p1}A}{(K_{p2}A - K_{p1}C)} e_5\right)^2 \\
&+ \frac{\left(-7K_{p1}A^2K_{p3} + K_{p1}A^2k_h\right)\left(K_{p2}A - K_{p1}C\right) - 2K_{p1}^2A^2CK_{p3}}{2CK_{p3}(K_{p2}A - K_{p1}C)^2} e_5^2 \\
&+ \frac{K_{p1}A^2m_m}{2CK_{p3}(K_{p2}A - K_{p1}C)} e_6^2
\end{aligned}
\tag{5.119}
$$

Function V is continuous. Next, V is proven positive and definite. In doing this, some conditions to the controller gains should be applied. Rewriting V as follows:

$$V = V_1 + V_2 \tag{5.120}$$

where:

$$V_1 = \left(\frac{7K_{p1}A^2}{16C(K_{p2}A - K_{p1}C)} + \frac{k_s}{2C}\right)e_1^2 + \frac{2K_{p1}C + (K_{p2}A - K_{p1}C)}{4(K_{p2}A - K_{p1}C)}e_3^2 + \frac{K_{p1}A}{(K_{p2}A - K_{p1}C)}e_1e_3 \tag{5.121}$$

and,

$$V_2 = \frac{m_s}{2C}e_2^2 + \frac{Ac_dw\tau}{2k_{sp}C\sqrt{\rho}(K_{p2}A - K_{p1}C)}e_4^2 + \frac{K_{p1}A^2}{16C(K_{p2}A - K_{p1}C)}(e_1 - 8e_5)^2 + \frac{1}{4}\left(e_3 - \frac{2K_{p1}A}{(K_{p2}A - K_{p1}C)}e_5\right)^2 + \frac{\left(-7K_{p1}A^2K_{p3} + K_{p1}A^2k_h\right)\left(K_{p2}A - K_{p1}C\right) - 2K_{p1}^2A^2CK_{p3}}{2CK_{p3}(K_{p2}A - K_{p1}C)^2}e_5^2 + \frac{K_{p1}A^2m_m}{2CK_{p3}(K_{p2}A - K_{p1}C)}e_6^2 \tag{5.122}$$

V_1 can be re-written in the following form:

$$V_1 = [e_1 \quad e_2]\, Q \begin{bmatrix} e_1 \\ e_2 \end{bmatrix} \tag{5.123}$$

where matrix Q is:

$$Q = \begin{bmatrix} \left(\frac{7K_{p1}A^2}{16C(K_{p2}A - K_{p1}C)} + \frac{k_s}{2C}\right) & \frac{K_{p1}A}{2(K_{p2}A - K_{p1}C)} \\ \frac{K_{p1}A}{2(K_{p2}A - K_{p1}C)} & \frac{2K_{p1}C + (K_{p2}A - K_{p1}C)}{4(K_{p2}A - K_{p1}C)} \end{bmatrix} \tag{5.124}$$

According to the Sylvester's theorem [92], for V_1 to be positive definite, a necessary and sufficient condition for the symmetric matrix Q is that its principal minors, i.e., Q_{11} and $(Q_{11}Q_{22} - Q_{12}Q_{21})$ must be strictly positive. Q_{11} is shown below:

$$Q_{11} = \left(\frac{7K_{p1}A^2}{16C(K_{p2}A - K_{p1}C)} + \frac{k_s}{2C}\right) \tag{5.125}$$

which is strictly positive subject to the following condition:

$$\frac{C}{A} < \frac{K_{p2}}{K_{p1}} \tag{5.126}$$

Term $(Q_{11}Q_{22} - Q_{12}Q_{21})$ is given below:

$$\begin{aligned} &(Q_{11}Q_{22} - Q_{12}Q_{21}) \\ &= \left(\frac{7K_{p1}A^2}{16C(K_{p2}A - K_{p1}C)} + \frac{k_s}{2C}\right)\left(\frac{2K_{p1}C + (K_{p2}A - K_{p1}C)}{4(K_{p2}A - K_{p1}C)}\right) \\ &- \left(\frac{K_{p1}A}{2(K_{p2}A - K_{p1}C)}\right)^2 \end{aligned} \tag{5.127}$$

which can be rewritten in the following form:

$$(Q_{11}Q_{22} - Q_{12}Q_{21}) = k_s \frac{K_{p2}A + K_{p1}C}{8C(K_{p2}A - K_{p1}C)} + \frac{K_{p1}A^2(7K_{p2}A - 9K_{p1}C)}{64C(K_{p2}A - K_{p1}C)^2} \tag{5.128}$$

The first term in (5.128) is positive given condition (5.126). To ensure $(Q_{11}Q_{22} - Q12Q21$ is strictly positive the following condition must hold:

$$\left(7K_{p2}A - 9K_{p1}C\right) > 0 \tag{5.129}$$

which applies the following condition to controller gains:

$$\frac{9C}{7A} < \frac{K_{p2}}{K_{p1}} \tag{5.130}$$

Note that satisfying condition (5.130) guarantees (5.126). For V_2, all terms are positive subject to satisfying condition (5.126), except for term pertaining to e_5^2 which is positive subject to satisfying the following condition:

$$\left(-7K_{p1}A^2K_{p3} + K_{p1}A^2k_h\right)\left(K_{p2}A - K_{p1}C\right) - 2K_{p1}^2A^2CK_{p3} > 0 \tag{5.131}$$

Condition (5.131) leads to the following relation:

$$K_{p3} < \frac{k_h\left(K_{p2}A - K_{p1}C\right)}{\left(7K_{p2}A - 5K_{p1}C\right)} \tag{5.132}$$

Note that using (5.130), the right hand side of (5.132) is positive. Thus, subject to satisfying conditions (5.130) and (5.132), function V is positive definite.

Now, V is proven to be a smooth Lyapunov function and $\dot{V}$ is negative and at least semi-definite. The derivative of V with respect to time is:

$$\begin{aligned}
&\dot{V} \\
&= \left(\frac{7K_{p1}A^2}{8C\left(K_{p2}A - K_{p1}C\right)} + \frac{k_s}{C}\right) e_1\dot{e}_1 + \frac{2K_{p1}C + \left(K_{p2}A - K_{p1}C\right)}{2\left(K_{p2}A - K_{p1}C\right)} e_3\dot{e}_3 \\
&+ \frac{K_{p1}A}{(K_{p2}A - K_{p1}C)}\dot{e}_1 e_3 + \frac{K_{p1}A}{(K_{p2}A - K_{p1}C)} e_1\dot{e}_3 + \frac{m_s}{C} e_2\dot{e}_2 \\
&+ \frac{Ac_d w\tau}{k_{sp}C\sqrt{\rho}(K_{p2}A - K_{p1}C)} e_4\dot{e}_4 + \frac{K_{p1}A^2}{8C(K_{p2}A - K_{p1}C)}(e_1 - 8e_5)(\dot{e}_1 - 8\dot{e}_5) \\
&+ \frac{1}{2}\left(e_3 - \frac{2K_{p1}A}{(K_{p2}A - K_{p1}C)} e_5\right)\left(\dot{e}_3 - \frac{2K_{p1}A}{(K_{p2}A - K_{p1}C)}\dot{e}_5\right) \\
&+ \frac{\left(-7K_{p1}A^2K_{p3} + K_{p1}A^2k_h\right)\left(K_{p2}A - K_{p1}C\right) - 2K_{p1}^2A^2CK_{p3}}{CK_{p3}(K_{p2}A - K_{p1}C)^2} e_5\dot{e}_5 \\
&+ \frac{K_{p1}A^2m_m}{CK_{p3}(K_{p2}A - K_{p1}C)} e_6\dot{e}_6
\end{aligned} \tag{5.133}$$

Replacing $\dot{e}_{i(i=1..6)}$ with right-hand sides of (5.117) and subject to the following condition:

$$K_{p4} = K_{p3}\frac{C}{A} \tag{5.134}$$

it can be shown that (details are not included for the sake of brevity):

$$\dot{V} = -\frac{d}{C}e_2^2 - \frac{Ac_d w}{k_{sp}C\sqrt{\rho}(K_{p2}A - K_{p1}C)}e_4^2 - \frac{k_d K_{p1}A^2}{CK_{p3}(K_{p2}A - K_{p1}C)}e_6^2 \tag{5.135}$$

$\dot{V}$ is continuous; thus, V is a smooth Lyapunov function for the non-smooth system described by (5.117). Moreover, $\dot{V}$ is negative semi-definite. Note that all parameters are positive numbers. Therefore, the control system is stable in the sense of Lyapunov, according to the theorem outlined in [89]. Conditions needed to prove the stability are summarized again for future reference:

$$\frac{9C}{7A} < \frac{K_{p2}}{K_{p1}} \tag{5.136}$$

$$K_{p3} < \frac{k_h\left(K_{p2}A - K_{p1}C\right)}{7K_{p2}A - 5K_{p1}C} \tag{5.137}$$

$$K_{p4} = K_{p3}\frac{C}{A} \tag{5.138}$$

5.4.3 Performance evaluation

The performance of proposed controller in this section is now validated by simulation and experimental studies.

5.4.3.1 Simulation results

Equation (3.13) was used as the system and equations (5.100) and (5.101) were used as controllers. For numerical simulations, 4th order Runge-Kutta method was used in C++ as the integration routine. The parameters used for the simulations are given in Table 3.1. The controller gains were chosen as $K_{p1} = 0.05$, $K_{p2} = 2.1 \times 10^{-11}$, $K_{p3} = 60.0$, and $K_{p4} = 1.8957 \times 10^{-8}$ which satisfy conditions (5.136), (5.137), and (5.138).

The controller gains were chosen based on the following procedure. First, a value for K_{p1} is chosen that is high enough to produce a fast response without saturating the control signal or causing unacceptable overshoots. Next, K_{p2} was chosen to be the smallest value satisfying (5.136). This makes position error between the master and slave smallest, given K_{p1} (see Remark 1 above). Rewriting (5.118) using (5.138), we have:

$$F_{mss} = K_{p3}\left(\frac{C}{A^2} - \frac{K_{p2}}{AK_{p1}}\right)F_{lss} \tag{5.139}$$

From (5.139), the value of K_{p3} is then determined based on the desired scaling factor between F_l and F_m while satisfying condition (5.137). Finally, K_{p4} is determined from (5.138).

In the first test, the input F_h was set to a constant value of 0.4N, and zero initial conditions for all states were chosen, i.e.

$$\vec{x}_{init} = [x_{1init} \quad x_{2init} \quad x_{3init} \quad x_{4init} \quad x_{5init} \quad x_{6init}]^T = [0.0\ \text{mm} \quad 0.0\ \text{m/s} \quad 0.0\ \text{Pa} \quad 0.0\ \text{mm} \quad 0.0\ \text{mm} \quad 0.0\ \text{m/s}]^T \tag{5.140}$$

The goal of this test was to show that the system can reach an equilibrium point for a constant input without interacting with the environment, i.e. free motion or $k_s = 0\text{N/m}$. From (5.112), the equilibrium point of the system was determined to be:

$$\vec{x}_{eq} = [x_{1\text{eq}} \quad x_{2\text{eq}} \quad x_{3\text{eq}} \quad x_{4\text{eq}} \quad x_{5\text{eq}} \quad x_{6\text{eq}}]^T = [40.0\ \text{mm} \quad 0.0\ \text{m/s} \quad 0.0\ \text{Pa} \quad 0.0\ \text{mm} \quad 40.0\ \text{mm} \quad 0.0\ \text{m/s}]^T \tag{5.141}$$

Figure 5.11 shows simulation results for all states. All states can be seen to reach the equilibrium point (5.141). This test shows that system is stable in free motion (non-contact) and will reach the equilibrium point very fast.

This test is then repeated except the hydraulic actuator is interacting with a spring with the stiffness of $k_s = 125\text{kN/m}$, the input F_h was again set to a constant value of 0.4N and system starts from zero initial condition of (5.140). The goal of this test was to show that the system can reach an equilibrium point while interacting with a stiff spring. The equilibrium point of the system was determined to be:

$$\vec{x}_{eq} = [x_{1\text{eq}} \quad x_{2\text{eq}} \quad x_{3\text{eq}} \quad x_{4\text{eq}} \quad x_{5\text{eq}} \quad x_{6\text{eq}}]^T$$
$$= [36.0\ \text{mm} \quad 0.0\ \text{m/s} \quad 7.1\text{MPa} \quad 0.0\ \text{mm} \quad 39.0\ \text{mm} \quad 0.0\ \text{m/s}]^T \tag{5.142}$$

Simulation results are shown in

Figure 5.12. All states can be seen to reach the equilibrium point (5.142). These two tests confirm the theoretical stability analysis performed earlier. The steady state error between master and slave displacements is $\left(\frac{K_{p2}k_s}{K_{p1}A}\right)x_{1ss} < 3\text{mm}$.

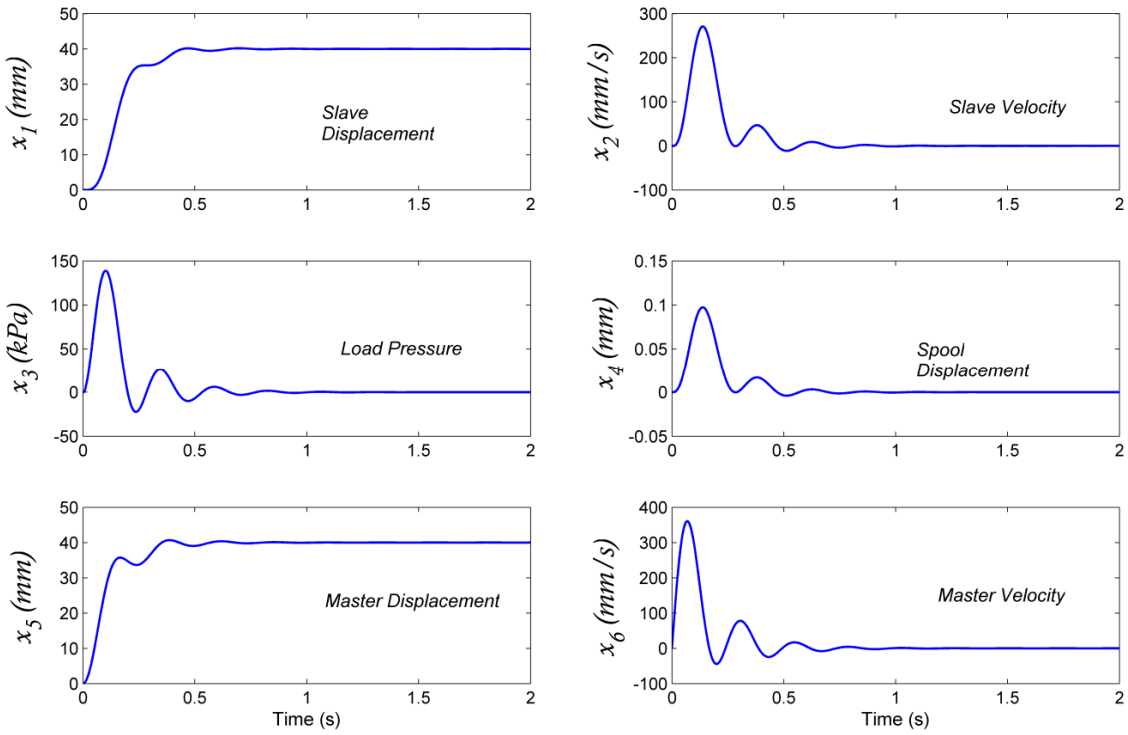

Figure 5.11 Simulation results for a constant operator input ($F_h = 0.4\text{N}$). The hydraulic

actuator moves in free motion (non-contact).

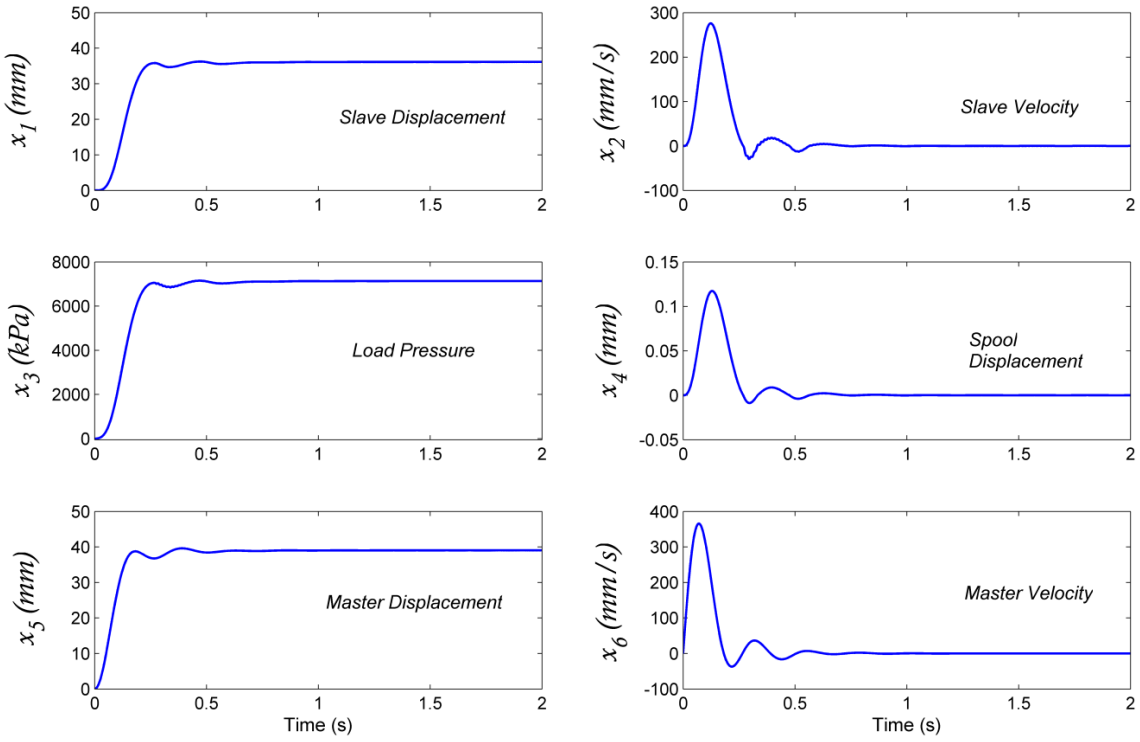

Figure 5.12 Simulation results for a constant operator input ($F_h = 0.4$N). The hydraulic actuator is in contact and interacts with environment having stiffness of $k_s = 125$kN/m.

5.4.3.2 Experimental results

The same controller gains as in the simulations were used. The load pressure, P_L, and the displacement of the hydraulic actuator, x_s, were sent from the slave side to the master. These data were used at the master side to compute the master force, F_m using (5.101). The displacement of the haptic device, x_m , was sent from the master side to the slave to determine the control signal of the hydraulic actuator, u using (5.100). The spring used in the experiments could not travel more than 20mm. Thus, during the experiments, the operator was restricted not to push beyond this limit. Other variables needed by the

controllers were pump pressure, P_s, and differential pressures, P_L, which were easily obtained via on-line measurements.

Experimental results of using the control laws developed in this section are shown on Figure 5.13 to Figure 5.19. With reference to Figure 5.13 and Figure 5.14, the operator applied a command to the haptic device similar to a step displacement. In Figure 5.13, hydraulic actuator moved in free motion (non-contact), while in Figure 5.14, the hydraulic actuator was in contact with the environment having stiffness of $k_s = 180\text{kN/m}$ all the time. As is seen, the system was stable and exhibited acceptable responses in term of position tracking. Note that in Figure 5.14, the error between the master and slave displacements at the steady-state was measured to be approximately 2.1mm which is consistent with the theoretical value that can be obtained from Remark 1.

The experimental results confirm that even though actuator dry friction was not explicitly considered as part of the controllers design, the experimental system performed well. Note that static and Coulomb frictions were estimated to be up to $F_s \approx 1000\text{N}$ and $F_c \approx 500\text{N}$ for the actuator in the test rig. They were estimated by the construction of the static friction-velocity map measured during constant velocity motions [99].

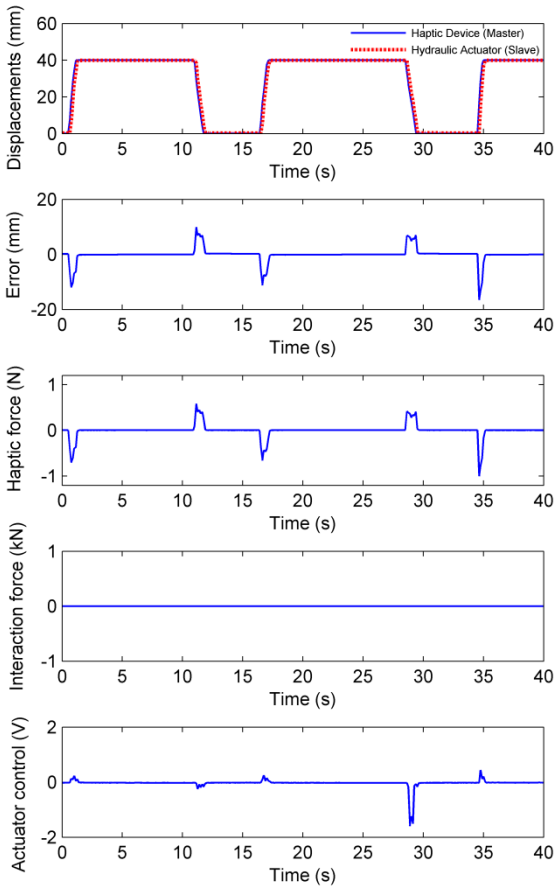

Figure 5.13 Experimental results given step-like operator input. The hydraulic actuator moves in free motion (non-contact).

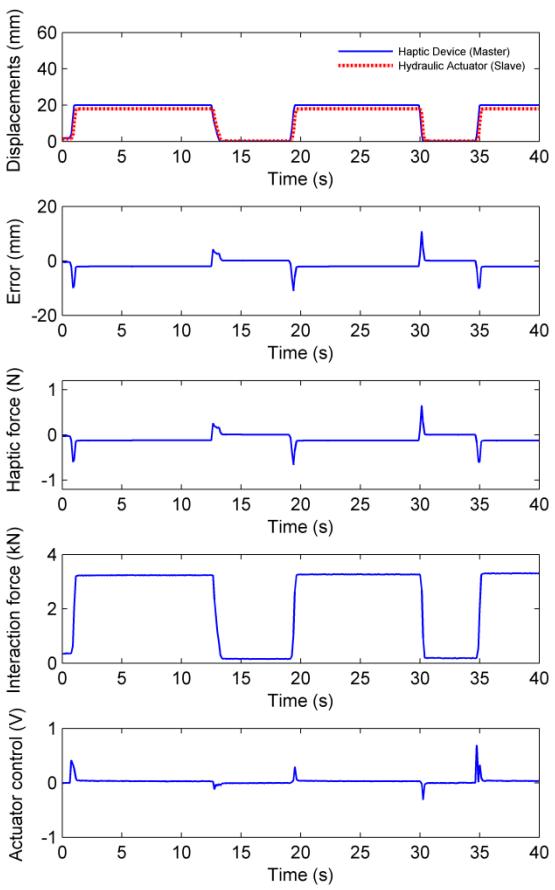

Figure 5.14 Experimental results given step-like operator input. The hydraulic actuator is in contact with the environment having stiffness of $k_s = 180\text{kN/m}$ all the time.

In the next set of experiments, the operator moves the haptic device back and forth. Figure 5.15 shows the results when the hydraulic actuator moved in free motion (non-contact). The displacement tracking error between the haptic device and the hydraulic actuator is roughly 5mm. Figure 5.16 shows results for a test whereby the hydraulic

actuator is pushing against a spring having the same stiffness as in the previous experiment. In both experiments, control signals are within the range and not saturated.

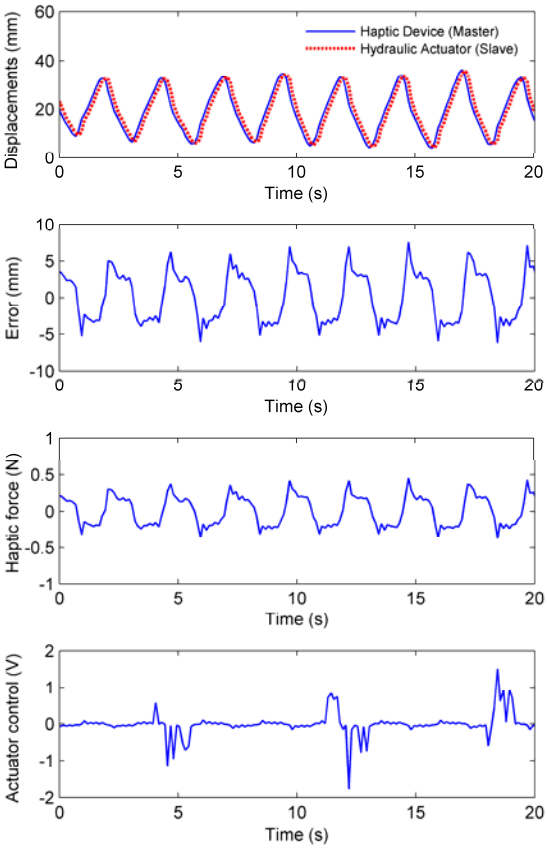

Figure 5.15 Experimental results given sinusoid-like operator input. The hydraulic actuator moves in free motion (non-contact).

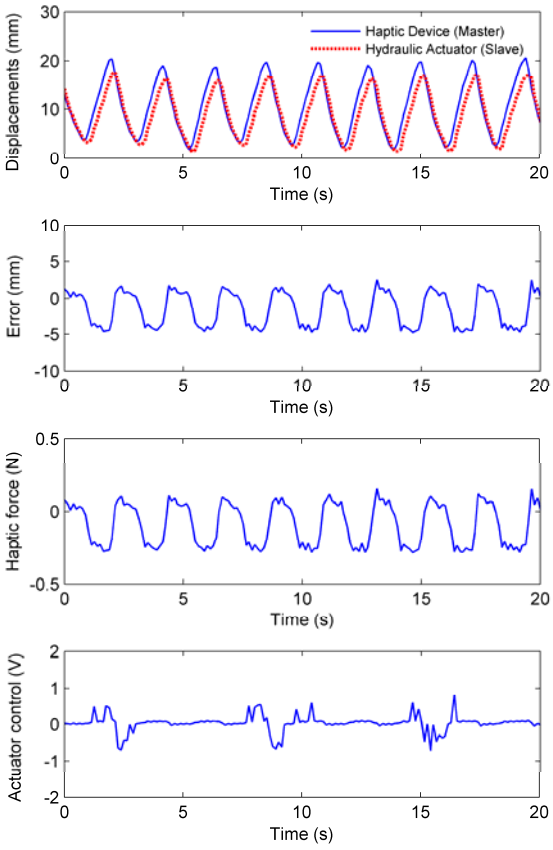

Figure 5.16 Experimental results given sinusoid-like operator input. The hydraulic actuator is in contact with the environment having stiffness of $k_s = 180\text{kN/m}$ all the time.

Figure 5.17 shows results of the next experiment in which the hydraulic actuator starts in free motion and comes in contact with a spring having stiffness of $k_s = 180\text{kN/m}$, at $x_s \approx 20\text{mm}$. As is seen, the system is stable and exhibits good tracking response while providing haptic force feedback to the operator. Plots show only 20-seconds while the actual tests are conducted for much longer.

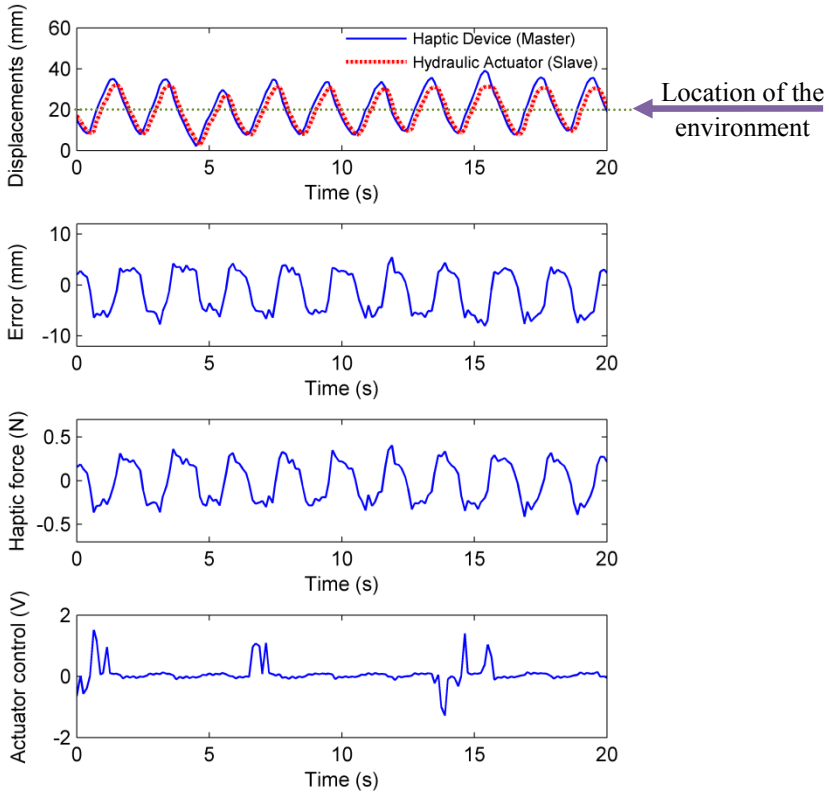

Figure 5.17 Experimental results given sinusoid-like operator input. The hydraulic actuator starts in free motion and makes contact with a spring having stiffness of $k_s = 180\text{kN/m}$ at $x_s \approx 20\text{mm}$. Supply pressure is $P_s = 17.2\text{MPa}$.

The last two experiments are conducted to investigate the effect of the stiffness of the environment and the supply pressure. As is seen on Figure 5.18, increasing the stiffness

of the environment, $k_s = 400\text{kN/m}$, increases the displacement error. In the last experiment, results of which are shown in Figure 5.19, the supply pressure is reduced to $P_s = 6.9\text{MPa}$ which increases the displacement error between the master and the slave, and causes a slower system response, and increases the control signal for the hydraulic actuator.

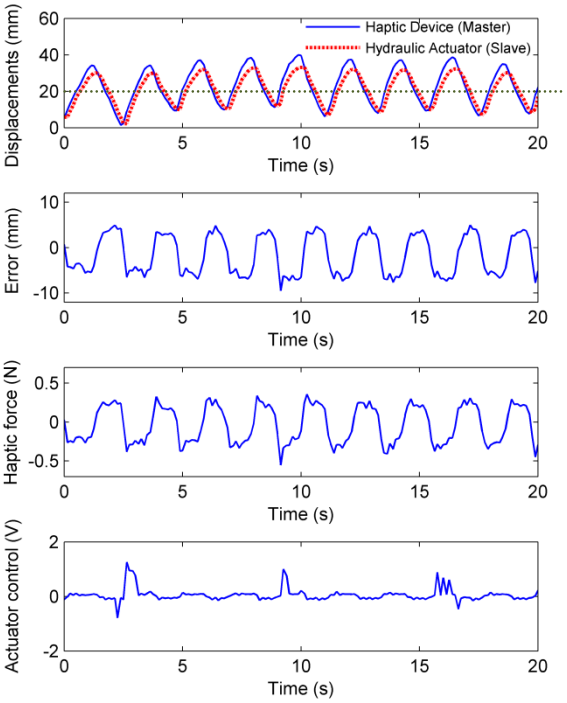

Figure 5.18 Experimental results given sinusoid-like operator input. The hydraulic actuator starts in free motion and makes contact with a spring having stiffness of $k_s = 400\text{kN/m}$ at $x_s \approx 20\text{mm}$. Supply pressure is $P_s = 17.2\text{MPa}$.

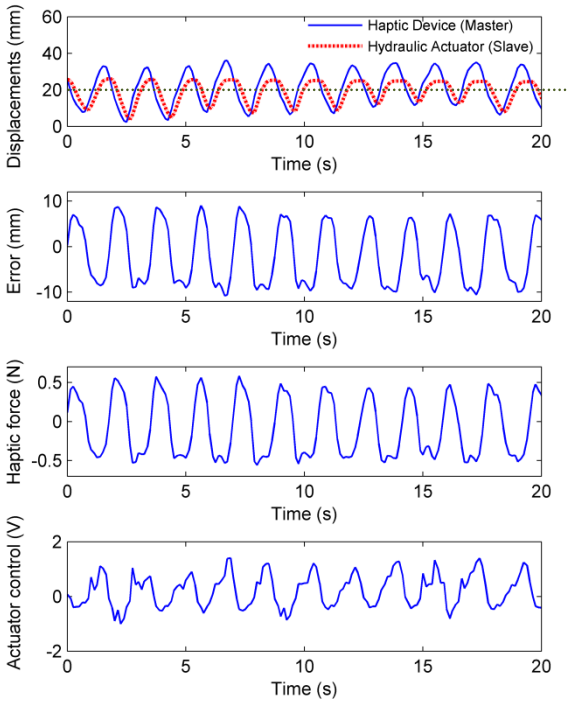

Figure 5.19 Experimental results given sinusoid-like operator input. The hydraulic actuator starts in free motion and makes contact with a spring having stiffness of $k_s = 180\text{kN/m}$ at $x_s \approx 20\text{mm}$. Supply pressure is $P_s = 6.9\text{MPa}$.

5.5 Summary

In this Chapter, three control schemes are designed for bilateral control of hydraulic actuators based on Lyapunov's stability technique. Stability and effectiveness of the proposed control schemes considering nonlinear hydraulic functions, and operator dynamics were analytically proven and experimentally validated. Due to the discontinuity in the control laws, the resulting control systems were non-smooth. Thus, the existence, continuation and uniqueness of the solution were first proven using Filippov's solution theories. The extended Lyapunov's stability theory was used next for the stability analysis of the resulting control systems. Specifically, the extension of LaSalle's invariance principle to non-smooth systems was employed to prove the asymptotic stability of the control systems and convergence of all solution trajectories to the equilibrium point. Simulation results were presented, which confirmed that the controller could effectively stabilize the system and have good position tracking at the slave side while providing haptic feel at the master side. Experiments were conducted to verify the practicality of the proposed control systems.

The first controller was designed in force-mode control for constrained motion. The force applied to the human operator by the haptic device, was scaled based on the maximum expected interaction force between the hydraulic actuator and the environment and the maximum force that can be generated by the haptic device. This controller can be used only for constrained motion, i.e., when hydraulic actuator is in contact and interacts with the environment all the time. Thus, the next controller was designed in Section 5.3 as a complement to the previous controller for unconstrained or free motion of the hydraulic

actuator.

The third controller, designed in Section 5.4, was based on position information of master and slave devices. This controller is the best choice in applications in which installing a force sensor on the end-effector of the hydraulic manipulator is not practical. In such applications, it is better to use position information instead of interaction force information measured by the force sensor installed at the implement. This type of haptic force can help the operator to "feel" the environment based on the position information. This haptic force notifies the operator about the position error between the master and slave manipulators and produces an opposing force to the operator's hand when the slave manipulator is behind/ahead in tracking master manipulator's displacement. This helps the operator to feel that he/she controls the hydraulic actuator by his/her own hand which in turn improves the level of telepresence, or the "feel" of the remote site available to the operator via the teleoperation system.

The results of this chapter contribute to enhancing the operator's ability to carry out stable bilateral teleoperation of hydraulic robots where physical presence of the human operator in the task environment is an issue.

Chapter 6

6 CONCLUDING REMARKS

6.1 Contributions of this thesis

Stability proven bilateral control schemes for haptic-enabled control of hydraulic actuators was designed and implemented in this thesis. The stability of the entire control system was proven analytically and the controller was validated by experimental results. Both unilateral and bilateral teleoperation of hydraulic manipulators has been thoroughly investigated in this thesis.

On the unilateral control front, the concept of virtual fixtures was adopted in this thesis to provide haptic feel for the operator. In unilateral telemanipulation, position accuracy is one of the most important issues that should be addressed. One source of inaccuracy in

position is the operator performance. Using the concept of virtual fixtures can effectively minimize the operator's errors in performing tasks which require general path tracing. Thus, the concept of virtual fixtures is adopted in this research to minimize these errors. The system combines the accuracy, power, and good performance of the robot with the intelligence of the operator. In this thesis, the application was towards live transmission line maintenance. A number of maintenance tasks were identified and proper virtual fixtures for many tasks were designed. All identified tasks were performed successfully by all operators using the experimental teleoperation test rig designed in this thesis. Different operators having different skills have performed maintenance tasks and they completed the tasks in a reasonable time. Using the system was very easy and special training was necessary. Expert linemen from Manitoba Hydro stated that using the haptic virtual fixture and the robotic system has the following advantages: it is easy to understand how the system works in general; it was easy to learn using the system and no special training is necessary; the virtual fixtures' concept is helpful in performing the tasks; it reduces the physical labor on the operator's body as compared to manual tasks; even novice linemen can use this system very easily.

On the bilateral control front, the extension of Lyapunov stability theory to non-smooth systems, based on Filippov's solution theory, was used to design a number of control schemes. Nonlinear hydraulic functions and the operator's dynamics were included in the analysis. Different types of haptic sensation were provided by proposed control schemes to the operator based on the reflected interaction force between the hydraulic actuator and the task environment or the position error between the haptic device and the hydraulic actuator positions. For the hydraulic actuator, both position-mode and force-mode control

methods were investigated. Proposed control schemes can be used in a wide variety of applications even if the interaction force between the hydraulic actuator and the task environment cannot be measured.

Individual theoretical stability of all control schemes were thoroughly investigated considering nonlinear hydraulic functions, servovalve dynamics, haptic device dynamics, human operator dynamics, and dynamics of the task environment in the analysis. All control schemes were individually tested experimentally on a hydraulic test rig to verify their practicality and effectiveness in real applications.

The results of this thesis contribute to enhancing the operator's ability to carry out stable haptic teleoperation of hydraulic robots where physical presence of the human operator in the task environment is an issue.

6.2 Future work

This work could be extended in many ways including but not limited to the following subjects:

- The model of the environment, currently assumed to be stationary, can be extended to a moving environment with a separate dynamics which can also be time varying.
- It would be instructive to design Lyapunov-based control schemes using the original hydraulic equations without imposing assumptions on the piston initial position and range of movements.
- A second order system can be used for servovalve dynamics.

- The hydraulic actuator's dry friction can be considered in dynamic equations.
- Results can be extended to multi-degree-of-freedom hydraulic manipulators.
- Instead of using measured interaction force between the hydraulic actuator and the task environment, the pressure information can be used to estimate this interaction force.
- The effect of delay and packet loss in the communication link can be considered and analyzed in designing new controllers for the system.

REFERENCES

[1] M. E. Kontz, J. Beckwith and W. J. Book, "Evaluation of a teleoperated haptic forklift," in *IEEE/ASME International Conference on Advanced Intelligent Mechatronics,* 2005, pp. 295-300.

[2] S. Tafazoli, S. E. Salcudean, K. Hashtrudi-Zaad and P. D. Lawrence, "Impedance control of a teleoperated excavator," *IEEE Transactions on Control System Technology,* vol. 10, pp. 355-367, 2002.

[3] E. Papadopoulos, B. Mu and R. Frenette, "On modeling, identification, and control of a heavy-duty electrohydraulic harvester manipulator," *IEEE/ASME Transactions on Mechatronics,* vol. 8, pp. 178-187, 2003.

[4] H. E. Merritt, *Hydraulic Control Systems*. NY: John Wiley, 1967.

[5] N. R. Parker, S. E. Salcudean and P. D. Lawrence, "Application of force feedback to heavy duty hydraulic machines," in *Proceedings of IEEE International Conference on Robotics and Automation,* 1993, pp. 375-381.

[6] M. E. Kontz and W. J. Book, "Position/rate haptic control of a hydraulic forklift," in *ASME International Mechanical Engineering Congress,* 2003, pp. 801-808.

[7] M. E. Kontz, M. C. Herrera, J. D. Huggins and W. J. Book, "Impedance shaping for improved feel in hydraulic systems," in *ASME International Mechanical Engineering Congress and Exposition,* 2008, pp. 185-194.

[8] J. K. Salisbury and M. A. Srinivasan, "Phantom-based haptic interaction with virtual objects," *IEEE Computer Graphics and Applications,* vol. 17, pp. 6-10, 1997.

[9] O. Y. Ming, D. V. Beard and F. P. Brooks Jr., "Force display performs better than visual display in simple 6-D docking task," in *IEEE International Conference on Robotics and Automation,* 1989, pp. 1462-1466.

[10] W. J. Book, "Haptics for and by Hydraulics," in *the 16th IEEE International Symposium on Robot and Human Interactive Communication,* 2007, pp. 1-2.

[11] B. Heinrichs, N. Sepehri and A. Thornton-Trump, "Position-based impedance control of an industrial hydraulic manipulator," *IEEE Control Systems Magazine,* vol. 17, pp. 46-52, 1997.

[12] M. R. Sirouspour and S. E. Salcudean, "On the nonlinear control of hydraulic servo-systems," in *IEEE International Conference on Robotics and Automation,* 2000, pp. 1276-1282.

[13] A. Alleyne and R. Liu, "A simplified approach to force control for electro-hydraulic systems," *Control Engineering Practice,* vol. 8, pp. 1347-1356, 2000.

[14] M. R. Sirouspour and S. E. Salcudean, "Nonlinear control of hydraulic robots," *IEEE Transactions on Robotics and Automation,* vol. 17, pp. 173-182, 2001.

[15] P. F. Hokayem and M. W. Spong, "Bilateral teleoperation: An historical survey," *Automatica,* vol. 42, pp. 2035-2057, 2006.

[16] H. Kang, Y. S. Park, T. F. Ewing, E. Faulring and J. E. Colgate, "Visually and haptically augmented teleoperation in DD tasks using virtual fixtures," in *10th International Conference on Robotics and Remote Systems for Hazardous Environments,* 2004, pp. 466-471.

[17] N. Turro, O. Khatib and E. Coste-Maniere, "Haptically augmented teleoperation," in *IEEE International Conference on Robotics and Automation,* 2001, pp. 386-392.

[18] S. Payandeh and Z. Stanisic, "On application of virtual fixtures as an aid for telemanipulation and training," i*n Proceedings of 10th Symposium on Haptic Interfaces for Virtual Environment and Teleoperator Systems,* 2002*,* pp. 18-23.

[19] C. A. Moore Jr., M. A. Peshkin and J. E. Colgate, "Cobot implementation of virtual paths and 3-D virtual surfaces," *IEEE Transactions on Robotics and Automation,* vol. 19, pp. 347-351, 2003.

[20] J. J. Abbott and A. M. Okamura, "Pseudo-admittance bilateral telemanipulation with guidance virtual fixtures," *International Journal of Robotics Research,* pp. 865-884, 2007.

[21] P. Marayong, A. Bettini and A. Okamura, "Effect of virtual fixture compliance on human-machine cooperative manipulation," in *IEEE/RSJ International Conference on Intelligent Robots and Systems,* 2002, pp. 1089-1095.

[22] V. Eduardo, K. Khokar, R. Alqasemi and R. Dubey, "Laser assisted real time and scaled telerobotic control of a manipulator for defense and security applications," in *Proceedings of the SPIE (The International Society for Optical Engineering) Unmanned Systems Technology XI,* 2009, vol. 7332, pp. 11.

[23] J. J. Abbott and A. M. Okamura, "Stable forbidden-region virtual fixtures for bilateral telemanipulation," *Transactions of the ASME, Journal of Dynamic Systems, Measurement and Control,* vol. 128, pp. 53-64, 2006.

[24] D. A. Lawrence, "Stability and transparency in bilateral teleoperation," *IEEE Transactions on Robotics and Automation,* vol. 9, pp. 624-637, 1993.

[25] B. Hannaford, "Stability and performance tradeoffs in bi-lateral telemanipulation," in *Proceedings of IEEE International Conference on Robotics and Automation,* 1989, vol. 3*,* pp. 1764-1767.

[26] K. Zarei-nia, G. A. Yazdanpanah, N. Sepehri and W. Fung, "Experimental evaluation of bilateral control schemes applied to hydraulic actuators: a comparative study." *Transactions of the Canadian Society for Mechanical Engineering,* vol. 33, pp. 377-398, 2009.

[27] A. Bonchis, P. I. Corke and D. C. Rye, "Experimental evaluation of position control methods for hydraulic systems," *IEEE Transactions on Control Systems Technology,* vol. 10, pp. 876-882, 2002.

[28] K. Toussaint, N. Pouliot and S. Montambault, "Transmission line maintenance robots capable of crossing obstacles: State-of-the-art review and challenges ahead," *Journal of Field Robotics,* vol. 26, pp. 477-499, 2009.

[29] M. Boyer, "Systems integration in telerobotics: Case study: Maintenance of electric power lines," in *Proceedings of IEEE International Conference on Robotics and Automation,* 1996, vol. 2, pp. 1042-1047.

[30] J. Lessard, J. Robert and P. Rondot, "Evaluation of working techniques using teleoperation for power line maintenance," in *Telemanipulator and Telepresence Technologies,* 1994, pp. 88-98.

[31] G. Clement, "An overview of CAT control in nuclear services," in *Proceedings of IEEE International Conference on Robotics and Automation,* 1985, vol. 2, pp. 713-718.

[32] M. Tavakoli, R. V. Patel and M. Moallem, "A force reflective master-slave system for minimally invasive surgery," in *IEEE/RSJ International Conference on Intelligent Robots and Systems,* 2003, pp. 3077-3082.

[33] A. J. Madhani, "The Black Falcon: a teleoperated surgical instrument for minimally invasive surgery," in *Proceedings of IEEE/RSJ International Conference on Intelligent Robots and Systems,* 1998, vol. 2, pp. 936-944.

[34] L. Sun, F. Van Meer, Y. Bailly and C. K. Yeung, "Design and development of a da Vinci surgical system simulator," in *IEEE International Conference on Mechatronics and Automation,* 2007, pp. 1050-1055.

[35] A. Baheti, "RoSS: virtual reality robotic surgical simulator for the da Vinci surgical system," in *Symposium on Haptic Interfaces for Virtual Environment and Teleoperator Systems,* 2008, pp. 479-480.

[36] Y. Matsumoto, "Dexterous manipulation in constrained bilateral teleoperation using controlled supporting point," *IEEE Transactions on Industrial Electronics,* vol. 54, pp. 1113-1121, 2007.

[37] F. Najafi and N. Sepehri, "A novel hand-controller for remote ultrasound imaging," *Mechatronics,* vol. 18, pp. 578-590, 2008.

[38] J. Funda, "A symbolic teleoperator interface for time-delayed underwater robot manipulation," in *Proceedings of Ocean Technologies and Opportunities in the Pacific for the 90's,* 1991, pp. 1526-1533.

[39] N. Diolaiti, "Teleoperation of a mobile robot through haptic feedback," in *IEEE International Workshop on Haptic Virtual Environments and their Applications,* 2002*,* pp. 67-72.

[40] Sun-Gi Hong, "Generating artificial force for feedback control of teleoperated mobile robots," in *Proceedings of IEEE/RSJ International Conference on Intelligent Robots and Systems*, 1999, vol. 3, pp. 1721-1726.

[41] J. Lim, J. Ko and J. Lee, "Internet-based teleoperation of a mobile robot with force-reflection," in *Proceedings of IEEE Conference on Control Applications,* 2003, pp. 680-685.

[42] O. J. Rosch, K. Schilling and H. Roth, "Haptic interfaces for the remote control of mobile robots," *Control Engineering Practice,* vol. 10, pp. 1309-1313, 2002.

[43] M. Boukhnifer, "Scaled teleoperation controller design for micromanipulation over Internet," in *Proceedings of IEEE International Conference on Robotics and Automation,* 2004, vol. 5, pp. 4577-4583.

[44] J. J. Abbott, G. D. Hager and A. M. Okamura, "Steady-hand teleoperation with virtual fixtures," in *The 12th IEEE International Workshop on Robot and Human Interactive Communication,* 2003, pp. 145-151.

[45] L. B. Rosenberg, "Virtual fixtures: Perceptual tools for telerobotic manipulation," in *Proceedings of IEEE Virtual Reality Annual International Symposium,* 1993, pp. 76-82.

[46] M. Li, M. Ishii and R. H. Taylor, "Spatial motion constraints using virtual fixtures generated by anatomy," *IEEE Transactions on Robotics,* vol. 23, pp. 4-19, 2007.

[47] A. Bettini, P. Marayong, S. Lang, A. M. Okamura and G. D. Hager, "Vision-assisted control for manipulation using virtual fixtures," *IEEE Transactions on Robotics,* vol. 20, pp. 953-966, 2004.

[48] R. J. Anderson, "Bilateral control of teleoperators with time delay," *IEEE Transactions on Automatic Control,* vol. 34, pp. 494-501, 1989.

[49] P. Arcara and C. Melchiorri, "Control schemes for teleoperation with time delay: A comparative study," *Robotics and Autonomous Systems,* vol. 38, pp. 49-64, 2002.

[50] T. Itoh, "Human-machine cooperative telemanipulation with motion and force scaling using task-oriented virtual tool dynamics," *IEEE Transactions on Robotics and Automation,* vol. 16, pp. 505-516, 2000.

[51] J. E. Colgate, "Robust impedance shaping telemanipulation," *IEEE Transactions on Robotics and Automation,* vol. 9, pp. 374-384, 1993.

[52] T. B. Sheridan, "Telerobotics," *Automatica,* vol. 25, pp. 487-507, 1989.

[53] T. B. Sheridan, "Space teleoperation through time delay: Review and prognosis," *IEEE Transactions on Robotics and Automation,* vol. 9, pp. 592-606, 1993.

[54] W. J. Book, H. Lane, L. J. Love, D. P. Magee and K. Obergfell, "A novel teleoperated long-reach manipulator testbed and its remote capabilities via the internet," in *Proceedings of IEEE International Conference on Robotics and Automation,* 1996, pp. 1036-1041.

[55] P. D. Lawrence, S. E. Salcudean, N. Sepehri, D. Chan, S. Bachmann, N. Parker, M. Zhu and R. Frenette, "Coordinated and force-feedback control of hydraulic excavators," in *Proceedings of 4th International Symposium on Experimental Robotics,* 1997, pp. 181-194.

[56] P. Sekhavat, N. Sepehri and Q. Wu, "Impact stabilizing controller for hydraulic actuators with friction: Theory and experiments," *Control Engineering Practice,* vol. 14, pp. 1423-1433, 2006.

[57] P. Sekhavat, Q. Wu and N. Sepehri, "Impact control in hydraulic actuators," *Transactions of the ASME. Journal of Dynamic Systems, Measurement and Control,* vol. 127, pp. 197-205, 2005.

[58] N. Niksefat, C. Q. Wu and N. Sepehri, "Design of a Lyapunov controller for an electro-hydraulic actuator during contact tasks," *Transactions of the ASME, Journal of Dynamic Systems, Measurement and Control,* vol. 123, pp. 299-307, 2001.

[59] A. Halanay, C. A. Safta, F. Ursu and I. Ursu, "Stability analysis for a nonlinear model of a hydraulic servomechanism in a servoelastic framework," *Nonlinear Analysis: Real World Applications,* vol. 10, pp. 1197-1209, 2009.

[60] P. Sekhavat, Q. Wu and N. Sepehri, "Lyapunov-based friction compensation for accurate positioning of a hydraulic actuator," in *Proceedings of the American Control Conference,* 2004, pp. 418-423.

[61] M. R. Sirouspour and S. E. Salcudean, "Nonlinear control of hydraulic robots," *IEEE Transactions on Robotics and Automation,* vol. 17, pp. 173-182, 2001.

[62] M. A. B. Cunha, "Adaptive cascade controller applied to a hydraulic actuator," in *International Conference on Control and Automation,* 2005, pp. 622-627.

[63] O. Becker, I. Pietsch and J. Hesselbach, "Robust task-space control of hydraulic robots," in *Proceedings of IEEE International Conference on Robotics and Automation,* 2003, pp. 4360-4365.

[64] S. Montambault and N. Pouliot, "The HQ LineROVer: Contributing to innovation in transmission line maintenance," in *Proceedings of the IEEE International Conference on Transmission and Distribution Construction and Live Line Maintenance,* 2003, pp. 33-41.

[65] N. Pouliot and S. Montambault, "LineScout technology: From inspection to robotic maintenance on live transmission power lines," in *IEEE International Conference on Robotics and Automation,* 2009, pp. 1034-1040.

[66] K. Tsukahara, Y. Tanaka, Yingxin He, R. Hori, K. Mano, A. Hibino, Y. Taru and K. Tatsuno, "An experimental robot system for power distribution line maintenance robots - system architecture and bolt insertion experiment," in *IEEE/RSJ International Conference on Intelligent Robots and Systems,* 2008, pp. 1730-1736.

[67] R. Aracil, L. F. Penin, M. Feme, L. M. Jimenez, A. Barrientos, A. Santamaria, P. Martinez and A. Tudun, "ROBTET: A new teleoperated system for live-line maintenance," in *Proceedings of IEEE 7th International Conference on Transmission and Distribution Construction, Operation and Live-Line Maintenance,* 1995, pp. 205-211.

[68] K. Takaoka, K. Yokoyama, H. Wakisako, K. Yano, K. Higashijima and S. Murakami, "Development of the fully-automatic live-line maintenance robot-phase III," in *Proceedings of the IEEE International Symposium on Assembly and Task Planning (ISATP) Assembly and Disassembly in the Twenty-First Century,* 2001, pp. 423-428.

[69] S. Lu, P. Ma, L. Bingqiang and X. BiCui, "Live woking robot for power distribution systems," in *Proceedings of 4th International Conference on Control and Automation,* 2003, pp. 906-910.

[70] N. Sepehri, A. A. Khayyat and B. Heinrichs, "Development of a nonlinear PI controller for accurate positioning of an industrial hydraulic manipulator," *Mechatronics,* vol. 7, pp. 683-700, 1997.

[71] Y. Yokokohji, "Bilateral control of master-slave manipulators for ideal kinesthetic coupling-formulation and experiment," *IEEE Transactions on Robotics and Automation,* vol. 10, pp. 605-620, 1994.

[72] I. Aliaga, A. Rubio and E. Sanchez, "Experimental quantitative comparison of different control architectures for master-slave teleoperation," *IEEE Transactions on Control Systems Technology,* vol. 12, pp. 2-11, 2004.

[73] A. Abdossalami and S. Sirouspour, "Adaptive control for improved transparency in haptic simulations," *IEEE Transactions on Haptics,* vol. 2, pp. 2-14, 2009.

[74] G. J. Raju, "Design issues in 2-port network models of bilateral remote manipulation," in *Proceedings of IEEE International Conference on Robotics and Automation,* 1989, vol. 3, pp. 1316-1321.

[75] G. A. V. Christiansson and D. H. Van, "The low-stiffness teleoperator slave - A trade-off between stability and performance," *International Journal of Robotics Research,* vol. 26, pp. 287-299, 2007.

[76] D. A. Lawrence and J. D. Chapel, "Performance trade-offs for hand controller design," in *Proceedings of IEEE International Conference on Robotics and Automation,* 1994, vol. 4, pp. 3211-3216.

[77] M. Karpenko, N. Sepehri and J. Anderson, "Decentralized coordinated motion control of two hydraulic actuators handling a common object," *Transactions of the ASME. Journal of Dynamic Systems, Measurement and Control,* vol. 129, pp. 729-741, 2007.

[78] N. Niksefat, N. Sepehri and Q. Wu, "Design and experimental evaluation of a QFT contact task controller for electro-hydraulic actuators," *International Journal of Robust and Nonlinear Control,* vol. 17, pp. 225-250, 2007.

[79] A. G. Alleyne and R. Liu, "Systematic control of a class of nonlinear systems with application to electrohydraulic cylinder pressure control," *IEEE Transactions on Control Systems Technology,* vol. 8, pp. 623-634, 2000.

[80] R. Liu and A. Alleyne, "Nonlinear force/pressure tracking of an electrohydraulic actuator," *Transactions of the ASME, Journal of Dynamic Systems, Measurement and Control,* vol. 122, pp. 232-237, 2000.

[81] M. Jerouane, N. Sepehri and F. Lamnabhi-Lagarrigue, "Dynamic analysis of variable structure force control of hydraulic actuators via the reaching law approach," *International Journal of Control,* vol. 77, pp. 1260-1268, 2004.

[82] L. An and N. Sepehri, "Leakage fault detection in hydraulic actuators subject to unknown external loading," *International Journal of Fluid Power,* vol. 9, pp. 15-25, 2008.

[83] T. Tsuji, P. G. Morasso, K. Goto and K. Ito, "Human hand impedance characteristics during maintained posture," *Biological Cybernetics,* vol. 72, pp. 475-485, 1995.

[84] M. C. Pierre and R. F. Kirsch, "Measuring dynamic characteristics of the human arm in three dimensional space," in *Annual Fall Meeting of the Biomedical Engineering Society,* 2002, pp. 2558-2560.

[85] K. Zarei-nia, X. Yang, P. Irani and N. Sepehri, "Evaluating factors that influence path tracing with passive haptic guidance," in *Proceedings of 4th International Conference on Haptic and Audio Interaction Design,* 2009, pp. 21-30.

[86] A. F. Filippov, "Differential equations with discontinuous right-hand side." *American Mathematical Society Translations,* vol. 42, pp. 199-231, 1964.

[87] A. F. Filippov, "Differential equations with second members discontinuous on intersecting surfaces." *Differential Equations,* vol. 15, pp. 1292-1299, 1980.

[88] Q. Wu, N. Sepehri, A. Thornton-Trump and S. Onyshko, "An extended integral method to derive Lyapunov functions for nonlinear systems," *International Journal of Control,* vol. 62, pp. 717-736, 1995.

[89] Q. Wu, S. Onyshko, N. Sepehri and A. Thornton-Trump, "On construction of smooth Lyapunov functions for non-smooth systems," *International Journal of Control,* vol. 69, pp. 443-457, 1998.

[90] Q. Wu and N. Sepehri, "On Lyapunov's stability analysis of non-smooth systems with applications to control engineering," *International Journal of Non-Linear Mechanics,* vol. 36, pp. 1153-1161, 2001.

[91] D. Shevitz and B. Paden, "Lyapunov stability theory of nonsmooth systems," *IEEE Transactions on Automatic Control,* vol. 39, pp. 1910-1914, 1994.

[92] J. J. Slotine and W. Li, *Applied Nonlinear Control.* Englewood Cliffs, NJ: Prentice-Hall Inc., 1991.

[93] P. A. Prokopiou, S. G. Tzafestas and W. S. Harwin, "A novel scheme for human-friendly and time-delays robust neuropredictive teleoperation," *Journal of Intelligent and Robotic Systems: Theory and Applications,* vol. 25, pp. 311-340, 1999.

[94] N. Sepehri, "Demonstration of an aspect of data acquisition in mechatronics education," *International Journal of Engineering Education,* vol. 17, pp. 538-45, 2001.

[95] K. Zarei-nia, N. Sepehri and Q. Wu, "A Lyapunov controller for stable haptic manipulation of hydraulic actuators," in press, *International Journal of Robust and Nonlinear Control,* DOI: 10.1002/rnc.1680, 2011.

[96] K. Zarei-nia, N. Sepehri, T. Olson and W. Mueller, "Haptic-enabled control of hydraulic manipulators applied to power line maintenance: Concept implementation," in *1st International Conference on Applied Robotics for the Power Industry,* 2010, pp. 6.

[97] W. S. Kim, "Developments of new force reflecting control schemes and an application to a teleoperation training simulator," in *Proceedings of IEEE International Conference on Robotics and Automation,* 1992, pp. 1412-1419.

[98] K. Zarei-nia, A. Y. Goharrizi, N. Sepehri and W. Fung, "Experimental evaluation of two bilateral control schemes applied to a tele-operated hydraulic actuator," in *ASME Dynamic Systems and Control Conference,* 2009, pp. 1265-1271.

[99] L. Marton, S. Fodor and N. Sepehri, "A practical method for friction identification in hydraulic actuators," *Mechatronics,* vol. 21, pp. 350-356, 2011.

[100] N. Hogan, "Impedance control: an approach to manipulation. I. Theory," *Transactions of the ASME, Journal of Dynamic Systems, Measurement and Control,* vol. 107, pp. 1-7, 1985.

[101] N. Hogan, "Impedance control: an approach to manipulation. II. Implementation," *Transactions of the ASME, Journal of Dynamic Systems, Measurement and Control,* vol. 107, pp. 8-16, 1985.

[102] N. Hogan, "Impedance control: an approach to manipulation. III. Applications," *Transactions of the ASME, Journal of Dynamic Systems, Measurement and Control,* vol. 107, pp. 17-24, 1985.

APPENDIX: LYAPUNOV STABILITY[6]

Lyapunov's stability theory is a powerful tool to prove the stability of nonlinear systems. In this appendix, a brief explanation about Lyapunov stability is provided. First, some terms used in Lyapunov stability are defined, and then, Lyapunov's stability is explained [92].

Autonomous and non-autonomous systems

An autonomous system is a system of ordinary differential equation of the form:

$$\frac{d}{dt}x(t) = f\big(x(t)\big)$$

or more simply $\dot{x} = f(x)$, in which $x(t)$ is the state vector $(n \times 1)$ and t is time (scalar). For nonlinear systems, f is a nonlinear vector function $(n \times 1)$. It means the rate of the state vector x is a function of x only, in other words, the system is time-invariant. The function f does not depend explicitly on time. It should be distinguished from systems of differential equations of the form:

$$\frac{d}{dt}x(t) = f(x(t), t)$$

or more simply $\dot{x} = f(x, t)$, in which the independent variable t explicitly appears in the function, or the system is time-variant. Such systems are not autonomous, or so-called non-autonomous.

---

[6] Contents of this appendix are obtained from: J. J. Slotine and W. Li, *Applied Nonlinear Control.* Englewood Cliffs, NJ: Prentice-Hall, Inc., 1991.

A special class of nonlinear systems are linear systems. The linear system can be shown as:

$\dot{x} = Ax$

where matrix A is a $(n \times n)$ matrix which can be dependent or independent of time, i.e. non-autonomous or autonomous, respectively.

Equilibrium point

The point $\hat{x} \in \mathbb{R}^n$ is an equilibrium point for the differential equation:

$\dot{x} = f(x, t)$

If $f(\hat{x}, t) = 0$ for all t. It means once $x(t_1) = \hat{x}$ then it remains there for ever, i.e. $\{x(t) = \hat{x},\ for\ t \geq t_1\}$. Equilibrium point (or points) can be found by solving this equation: $\dot{x} = 0$. We usually transform the system differential equations in such a way to have the equilibrium point as the origin of the state space.

Lyapunov stability

Consider an autonomous nonlinear dynamical system as follows:

$\dot{x} = f(x(t)), \quad x(0) = x_0$

where $x(t) \in \mathcal{M} \subseteq \mathbb{R}^n$ denotes the system state vector, $\mathcal{M}$ is an open set containing the origin, and $f: \mathcal{M} \to \mathbb{R}^n$ continuous on $\mathcal{M}$. Suppose that x_{eq} is an equilibrium point of function.

1. The equilibrium point of the above system is said to be Lyapunov stable if for every $\varepsilon > 0$, there exists a $\delta(\varepsilon) > 0$, such that, if $\|x(0) - x_{eq}\| < \delta(\varepsilon)$, then $\|x(t) - x_{eq}\| < \varepsilon$, for every $t \geq 0$.

2. The equilibrium of the above system is said to be asymptotically stable if it is Lyapunov stable, and, if there exists a $\delta(\varepsilon) > 0$, such that, if $\|x(0) - x_{eq}\| < \delta(\varepsilon)$, then $\lim_{t\to\infty}(x(t) - x_{eq}) = 0$.

The above statements can be rephrased as follows:

1. Lyapunov stability of an equilibrium means that solutions starting "close enough" to the equilibrium (within a distance δ from it) remain "close enough" forever (within a distance ε from it). Note that this must be true for any ε that one may want to choose.

2. Asymptotic stability means that solutions that start close enough not only remain close enough but also eventually converge to the equilibrium.

Lyapunov's second method for stability

The basic philosophy of the Lyapunov`s second method is that if the total energy of the electrical or mechanical system is continuously dissipated, then the system should eventually settle down at an equilibrium point. The Lyapunov's second method is commonly used to prove the stability of nonlinear systems, makes use of a Lyapunov`s function as follows. Consider a function $(x) : \mathbb{R}^n \to \mathbb{R}$, with continuous first order derivative such that:

- $V(x) \geq 0$

- $V(x) = 0$ if and only if $x = 0$
- $\dot{V}(x) = \frac{d}{d_t}V(x) \leq 0$

The first two conditions imply that the function $V(x)$ is positive definite, and the third condition implies that $\dot{V}(x)$ with respect to time is negative semi-definite. In other words, if we can find such a scalar function that satisfies the above conditions, then the system is stable in the sense of Lyapunov. Finding a proper Lyapunov function is not a straightforward process for all systems and we may not be able to find one for a particular system. However, if one cannot be found for a system, it does not mean that the system is not stable, i.e., failure of proof is not proof of failure.

Asymptotic stability

If in addition to the conditions for stability in the sense of Lyapunov, $\dot{V}(x)$ is negative definite, then the stability is asymptotic, i.e.

- $V(x) \geq 0$
- $V(x) = 0$ if and only if $x = 0$
- $\dot{V}(x) = \frac{d}{d_t}V(x) \leq 0$
- $\dot{V}(x) = 0$ if and only if $x = 0$

Global stability

If in addition to the conditions for Lyapunov stability, we have:

$V(x) \to \infty \; as \; \|x\| \to \infty$

Then the equilibrium point at the origin is globally stable, i.e.

- $V(x) \geq 0$
- $V(x) = 0$ if and only if $x = 0$
- $\dot{V}(x) = \frac{d}{d_t} V(x) \leq 0$
- $V(x) \to \infty \; as \; \|x\| \to \infty$

Invariant set theorems

The invariant set theorem is used for determining the asymptotic stability of the system with a Lyapunov function with negative semi-definite derivative. A set G is an invariant set for a dynamic system $\dot{x} = f(x)$ if every trajectory $x(t)$ which starts from a point in G remains in G for all time. For example, any equilibrium point is an invariant set. The domain of attraction of an equilibrium point is also an invariant set.

Local invariant set theorem

Consider an autonomous system of the form $\dot{x} = f(x)$, with f continuous and let $V(x) : \mathbb{R}^n \to \mathbb{R}$ be a scalar function with continuous first partial derivatives. Assume that:

- for some $l > 0$, the set Ω_l defined by $V(x) \leq l$ is bounded.
- $\dot{V}(x) \leq 0$ for all x in Ω_l.

Let R be the set of all points within Ω_l where $\dot{V}(x) = 0$ and M be the largest invariant set in R. Then, every solution $x(t)$ originating in Ω_l tends to M as $t \to \infty$.